PRODUCTION OF POSITRONIUM AND MUONIUM IN OXIDE POWDERS

by

ROBERT FRANCIS KIEFL

B.Sc., Carleton University, 1976

A THESIS SUBMITTED IN PARTIAL FULFILLMENT

OF THE REQUIREMENTS FOR THE DEGREE OF

MASTER OF SCIENCE

in

THE FACULTY OF GRADUATE STUDIES

(Physics)

We accept this thesis as conforming

to the required standard

THE UNIVERSITY OF BRITISH COLUMBIA

October, 1978

In presenting this thesis in partial fulfilment of the requirements for an advanced degree at the University of British Columbia, I agree that the Library shall make it freely available for reference and study. I further agree that permission for extensive copying of this thesis for scholarly purposes may be granted by the Head of my Department or by his representatives. It is understood that copying or publication of this thesis for financial gain shall not be allowed without my written permission.

Department of Physics

The University of British Columbia
2075 Wesbrook Place
Vancouver, Canada
V6T 1W5

Date October 11 1978

ABSTRACT

A short review of positrons and muons, and their interactions with matter is presented. The experimental techniques for studying these short lived particles are discussed. Attention is focussed on the formation, properties, and uses of the hydrogen-like atoms, positronium (e^+e^-) and muonium (μ^+e^-), in gases and insulators.

Also, positrons have been injected into extremely fine evacuated powder samples of SiO_2, Al_2O_3, MgO, and ZnO. The fraction of positrons forming o-Ps within the powder grains and diffusing out into the vacuum region has been measured. The largest measurement of 26±3.% was made for the 35Å radius SiO_2 powder. Using this powder as a moderator the O_2 quenching rate coefficient has been determined to be $1.43\pm.04 \times 10^{-12}$ cm³/sec. Doppler broadening measurements of the annihilation line verify that the quenching involves conversion of o-Ps to p-Ps.

In addition polarized muons have been injected into SiO_2, Al_2O_3, MgO, CaO, SnO_2, GeO_2 and SiO powders. Using the techniques of μ^+SR and MSR, upper and lower limits on the muonium fraction have been determined. Non-zero muonium precession signals are reported for SiO_2, CaO, MgO, and Al_2O_3. Evidence is presented that suggests that the muonium is diffusing into the intergranular regions for Al_2O_3 and MgO as reported earlier for SiO_2.

Results from these two experiments indicate that the

formation and behaviour of muonium and positronium are correlated in insulators, at least in a qualitative sense. Future experiments using oxide powders to produce positronium and muonium are discussed.

TABLE OF CONTENTS

LIST OF FIGURES

LIST OF TABLES

ACKNOWLEDGEMENTS

I would especially like to thank Dr. J.B. Warren for his guidance and helpful discussions throughout this research project, and Glen M. Marshall and Dr. C. J. Oram for their constant assistance throughout all phases of the experiment and analysis. I would also like to express my gratitude to Dr. B. Bergersen for his helpful discussions and to Dr. J. H. Brewer and the entire MSR group since they made this research possible. I wish to thank Dr. D. J. Judd and Larry Spires for their generous participation. In addition I would like to thank George Clarke for his most effective data transfer system and computer programs and Dr. R. Albrecht for the use of his lifetime fitting program. Finally, I would like to thank the technicians of the UBC nuclear physics laboratory for their co-operation and assistance.

CHAPTER 1 INTRODUCTION

The fundamental dynamical postulate of quantum mechanics states that the time dependence of a physical state is determined by the full Hamiltonian according to

$$i\hbar\frac{\partial}{\partial t}|\psi(t)\rangle = H|\psi(t)\rangle$$

where $H = H_o + H_{int}$ and H_{int} is the full interaction Hamiltonian which is composed of weak, electromagnetic, and strong interaction terms, and accounts for both elastic and inelastic processes. Experiments in nuclear, and particle physics invariably involve the preparation of an initial state followed by the determination of a final state. The initial state, $|i\rangle$, can be determined precisely by measuring a complete set of compatible observables. The final state, $|f\rangle$, cannot be determined precisely with one set of measurements because the act of measuring is equivalent to projecting $|f\rangle$ onto the eigenstate corresponding to the measured quantities. The probability for making a set of measurements, which projects $|f\rangle$ onto $|m\rangle$ is $|\langle m|f\rangle|^2$. Expanding $|f\rangle$ in terms of $|m\rangle$ s gives

$$|f\rangle = \sum_m |m\rangle\langle m|f\rangle$$

The probabilities, $|\langle m|f\rangle|^2$, are determined experimentally, to within a statistical error, by performing many sets of measurements.

These efforts are directed at studying the time dependence of a physical state in order to obtain knowledge about the interaction Hamiltonian. All conservation laws in particle physics are the result of these types of experiments. The confidence in any conclusion reached obviously depends on the statistics of the experiment.

The simplest initial state to prepare is, of course, a one body state. The decay of single particles provides valuable insight into the fundamental interactions and properties of particles. Examples are

$$\mu^+ \rightarrow e^+ + \nu_e + \bar{\nu}_\mu \qquad \text{(weak)}$$

$$\pi^o \rightarrow 2\gamma \qquad \text{(electromagnetic)}$$

$$\Delta^{++} \rightarrow p + \pi^+ \qquad \text{(strong)}$$

The next simplest inital state to prepare is, naturally, the two body state. A very useful subset of these two body states are those bound together by the Coulomb force which are sometimes referred to as "onium" states. These Coulomb bound states are well defined eigenstates of orbital angular momentum. Also , the wave functions, $\langle E|x\rangle$, are easily calculated. These properties make "onium" systems invaluable in the study of the fundamental interactions. The vast majority of these "oniums" have not been observed because both partners are short lived and must be produced artificially. The production problem simplifies if one

partner is stable and naturally occurring. "Oniums" such as e^+e^-, $p\pi^-$, μ^+e^-, $p\mu^-$, and $\bar{p}p$, have already been observed. At the present time the search is on for the more elusive pi-muonium, $\pi^+\mu^-$.

The interest in the diffusion and chemistry of hydrogen atoms extends naturally to muonium and positronium because they provide an opportunity to study the chemical interactions and motion of hydrogen-like atoms on a time scale as small as 10^{-9} sec.

Muonium and positronium are also of special interest in particle physics. For example, the decay of the positronium ground state with spin=1, written

$$o\text{-}Ps \rightarrow 3\gamma$$

is of great interest because the lifetime in vacuum provides a test for the theory of quantum electrodynamics. A major difficulty in the experiment is to isolate the e^+e^- atom from other electrons which tend to shorten the observed lifetime.

The conversion rate of muonium to anti-muonium has important consequences in weak interaction theory. Such a conversion is possible only if the weak interaction conserves muon number in a multiplicative or parity-like fashion. Again, a major difficulty in measuring the true vacuum conversion rate is to isolate the μ^+e^- atom.

An experiment at TRIUMF has been planned for early 1979 that will produce and detect pionium, π^+e^-.

The purpose of this work was primarily to explore the

similarity in formation and behaviour between positronium and muonium in materials, particularly powdered oxides, where copious amounts of positronium had already been observed. Such comparisons are essential to a broader understanding of the behaviour of these "onium" systems and will inevitably help to realize their full potential in physics.

CHAPTER II POSITRONS AND POSITRONIUM IN MATTER

Section II.1 Introduction

Dirac (1930) postulated that vacancies in a filled sea of negative energy electron states would manifest themselves physically as anti-electrons or positrons. Anderson (1933) was the first to observe positrons in cloud chamber photographs of cosmic ray showers. The production of positron-electron pairs from high energy gamma rays was observed shortly afterwards (Blackett, 1933). These experimental results sparked a large effort to develop a theory for positrons in matter. Mahorovicii (1934) was the first to suggest the existence of a bound e^+e^- state, named positronium or Ps. Pirenne (1946) was one of the first to perform calculations on the positronium energy levels. Wheeler (1946) and Ore and Powell (1949) calculated annihilation rates from the S=0 and S=1 ground states respectively. In the meantime the experimental studies on positronium were just becoming possible as positron sources such as Na^{22} and Cu^{64} became available. The work of Deutsch (1951) firmly established the existence of positronium.

Despite the great amount of experimentation since those early days, it was not until 1974 that the first excited state of positronium, Ps*, was observed (Canter, 1975). This and many other experiments have been made possible by the

development of monoenergetic beams of low energy positrons (Canter, 1972).

Sections II.2 and II.3 of this chapter review the basic interactions of positrons and positronium with matter and the experimental techniques for observing these interactions. Sections II.4 and II.5 discuss Ps formation in matter and some previous positronium experiments in gases, powders, and gels which are relevant to this study.

Sect II.2 Properties of Positrons and Positronium in Matter

i Conservation of Charge Conjugation Parity in e^+e^- Annihilation

Although positrons and electrons are individually stable spin 1/2 states, the positron-electron state is unstable to annihilation into gamma rays through electromagnetic interaction. The charge conjugation or C parity for an e^+e^- state is $(-1)^{L+S}$ (see Appendix I(a)) where L is the orbital angular momentum and S is the total spin. The C parity for a state containing n gamma rays is $(-1)^n$ (see Appendix I(b)). Electromagnetic interactions conserve C parity which implies $(-1)^{L+S} = (-1)^n$. Since in many cases one need only consider the L=0 states, this restricts the annihilation from spin 0 and spin 1 states to an even and odd number of γs respectively. Annihilation into a single γ from a two body inital state cannot conserve both momentum and energy so that a spin 1 state must decay into $(2m+1)$ γs where m is a positive non-zero integer. The annihilation rate into m γs decreases rapidly like α^m where α is the fine structure constant $(=e/\hbar c=1/137)$ so that the spin 0 and spin 1 states decay primarily into 2 γs and 3 γs respectively.

ii Free Positron Annihilation

In low energy e^+e^- scattering only the L=0 state contributes and thus restricts the final state to 2γ s and 3γ s for the S=0 and S=1 states respectively. Dirac (1930) calculated the spin averaged 2γ cross section for e^+e^- scattering to be

$$\sigma_{2\gamma} = \pi r_e^2 c/v \quad v<<c \quad \text{eqn II.1}$$

where r_e is the classical electron radius, e^2/mc. Ore and Powell (1949) calculated the spin averaged cross section for annihilation into 3γ s to be

$$\sigma_{2\gamma} = 4(\pi^2-9)r_e^2 c\alpha/3v = 1/371\sigma_{2\gamma} \quad v<<c$$

The single γ annihilation requires a third body in the initial state to conserve both energy and momentum, such as an electron or a nucleus. In the case of an electron the decay rate involves an e^-e^- correlation coefficient. West (1973) estimates that the annihilation rate into a single γ in this manner to be smaller than the 3γ annihilation rate by a factor $\lambda_c^3\rho$ where λ_c is the compton wavelength for an electron and ρ is the second electron density. On this basis the most optimistic ρ leads to a branching ratio

$$\sigma_\gamma/\sigma_{3\gamma} = \alpha^3$$

Attempts to observe this rare annihilation mode have been unsuccessful (Reddy, 1970)

The single gamma annihilation involving a nucleus is much more likely and has been observed (Sodickson, 1961). The cross section is approximately $\alpha^4 Z^5 r_e^2$.

Annihilation into 0 gamma rays has also been observed (Shimizu, 1968). In this process the positron annihilates with a core electron and imparts the the resulting energy to another core electron. The Feynman diagrams for all these annihilation modes are shown in fig II.1. Free positrons are useful probes into the many electron state of the host substance since that state characterizes the subsequent annihilation. For a thermalized free positron annihilating with an electron, where the total spin =0, the angle between the resulting 2γ s provides a measure of the e^+e^- pair momentum which depends primarily on the electron momentum distribution of the host. This has proven to be particularly useful in studying metals.

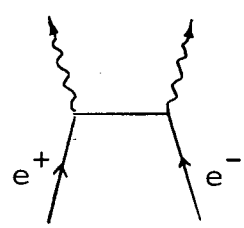

(a)

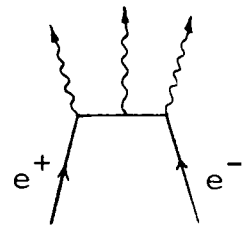

(b)

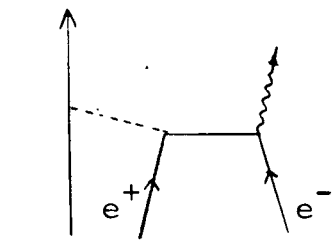

(c)

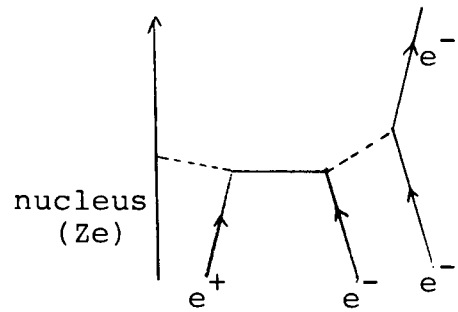

(d)

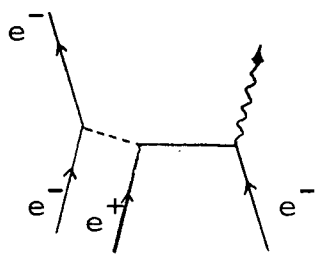

(e)

Fig II.1 Feynman diagrams for (a) 2 gamma annihilation ,(b) 3 gamma annihilation, (c) 1 gamma annihilation involving a nucleus , (d) 0 gamma annihilation involving a nucleus and a second electron , (e) 1 gamma annihilation involving a second electron.

Iii Bound State Annihilations

The factors that effect Ps formation in a substance will be discussed in Sect II.3. Given that it does form, the singlet (S=0 or para-positronium or p-Ps) state and the triplet (S=1 or ortho-positronium or o-Ps) state form in the statistical ratio 1:3. p-Ps decays into two 511 KeV γ's whereas o-Ps decays into 3 γs. The energy spectrum is continuous and is shown in fig II.2. The mean decay rate (=1/lifetime) in vacuum for p-Ps and o-Ps from theory and experiment are

$\lambda^{th}_{p-Ps} = .7985 \times 10^{10} sec^{-1}$ [1] (Kolbig, 1969)

$\lambda^{exp}_{p-Ps} = .799 \pm .011 \times 10^{10} sec^{-1}$ (Theriot, 1967)

$\lambda^{th}_{o-Ps} = 7.0379 \pm .0012 \times 10^{6} sec^{-1}$ (Caswell, 1977)

$\lambda^{exp}_{o-Ps} = 7.056 \pm .007 \times 10^{6} sec^{-1}$ (Gidley, 1978)

The difference in annihilation rates for o-Ps and p-Ps is of order α and can be understood in terms of the additional vertex for the Feyman diagram for the o-Ps decay (see fig II.1).

[1] no error given

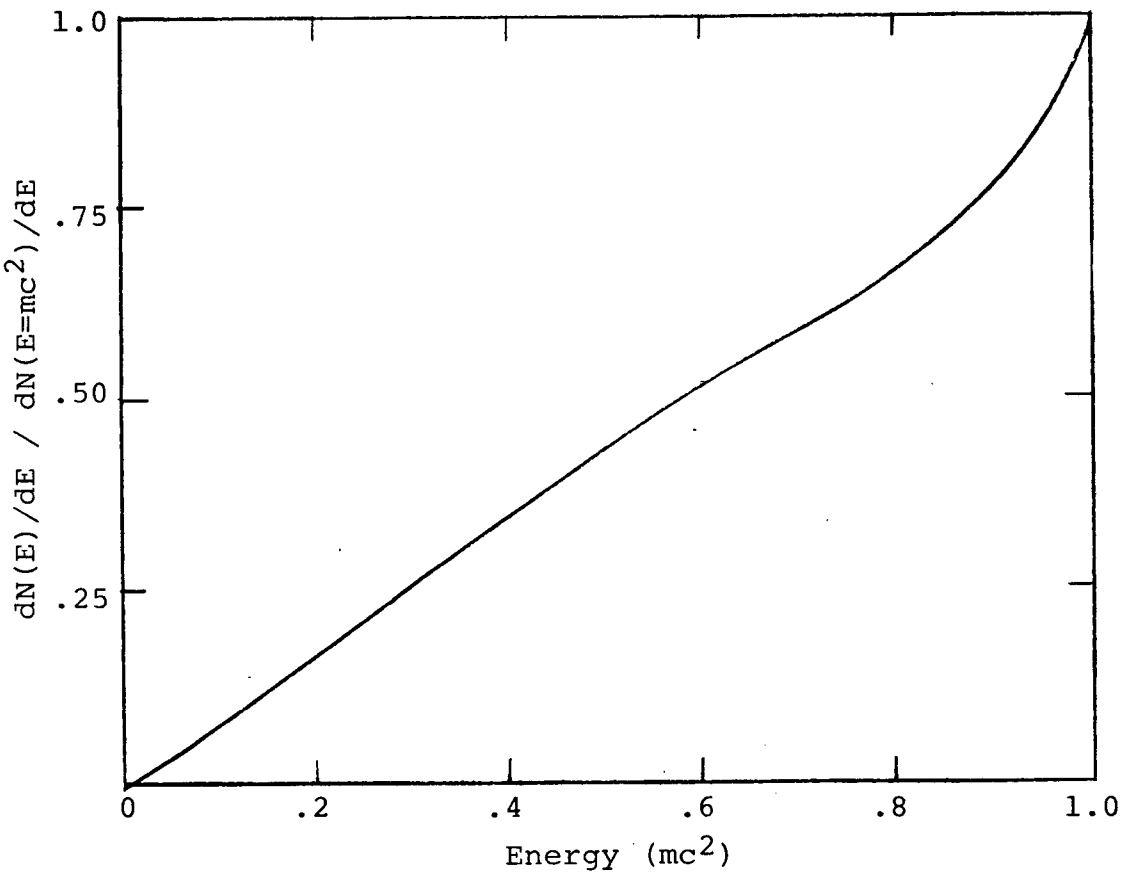

Fig II.2 . The photon energy spectrum from the annihilation of o-Ps. (Ore,1949)

Sect II.3 Experimental Techniques

i General

The study of positrons in matter is based on the detection of the annihilation quanta. The relevant observables are the time before annihilation, the angle between the annihilation quanta, the energy of the annihilation quanta, and the number of annihilation quanta.

ii Lifetime Technique

Na^{22} sources are commonly used for measuring positron lifetimes because the emission of a positron is followed, in most decays ,by the emission of a nuclear γ of energy 1274 KeV within 10^{-11} sec (see fig II.3) and thus provides a convenient method of signaling a positron emission. One counter is used to start the clock on an e^+ emission and up to three γ counters in coincidence can be used to stop the clock. Small plastic scintillators provide excellent timing resolution ($.3 \times 10^{-9}$ sec), but have poor energy resolution and are very inefficient. For studying short lifetimes in solids and liquids, plastic scintillators are essential. Larger NaI detectors are often preferred for measuring the long lifetime of o-Ps where sometimes a triple coincidence stop is required (Bird, 1973). The efficiency and energy resolution are increased substantially using this type of detector although the timing resolution (3 or 4 nsec) is not as good as may be achieved with plastic scintillators.

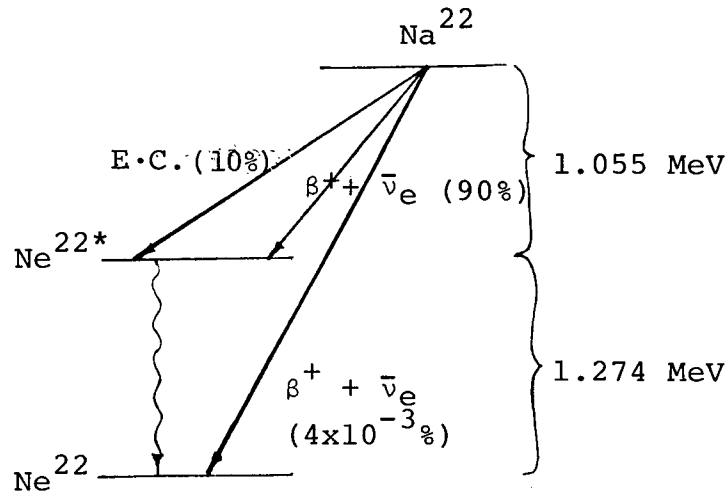

Fig II.3 . Na^{22} decay scheme. The maximum enegy for a positron resulting from the decay into Ne^{22*} is .544 MeV. The lifetimes for Na^{22} and Ne^{22*} are 2.6 years and 10^{-11} sec respectively.

iii Angular Correlation Technique

If an S=0 e^+e^- state has a pair momentum component, $p_\perp$, perpendicular to one of the photon emission directions then the two photons will be emitted at an angle, $180^o + \theta$ where

$$\theta \sim p_\perp / m_o c \qquad p_\perp \lesssim m_o c \text{ (West,1972)}$$

If the positron is thermalized then the pair momentum is approximately equal to the electron momentum. Thus if $p_\perp$ of the electron is 0.5 KeV/c, corresponding to an energy $p_\perp^2/2m_o = 0.25$ eV, then the two photons will be emitted at an angle of 1 mrad or $.057^o$.

The angular distribution between the annihilation quanta is measured using a long slit angular correlation apparatus. This apparatus measures the coincidence counting rate between two detectors as a function of the angle defined by detector 1, the source and detector 2. A typical angular resolution would be .5 mrad.

iv Doppler Broadening Technique

Information on the pair momentum distribution can also be obtained by using a high resolution Ge or GeLi detector to measure the Doppler broadening of the annihilation line at 511 KeV. To first order, the shift in energy produced by a longitudinal pair momentum component, $p_{\parallel}$, is given by

$$\Delta E \mp h\nu - mc^2 \approx p_{\parallel} c/2 \qquad \text{(Hotz, 1968)}$$

where $h\nu$ is the energy of the detected photon. Thus, if $p = 0.5$ KeV/c then $\Delta E = 0.25$ KeV. In cases where the sampled e^- momentum distribution is isotropic, the techniques of Doppler broadening and angular correlation ,applied to annihilation quanta in a given direction, yield the same information. Charalambois (1976) has reported a system resolution of 1.08 KeV at 514 KeV using an intrinsic Ge detector, which is equivalent to an angular correlation apparatus with an angular resolution of 4 mrad.

The Doppler broadening technique analyzes all momentum channels simultaneously and is therefore much faster. Also, it does not require high e^+ stopping densities nor strong sources as does the angular correlation technique. The obvious disadvantage is the poorer resolution which is limited by the intrinsic properties of semi-conductors such as GeLi.

v $2\gamma/3\gamma$ Decay Ratio Technique

3γ decays resulting from o-Ps formation can be detected using a 3γ coincidence technique (Celitans, 1964a), but normalizing the detection rate to that of 2γ decays is difficult because 3γ decays result in a continuous energy spectrum. This will be discussed further in Sect IV.1. Changes in the $3\gamma/2\gamma$ ratio are however, directly observable in the annihilation spectra. An increase in the $3\gamma/2\gamma$ ratio is characterized by a reduction in the 511 KeV photopeak and an increase in the counting rate below 511 KeV. NaI detectors previously and GeLi detectors more recently (Sen and Patro, 1969) have been used to study the $3\gamma/2\gamma$ ratio in this manner.

Sect II.4 Ps Formation

i Slowing Down in Gases

High energy positrons lose energy through inelastic collisions leading to ionization or the emission of Bremsstrahlung radiation. The ratio between the energy loss rates for the two processes is given as

$$\frac{\left(\frac{dE}{dx}\right)_{rad}}{\left(\frac{dE}{dx}\right)_{ion}} \simeq EZ/800 \qquad \text{(Segré, 1964a)}$$

where E is the positron energy in MeV and Z is the atomic number of the atomic species. Below energies of a few MeV, ionization dominates whereby the fast positron loses approximately 30 eV per ion formed (Segre, 1964b). The loss to free annihilation is small because 1/(slowing down time) is large in comparison to the free annihilation rate given by

$$\lambda_2 = nZv\sigma_2$$
$$= nZ\pi r_e^2 c \qquad \text{using eqn II.1}$$

where n is the number density for the gas and Z is the atomic number for the gas.

ii Ore Gap in Gases

Fig. II.4 shows the different channels that a positron can take before it annihilates. For the energy interval (E_{ion}, E_{exc}) the processes of atomic or molecular excitation and Ps formation are in competition. The Ore gap is defined as the energy interval (E_{exc}, E_{ion} -6.8 eV). It is generally believed that Ps forming collisions dominate the dE/dX in this energy range. The Ps atom has a kinetic energy less than that of the incident positron by E_{ion} -6.8 eV. A positron with an energy below the threshold for Ps formation (E_{ion} -6.8 eV) will collide elastically until it annihilates freely. The positron usually thermalizes before annihilating.

The Ore limits on Ps formation are arrived at by assuming that the last ionizing collision above E_{ion} leads to a uniform population density in the energy interval (0, E_{ion}). It is further assumed that a positron in the Ore gap (E_{exc}, E_{ion} -6.8 eV) forms Ps 100% of the time. The lower limit on f_{Ps} is then (E_{exc} - (E_{ion} -6.8 eV)) / E_{ion} . If the positron finds itself in the energy interval (E_{exc}, E_{ion}) it may or may not form Ps since excitation is a competing process. Thus the upper limit on f_{Ps} is 6.8 eV/E_{ion} .

As an example, the Ore limits for argon and helium are (16-43)% and (90-28)% respectively, whereas the observed fractions are 27±3% (Gittleman, 1956) and 32±3% (Pond, 1952) respectively.

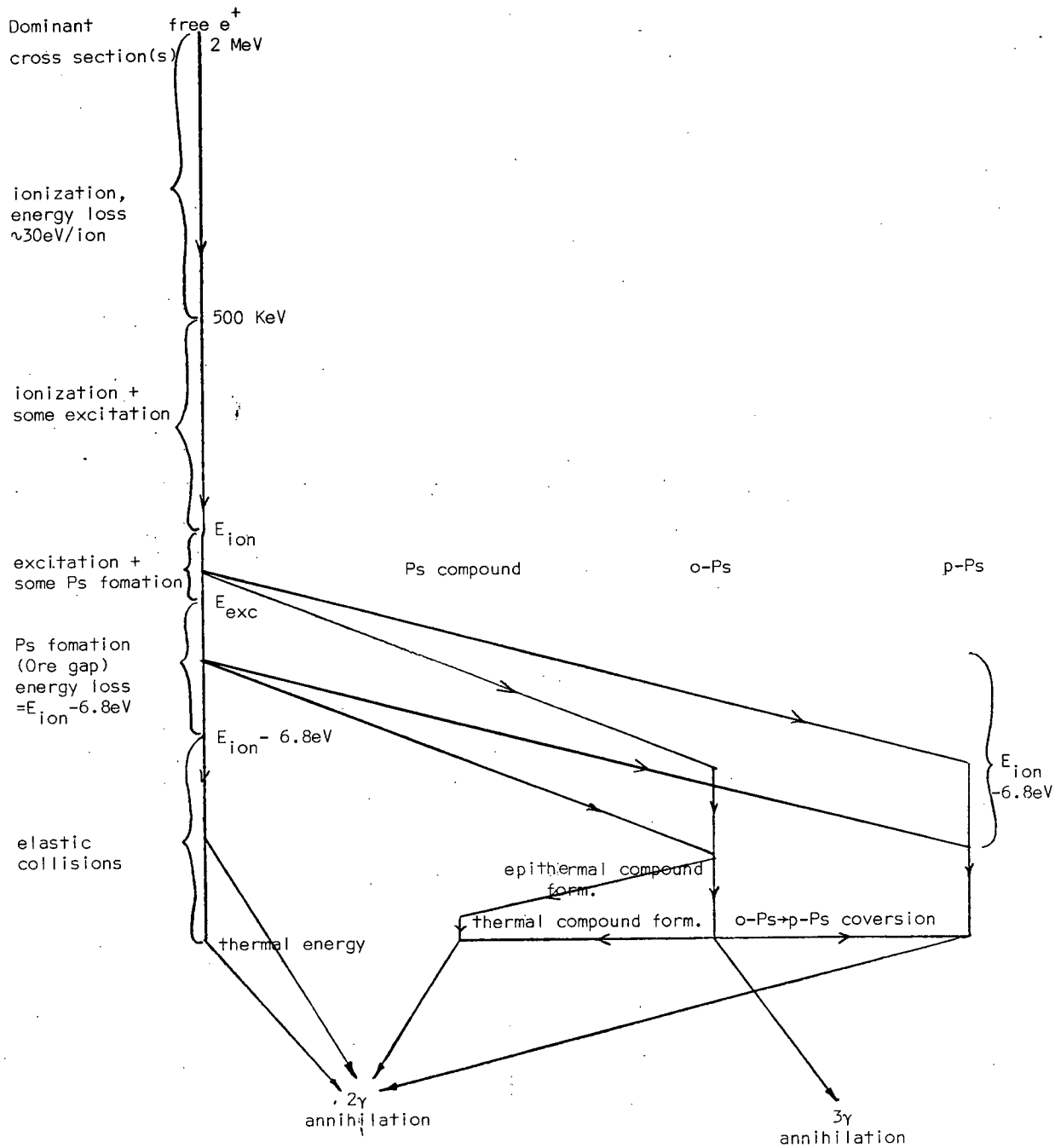

Fig II.4 . Flow diagram for free positrons in a gas with ionization energy E_{ion} and excitation energy E_{exc}.

iii Low Energy Positron Beams in Gases

Unfortunately, the Ore predictions have had only limited success, one case being argon . It has been suggested low energy resonances just above E_{ion} could result in an non-uniform population density below E_{ion} (Lee,1967). This would explain the failure of the Ore limits.

Since 1970,scurces of thermal positrons from the back scattering of high energy positrons off various surfaces have become available. The highest efficiency thus far (3×10^{-3}%) was obtained by using a gold surface coated with MgO (Canter,1974). These thermal positrons have been used to generate monoenergtic beams of low energy positrons. Such beams have been used to measure total cross sections in noble gases (Harris,1976 & Canter,1974). The technique involves passing a positron beam through a gas cell of length d, in which the number density for the gas is n. The pressure is chosen so that only single scattering is likely. The transmission coefficient through the gas is measured at the end of the cell using a NaI counter to detect annihilation radiation with and without the gas. The total cross section for the gas,ignoring small angle scattering, is then given by

$$\sigma_{tot} = [\ dN/dt_{vac} - dN/dt_{gas}\ ]/[\ n\ d\ dN/dt_{vac}\ ]$$

and represents the sum of all possible cross sections, elastic and inelastic. Although sharp resonances are not present (see fig II.5) the total cross section does drop off

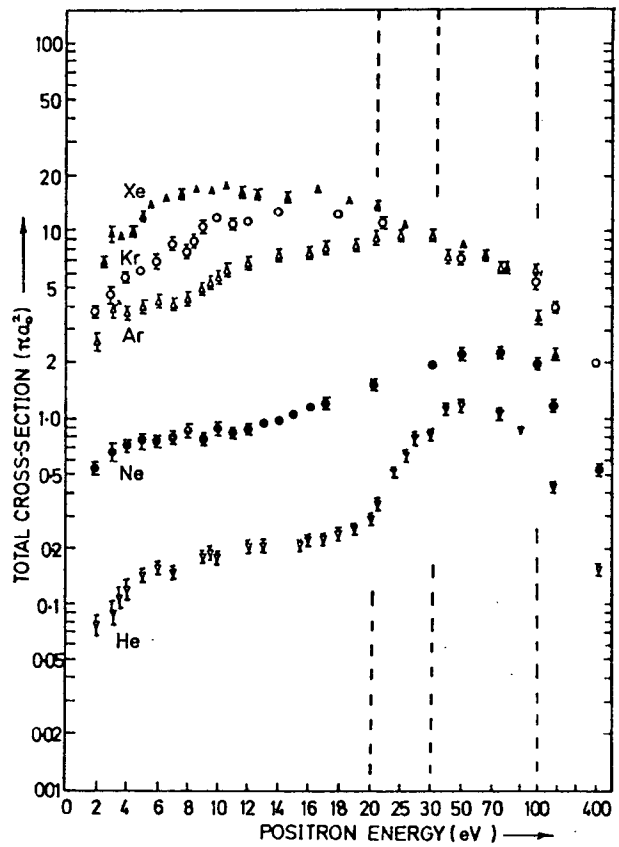

Fig II.5 . Total cross section measurements in noble gases for low energy positrons.(Canter,1974)

rapidly below 50 eV in some cases. This could be responsible for a non-uniform population density below E_{ion} and would therefore help to explain the failure of the Ore limits in cases such as Kr and He.

In principle it should be possible to monitor the three gamma coincidence rate as a function of positron energy and thus determine explicitly the energy dependence of the Ps forming cross section. This would be a firm test of the Ore gap theory.

iv Formation in Solids

The Ore gap analysis cannot be extended in a straight forward manner to include solids. Positronium has been observed in insulators (e.g. quartz and ice) but has not been observed in covalent semi-conductors such as Ge and Si. The energy of the positronium state is modified by the dielectric properties of the medium and is only well defined if the electronic energy lies in a forbidden gap. High yields of positronium formation (e.g. 30%) have been observed in oxide powders (Paulin and Ambrosino, 1969). The positrons are slowed down within the grains and eventually reach the intergranular region as positronium. Paulin and Ambrosino (1969) have reported an increased Ps fraction for amorphous SiO_2 powder compared with the crystaline form.

It should be stressed that a Ps state in a solid cannot be treated independently of the electrons in the solid. In an unreactive gas at low pressure the perturbing effects of the neighbouring electrons on a Ps state are small, whereas in a solid this is not true. For example, angular correlation measurements in single crystal ice (see fig II.6) reveal a delocalized p-Ps state whereby the pair momentum distribution has side peaks reflecting the

periodicity of the p-Ps centre of mass position wave function.

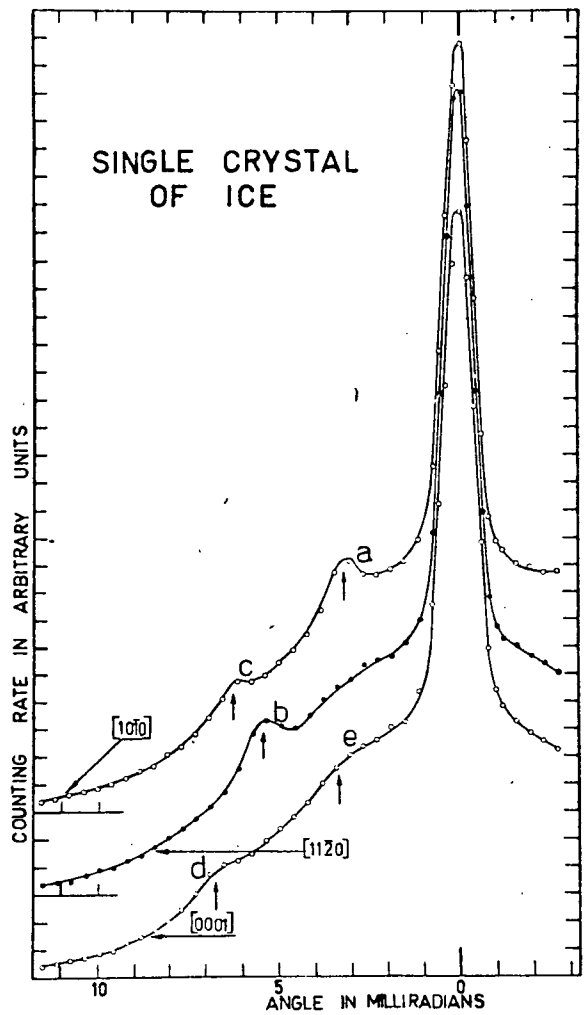

Fig II.6 . Angular correlation measurements in single crystal ice for the different crystal orientations. The arrows indicate the theoretical position of the peaks assuming a periodic wave function for p-Ps.The broad Gaussian background is due to free positron annihilation. (Mogensen,1971)

v Summary of Ps Formation

In summary, the Ore gap is a useful concept in gases where the formation process is thought to be represented well by charge exchange collisions with individual atoms. Now that monoenergetic beams of low energy positrons are available it should be possible to firmly test the validity of this approach. In solids the situation is more complex so that a more sophisticated approach is required.

Sect. II.5 o-Ps in Gases, Powders and Gels

i Quenching in Gases

Positronium gas chemistry makes use of the relatively small mean decay rate of free o-Ps of 7.056±.007 μsec^{-1} (Gidley,1977). In gases this mean decay rate is increased in two ways, pickoff annihilation and o-Ps to p-Ps conversion. Both processes are said to quench the o-Ps. Pickoff annihilation is when the bound positron in o-Ps annihilates with an electron from the surrounding medium. In gases this can happen to a small degree during elastic collisions or to a much greater degree if a chemical compound is formed. The resulting pair momentum is of order 3 KeV/c corresponding to the momentum distribution of the valence electrons of the gas molecules. If a gas has an unpaired electron, a spin flip process may occur during a collision so that the o-Ps is converted to p-Ps. The pair momentum for thermal p-Ps is order 0.1 KeV/c and thus makes quenching due to a conversion process easily distinguishable from pickoff quenching associated with a chemical bond formation.

ii Quench Rate Coefficient in Gases

The mean quenching rate for o-Ps atoms with velocity v in a gas with number density n and quenching cross section σ_q is

$$\lambda_q = \sigma_q v n \qquad \text{(see Appendix II).}$$

If the Ps thermalizes fast, v is the mean thermal velocity. The mean quenching rate is proportional to n where the constant of proportionality, $\sigma_q v$, is referred to as the quench rate coefficient.

For gases which possess a quench rate coefficient that is much larger than that for argon ($2.51 \pm .05 \times 10^5$ sec^{-1}/atm., Cetitans, 1964b), argon + gas mixtures can be used to study the reaction. The argon acts as a moderator producing 27% Ps, but has very little quenching effect. The quench rate coefficient for a particular gas is then the slope of the quench rate versus gas concentration in argon + gas mixtures.

iii Ps in Powders and Gels

Paulin and Ambrosino (1969) have studied positron lifetimes in fine MgO, SiO_2, and Al_2O_3 powders. The lifetime spectra exhibited three components at <.4 nsec, 2 nsec and 140 nsec. They attributed the <.4 nsec component to free positron annihilation and p-Ps annihilation, the 2 nsec component to pickoff of o-Ps within the grains, and the 140 nsec component to o-Ps in the intergranular regions. Brandt and Paulin (1969) interpreted these results in terms of a diffusion model whereby the o-Ps forms within the grains and then diffuses out into the intergranular region.

Since that time many experiments have been done with fine powders. Stedlt and Varlashkin (1972) have performed angular correlation measurements on compressed SiO_2 powders. They investigated the effect of powder size, powder density, baking, and temperature on the narrow component associated with p-Ps . They interpreted the results in terms of the diffusion model suggested by Brandt and Paulin (1969).

Gidley and Marko (1976) have measured the linear dependence of the o-Ps mean decay rate in fine SiO_2 on powder density. They extrapolated back to zero powder density and obtained a value of 7.09±.02 μsec^{-1} for the mean decay rate of o-Ps in vacuum. Systematic errors were later discovered (Gidley, 1978) which lower this value to 7.067±.021 μsec^{-1}.

Positrons have also been injected into silica gels with a mean pore size of 22 $\mathring{A}$ (Chuang, 1974). After evacuating the

gel they observed a long component in the lifetime spectrum with a mean decay rate of 31 μsec^{-1} which they attributed to o-Ps in the pores. After adsorbing different amounts of Br_2, NO, I_2, O_2, and NO_2, they measured quenching rate coefficients for these gases. They also performed angular correlation measurements to determine the quenching mechanisms.

CHAPTER III POSITIVE MUONS AND MUONIUM IN MATTER

Sect III.1 Introduction

In 1935 Yukawa postulated that the nucleus was held together by an exchange force whereby heavy quanta are exchanged between the nucleons within the nucleus. He estimated on the basis of the strength and range of the nuclear force that the heavy quanta should possess a mass between 50 and 100 Mev/c^2. Cosmic ray experiments performed by Anderson and Neddermeyer (1937,1938) and Street and Stevenson (1937) showed the existence of a pair of oppositely charged particles with a mass $\sim$ 100 Mev/c^2. However, further experiments (Conversi, 1947) revealed that the nuclear absorption lifetime in carbon of the negatively charged partner was of order 10^{-6} sec. instead of 10^{-18} sec. as expected if the particles were strongly interacting. These two particles are now called muons. The Yukawa meson , which is now referred to as the pion, was discovered later that year (Lattes, 1947) in an experiment which showed that pions decayed into a neutral particle plus a muon.

Section III.2 of this chapter discusses the properties of muons and muon decay, and points out some of their uses as probes. Section III.3 reviews the basic features of μ^+SR and MSR. Section III.4 discusses muonium formation with specific reference to the analogous situation in hydrogen formation.

Sect III.2 Properties and Uses of Muons

i Properties

The properties of muons have provided valuable insight into elementary theories for weak interactions and electromagnetic interactions.

For example, the gyromagnetic ratio of the muon which is defined as

$$g_\mu = \mu_\mu 4\, m_\mu c / e\hbar$$

(where μ_μ is the muon magnetic moment and m_μ is the muon mass) is very close to 2 as predicted by the Dirac equation for a spin 1/2 particle. The difference $a_\mu = (g_\mu - 2)/2$ has provided one of the best tests for the theory of quantum electrodynamics since it has been measured and calculated to 1 part in 10^8. The results as of 1977 are

$$a_\mu^{exp} = 1{,}165{,}910(9) \times 10^{-9} \quad \text{(Bailey,1977)}$$
$$a_\mu^{th} = 1{,}165{,}915(10) \times 10^{-9} \quad \text{(Calmet,1977)}$$

Muons decay weakly with a lifetime of 2199.4 nsec into an electron and two neutrinos in the following way:

$$\mu^+ \rightarrow e^+ + \nu_e + \bar{\nu}_\mu$$
$$\mu^- \rightarrow e^- + \bar{\nu}_e + \nu_\mu$$

It was discovered in 1956 from the β-decay of Co^{60} (Wu, 1957) that weak interactions do not conserve parity. Non conservation of parity in muon decay allows the weak

interaction Hamiltonian to contain a pseudoscalar term $\sigma_\mu \cdot p_e$ where σ_μ is the muon spin operator and p_e is the electron momentum operator. The obvious consequence of such a term is that the distribution of decay electrons depends on $\cos\theta$ where θ is the angle between the muon polarization vector and the electron momentum. The simplest interaction Hamiltonian containing such a term leads to the following energy-angular distribution

$$\frac{dN}{d\Omega dw} = \frac{C(w)}{2\pi}\left[\, 1 \pm |\bar{P}| D(w) \cos\theta \,\right] \quad \text{(eg. Williams ,1971)}$$

$+$ for positrons

$-$ for electrons

where $\bar{P}$ is the polarization vector, θ the angle between and the electron momentum, and $w = E/E_{max}$ is the energy of the electron expressed in units of $E_{max}=m_\mu/2$. Fig III.1 shows the parameters C(w) and D(w) as a function of w. It should be noted that D(w) changes sign going from small electron energies to large electron energies. Also, the distribution of energies, C(w), is weighted towards E_{max}. The value of D(w) averaged over all energies is .324±.004 (Cronin,1968)

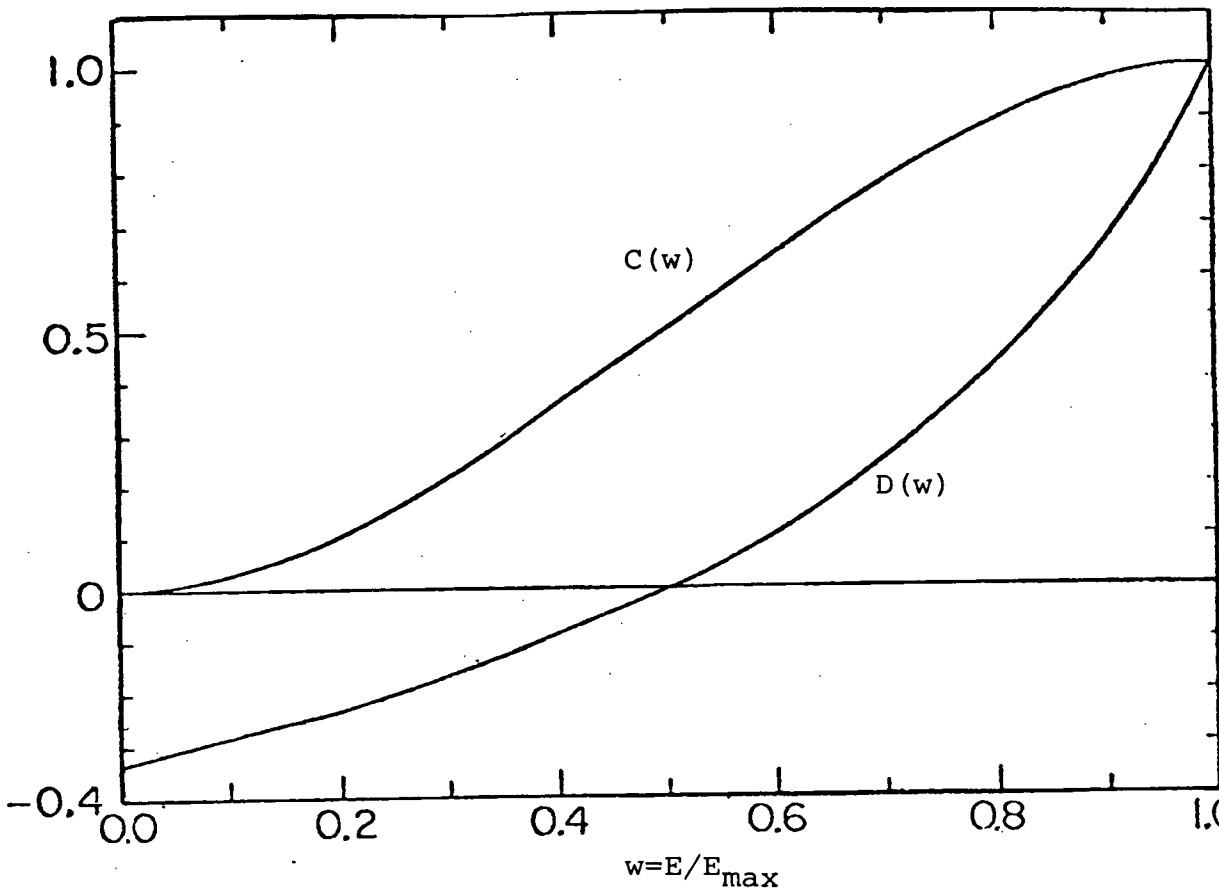

Fig III.1 . Muon decay parameters for $dN(w,\Omega)/dwd\Omega$ (e.g. Brewer,1975)

ii Muons as Probes

Muons are also proving to be very useful probes into atomic and nuclear structure. When negative muons stop in matter they are captured into weakly bound atomic orbits and then proceed to cascade through the lower orbits until they reach the ground state. The muon lifetime is shortened in this ground state due to the process whereby the muon is captured by the nucleus. Since the radii of atomic orbitals vary inversely with the reduced mass in a hydrogen-like atom, the muonic orbits are approximately 200 times smaller than the corresponding electronic orbits. In the upper part of the cascade, where there is substantial overlap between muonic orbits and the K and L electronic orbits, Auger transitions dominate. In such a transition the transition energy is imparted to a K or L electron. Transitions between the lower orbits are electromagnetic in nature whereby the transition energy is released in the form of an X ray. The lower orbits are often inside the nucleus so that the X ray energies are shifted from those calculated by an ordinary Coulomb potential because of the perturbing effects of the nuclear charge distribution.

The present study is directed towards positive muons. Polarized positive muons can be used as magnetic probes into the many electron states in matter. The time dependence of the muon polarization vector is determined by the magnetic environment in which it exists. The muon polarization vector is easily observable because of the asymmetric muon decay.

In addition, the bound state (Mu) provides a unique opportunity to study the chemistry and motion of hydrogen-like atoms. Moreover, macroscopic quantities of muonium are not required to obtain information on the system as is the case for hydrogen studies. Each muonium atom is detected separately so that a million muons are sufficient to determine the time dependence of the muon polarization vector. Such experiments will inevitably help to clarify our understanding of the macroscopic properties of hydrogen in matter.

Sect III.3 The Techniques of μ^+ Spin Resonance (μ^+SR) and Mu Spin Resonance (MSR) in Transverse Magnetic Fields

i General

The techniques of μ^+SR and MSR both involve measuring the time evolution of the muon polarization vector in the presence of an externally applied magnetic field. The difference is that in μ^+SR the muon exists in a diamagnetic environment whereas in MSR the muon is strongly coupled to the large magnetic moment of an electron. The time dependence of the muon polarization vector yields information on the magnetic environment of the free muon or muonium atom. This time dependence for muonium is radically different from that for free muons.

ii μ^+SR

The spin Hamiltonian for a free muon in the presence of an external magnetic field of magnitude $|B|$ applied along the z direction is

$$H^{\mu} = \frac{\hbar}{2}\,\bar{\omega}\cdot\bar{\sigma}^{\mu} = \frac{\hbar\omega\sigma_z}{2}$$

where $\bar{\omega} = g_{\mu}\, e\, \bar{B}/2m_{\mu}c$ and the components of $\bar{\sigma}^{\mu}$ are the Pauli spin matrices. It follows that the energy eigenstates are $|\alpha> = |\sigma_z/2 = 1/2>$ and $|\beta> = |\sigma_z/2 = -1/2>$ with energy eigenvalues $\frac{\hbar g_{\mu} e|\bar{B}|}{2m_{\mu}c}$ and $\frac{-\hbar g_{\mu} e|\bar{B}|}{2m_{\mu}c}$, respectively.

The technique of μ^+SR involves preparing an initial free muon state polarized in a direction perpendicular to the field direction, say the x direction. The initial state can then be written $|\psi(0)> = |\sigma_z = 1/2>$. The muon polarization vector is the expectation value of $\bar{\sigma}^{\mu}$ and therefore can be written

$$\bar{P}(t) = <\psi(0)|e^{\frac{iH^{\mu}t}{\hbar}}\ \bar{\sigma}^{\mu}\ e^{\frac{-iH^{\mu}t}{\hbar}}\ |\psi(0)>$$

$$= \cos\omega^{\mu}t\ \hat{x} + \sin\omega^{\mu}t\ \hat{y} \qquad \text{see Appendix III}$$

where $\omega^{\mu} = 2\pi \times 13.55\ \text{KHz/G} \times |\bar{B}|$

iii MSR

The corresponding problem for muonium is more difficult to solve because it involves two spin 1/2 particles interacting with one another as well as with an external field. The spin Hamiltonian for Mu in an external field, $\bar{B}$, is given as

$$H^{Mu} = \frac{\hbar\omega_o}{4}\bar{\sigma}^{\mu}.\bar{\sigma}^{e} + \hbar\bar{\omega}^{\mu}.\frac{\bar{\sigma}^{\mu}}{2} + \hbar\bar{\omega}^{e}.\frac{\bar{\sigma}^{e}}{2}$$

where $\hbar\omega_o = 1.84 \times 10^{-5}$ eV is the hyperfine splitting of Mu, $\hbar\bar{\sigma}^{\mu}/2$ and $\hbar\bar{\sigma}^{e}/2$ are muon and electron spin operators, and $\bar{\omega}^{\mu}$ and $\bar{\omega}^{e}$ are $-g_{\mu}e\bar{B} / 2m_{\mu}c$ and $g_{e}e\bar{B} / 2m_{e}c$, respectively.

The procedure for evaluating the time dependent muon polarization vector is the same as for the free muon case. It involves the diagonalization of H^{Mu} which is a 4 x 4 matrix in order to evaluate its eigenvalues and eigenvectors. The details can be found in many sources (eg:Brewer, 1975). Fig III.2 shows the familiar Breit-Rabi diagram for the muonium energy eigenvalues in units of h for L=0 as a function of the dimensionless quantity $x=B/B_o$ where

$$B_o = \hbar\omega_o/[\, g_e\mu_e - g_{\mu}\mu_{\mu}] = 1585 \text{ G}$$

is the effective magnetic field experienced by the muon due to the electron.

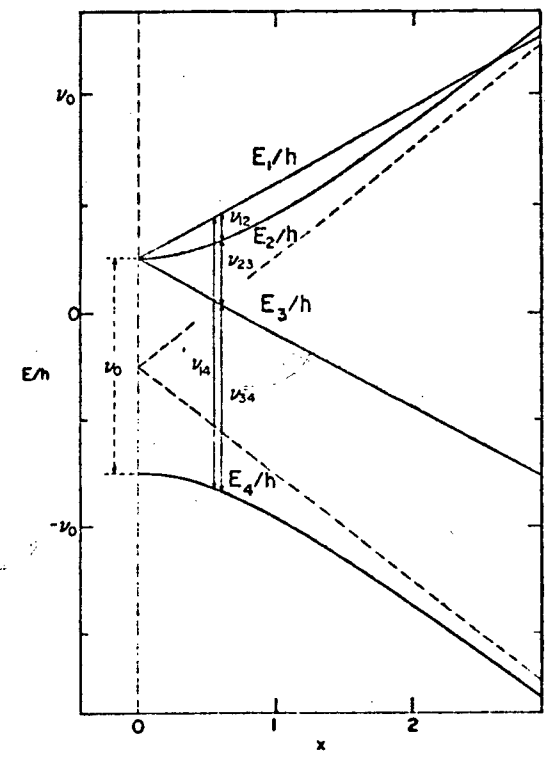

Fig III.2 . Muonium energy eigenvalues as functions of x=B/1585G.The ν_{ij} are the allowed transition energies in units of h. $\nu_{ij} = \omega_{ij}/2\pi$

If the external field is applied along the z direction, transverse to the initial muon polarization vector then the initial muonium state can be written

$$|\psi(0)\rangle = \frac{1}{\sqrt{2}}\left(\left|\sigma_x^{\mu}=\frac{1}{2}\ ,\sigma_x^{e}=\frac{1}{2}\right\rangle + \left|\sigma_x^{\mu}=\frac{1}{2}\ ,\ \sigma_x^{e}=-\frac{1}{2}\right\rangle\right)$$

where it is assumed that half the Mu forms with the muon and electron spins aligned and half with them anti-aligned. The x component of the muon polarization vector as a function of time is defined as

$$P_x(t) = \langle\psi(0)\left|e^{\frac{iH^{Mu}t}{\hbar}}\ \sigma_x^{\mu}\ e^{\frac{-iH^{Mu}t}{\hbar}}\right|\psi(0)\rangle$$

If $B \ll B_0$ this may be approximated

$$P_x(t) \sim \frac{1}{2}\cos\omega_- t[\cos\Omega t + \cos(\omega_0+\Omega)t] \quad \text{(e.g.Brewer 1975)}$$

where

$$\omega_- = \frac{1}{2}(\omega_{12}+\omega_{23})$$
$$\Omega = \frac{1}{2}(\omega_{23}-\omega_{12})$$
$$\hbar\omega_{ij} = h\nu_{ij} = E_i - E_j$$

The oscillations corresponding to the angular velocity $\omega_0 + \Omega$ are too fast to resolve experimentally since they correspond to a period of .225 nsec. Thus the observed x component of the polarization vector is

$$P_x^{exp}(t) = \frac{1}{2}\cos\omega_- t\ \cos\Omega t$$

whose maximum value (1/2) is exactly half that of the actual maximum of $P_x(t)$. For intermediate fields $\sim$70 G , $P_x^{exp}(t)$ displays a fast oscillation $\omega_- = \frac{1}{2}(\omega_{12}+\omega_{23})$ enveloped by a

beat frequency $\Omega=\frac{1}{2}(\omega_{23}-\omega_{12})$. In very low fields (B<10G) $\Omega\sim 0$ so that only a single precession frequency is oberservable corresponding to $\omega_-\sim\omega_{12}\sim\omega_{23}\sim 1.4$ MHz per Gauss.

iv Spectral Form

The observable quantity in μ^+SR and MSR is the number of positrons emitted in a direction in the plane of precession as a function of time after the μ^+ stop. For a low transverse field the usual spectral form is

$$\frac{dN}{dt} = N_o e^{-t/\tau_\mu}[1 + Asy_{\mu+}(t)\cos(\omega^\mu t+\phi) + Asy_{Mu}(t) \cos(\hat{\omega}_- t+\theta)] + B$$

where τ_μ is the muon lifetime, $Asy_{\mu+}(t)$ is time dependent asymmetry of the free muons, and $Asy_{Mu}(t)$ is the time dependent asymmetry of the muonium. In many cases the asymmetry relaxes exponentially so that

$$Asy_{Mu}(t) = Asy_{Mu}(0) \exp[-\lambda^R_{Mu} t]$$

and

$$Asy_{\mu+}(t) = Asy_{\mu+}(0) \exp[-\lambda^R_{\mu+} t]$$

Such is the case for muons or muonium propagating freely through matter where the probability for depolarization per unit distance is a constant. The inital asymmetries depend on the solid angle subtended by the positron detectors, the energy selection of the positron counters, the initial polarization, and the fraction of muons precessing in a free state or muonium state. The B term allows for a flat background.

V Source of Polarized Muons

The source of polarized muons originates from pion decay

$$\pi^+ \rightarrow \mu^+ + \nu_\mu$$

The neutrino state obeys a two component Weyl equation

$$-\bar{\sigma}.\bar{P}\,|\nu_\mu> = |\bar{p}|c\,|\nu_\mu>$$

with an helicity eigenvalue -1. Conservation of angular momentum and linear momentum require that the μ^+ is also an helicity eigenstate in the rest frame of the pion. The first stopping muon channels were designed to collect backward decaying muons from pions in flight. These types of channels are characterized by a relatively high energy of $\sim$50 MeV and a polarization < .8 .

The pions usually originate from energetic protons incident on a production target. Recently it was discovered (Pifer, 1976) that there exists a sizeable flux of μ^+s resulting from pions stopping on or near the surface of the production target. The resulting "surface muons" are monenergetic at 4.2 MeV and momentum 29 MeV/c and are almost completely polarized because the pions are at rest in the lab.

Sect. III.4 Mu Formation

i Gases

50 MeV positively charged muons lose energy in gases primarily through ionization collisions, losing $\sim$ 30 eV per ion formed (Segrè, 1964b). When the muons reach an energy of several KeV their velocity is comparable with the velocity of the valence electrons in the gas molecules so that they begin to capture and lose electrons in rapid succession. The final charge state of the muon system as it approaches thermal energies is primarily a function of the cross sections for electron capture by a muon, σ_{10}†, and electron loss by a muonium atom, σ_{01} . The cross sections σ_{1-1} and σ_{0-1} in noble gases are a few orders of magnitude smaller than σ_{-10} so that the simplification is valid in noble gases.

As yet no measurements on the $\mu^+e^-e^-$ system, bound by .75eV, have been performed although it surely must exist. Production of Mu^- ions in a non-depolarizing environment must be considered an extremely difficult task.

Very little information exists on the charge exchanging cross sections for muons, but a large amount of data exists for proton charge changing cross sections in the energy range 2 KeV-1 MeV. These cross sections are thought to be velocity dependent, not mass dependent, so that much can be inferred about the muon charge state in gases at near thermal energies by considering the corresponding situation

† The i j in σ_{ij} refer to the initial and final charge states.

for protons.

Figs III.3 (a), (b), (c), (d) and (e) show σ_{10} and σ_{01} for protons in H_2 , He, Ar, Ne, Kr, and Ar. The behaviour of σ_{10} for He and Ne is noticeably different in that it drops off rapidly below 10 KeV. For He $\sigma_{10}/\sigma_{01} \sim .15$ at 2 KeV implying that the neutral fraction is decreasing, whereas for Xe $\sigma_{10}/\sigma_{01} \sim 30$, suggesting that the protons are quickly neutralizing.

Table I gives the muonium fractions, the ionization energies, and the expected muon charge exchange cross sections at 220 eV on the basis of the proton data for several noble gases.

The high probability for formation in Xe is easily understood after considering the expected ratio between the capture cross section and the stripping cross section at muon energies of 220 eV as suggested by the proton data. Moreover, there is no threshold energy for Mu formation in Xe because the ionization energy (12.127 eV) is exceeded by the Mu binding energy (13.6 eV).

The proton data for Ar suggests that the muons are also quikly neutralizing at near thermal energies as in the case for Xe. However, in Ar σ_{10} must go to zero below 2.15 eV where Mu fomation is energetically forbidden. The free muon fraction in Argon may result in part from Mu in the energy gap (E_{ion}, 13.6 eV) being stripped of its electron. The competing processes for energy loss in this gap are Mu excitation Ar excitation and elastic

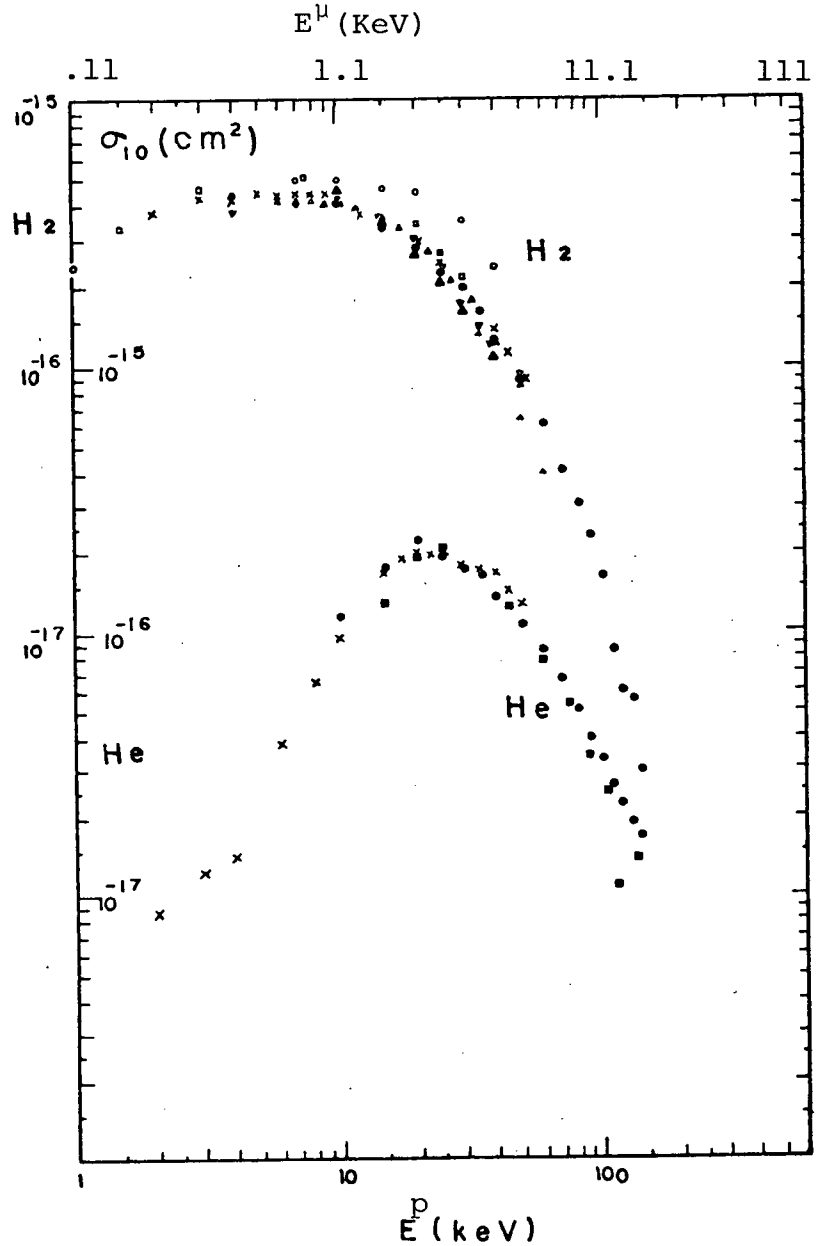

Fig III.3(a) . The electron capture cross section for protons in hydrogen and helium.(Tawara,1973)

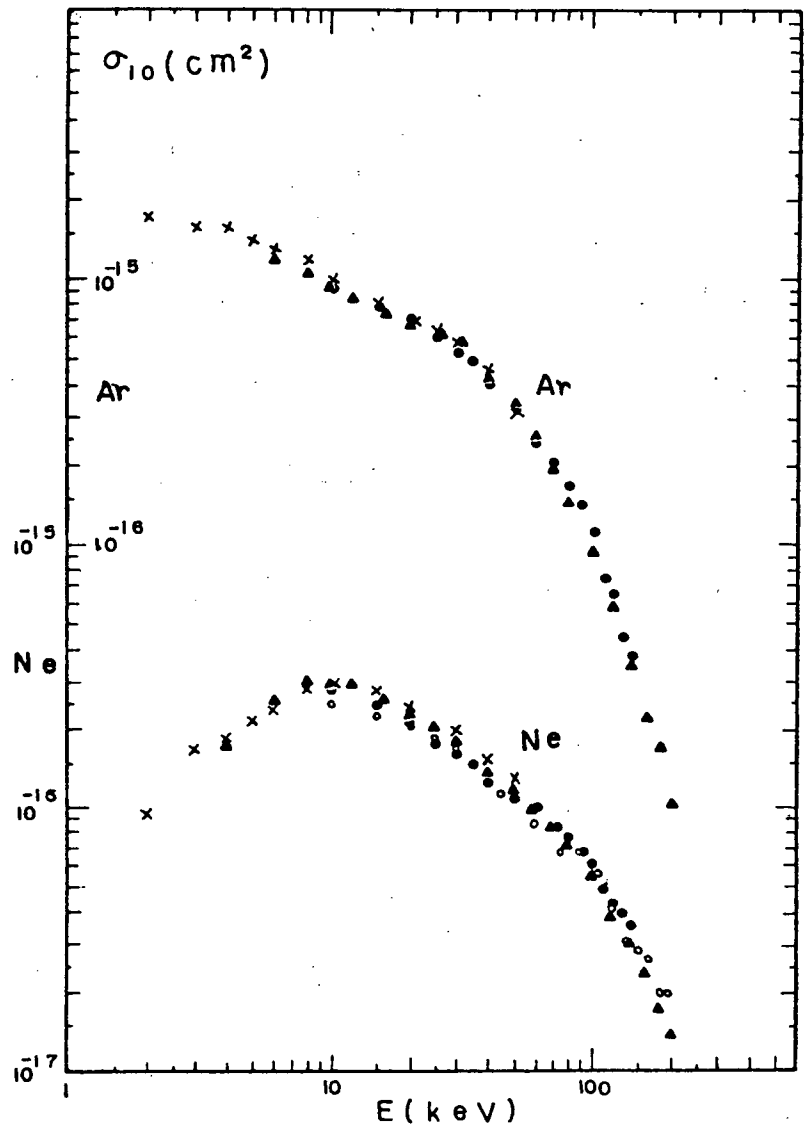

Fig III.3(b) . The electron capture cross section for protons in argon and neon. (Tawara,1973)

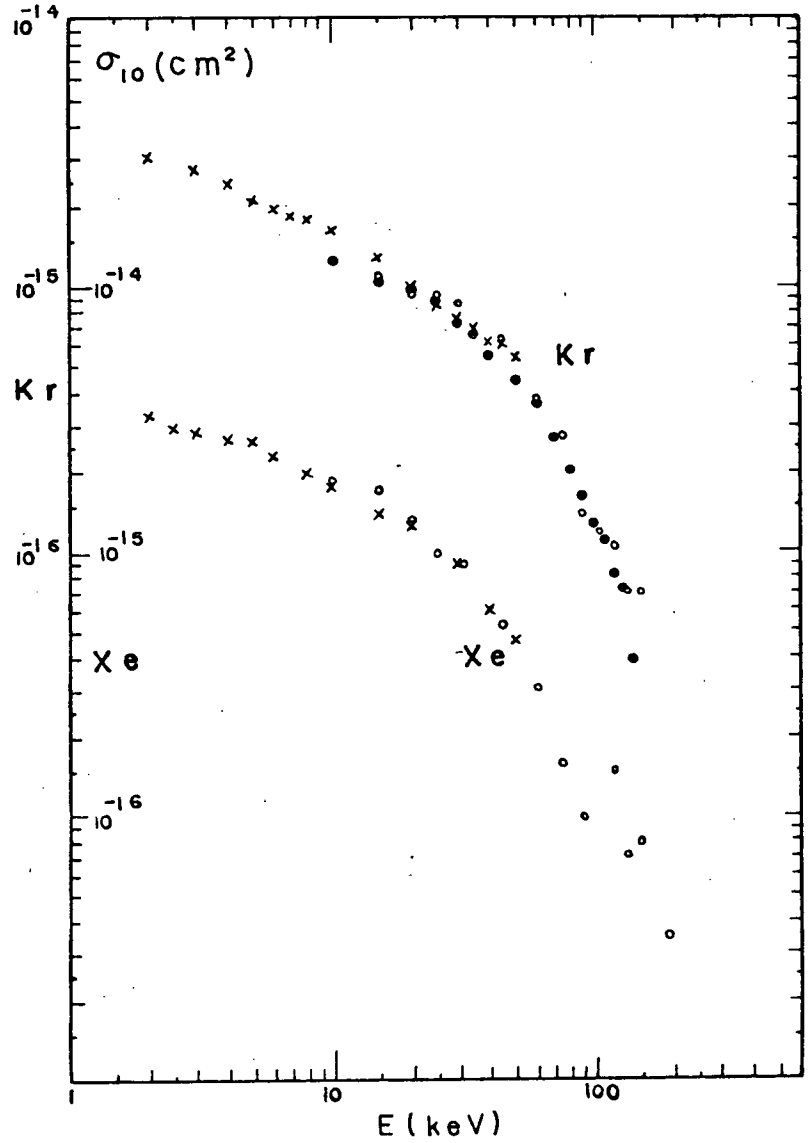

Fig III.3(c) . The electron capture cross section for protons in krypton and xenon. (Tawara, 1973)

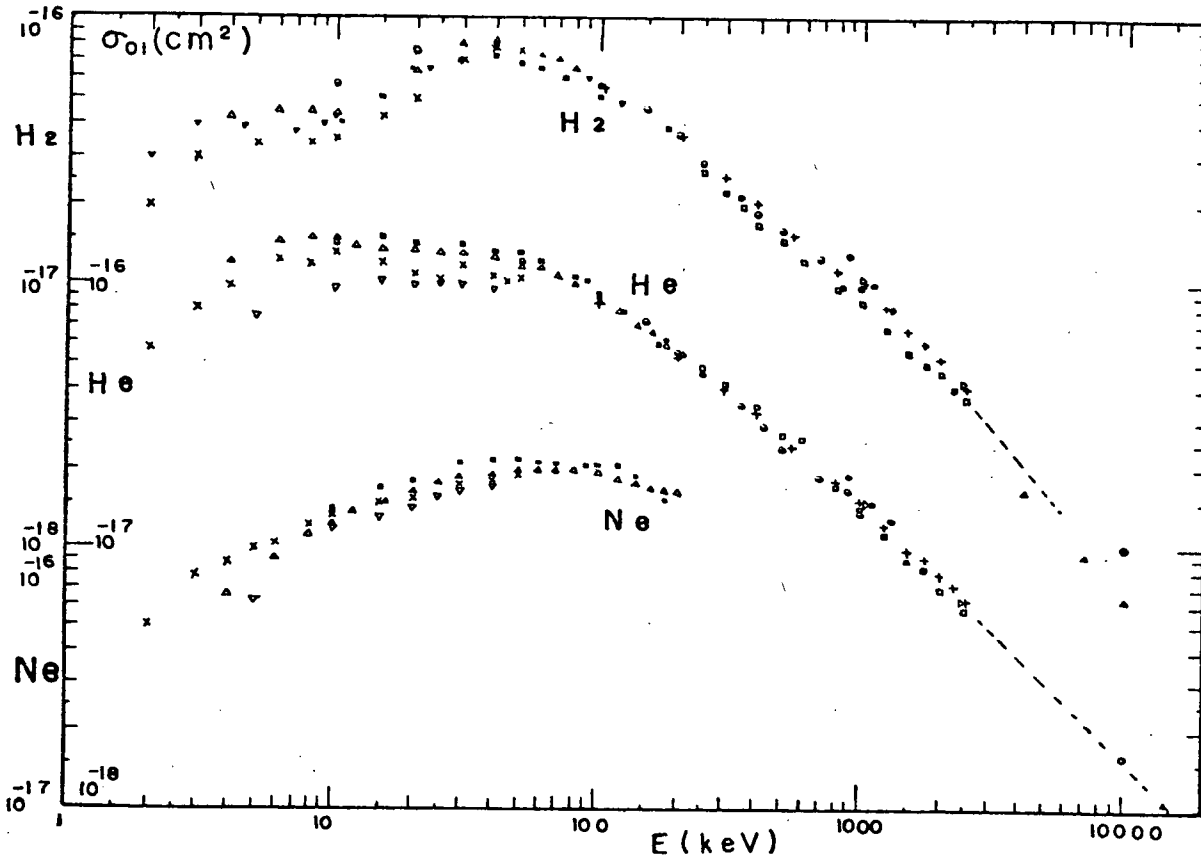

Fig III.3(d) . The electron loss cross section for hydrogen atoms in hydrogen , helium , and neon. (Tawara, 1973)

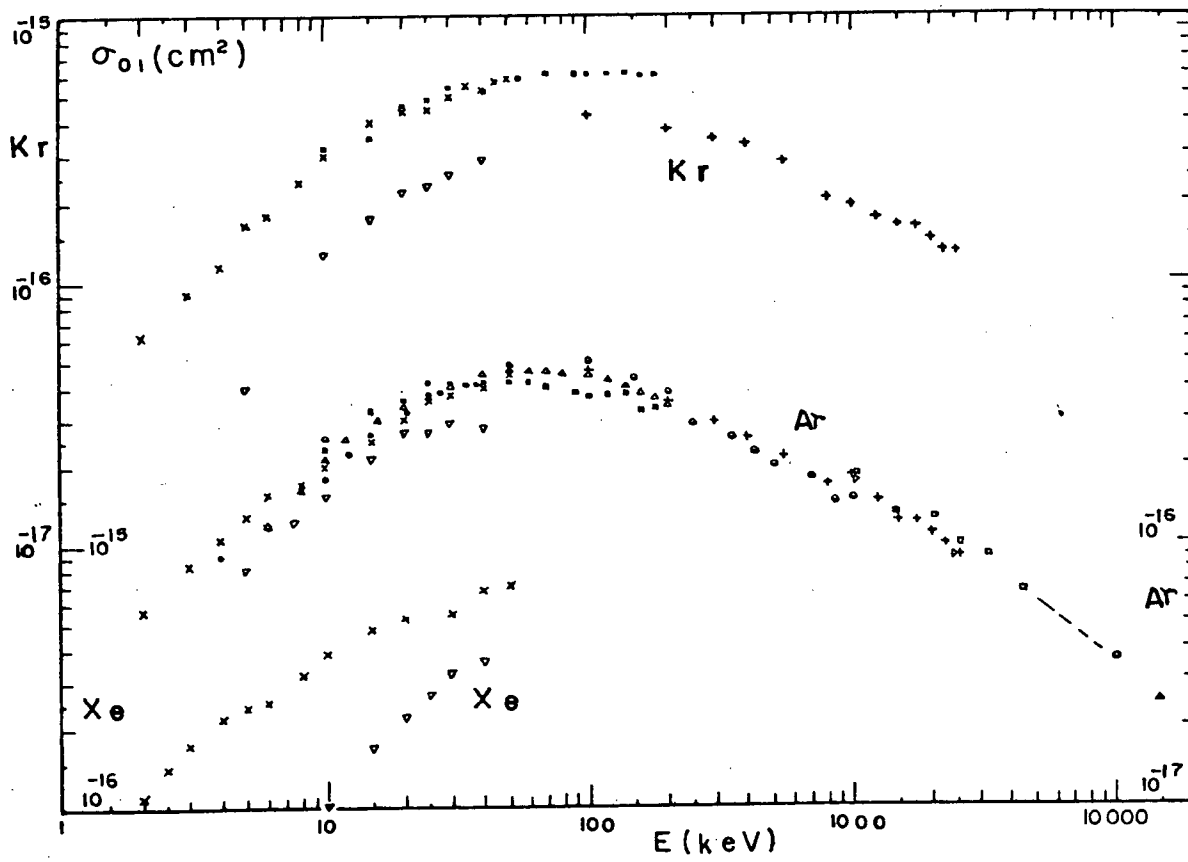

Fig III.3(e) . The electron loss cross section for hydrogen atoms in krypton , argon , and xenon.(Tawara,1973)

TABLE I. Mu Fraction in Noble Gases. (Stambaugh, 1974)

Gas	Pressure	Mu Fraction	Ionization Energy	Electron capt. cross section for 220 eV muons	Electron loss cross section for 220 eV muonium		
	atm	%	eV	cm^2	cm^2		
He	50	1±5	24.48	9×10^{-18}	5×10^{-17}		
Ne	26	0±2	21.56	9×10^{-17}	4×10^{-18}		
Ar	30	65±5	15.75	1.7×10^{-15}	5×10^{-17}		
Xe	44	100±(not given)	12.13	3×10^{-15}	10^{-16}		

scattering. If stripping occurs the resulting muon can have as much as 13.6 eV of kinetic energy less than that of the incident Mu atom and thus may get trapped below the threshold for Mu formation.

The proton data for He and Ne indicate that muons approach thermal energies as free muons so that the absence of Mu precession in these gases is consistent with the proton data. The ionization energies for He and Ne are much larger than for Xe or Ar. It appears that the capture and loss cross sections are strongly correlated with either the ionization energy or possibly the Coutere electron velocity distribution. Theoretical attempts to explain the behaviour of σ_{10} and σ_{01} for protons, even in noble gases, are inadequate at present.

ii Insulators and Semi-Conductors

The formation process of Mu in matter is a complex many body problem. Measurements of the Mu fraction in noble gases have been made but no theory has emerged that successfully explains the results. In solids, even less experimental information is available. It should be stressed that the Mu states may be strongly perturbed in solids and should be treated as Mu-(many electron states), denoted |Mu (n-1)e⁻> .

In insulators it is believed that Mu exists in the large interstitial sites and behaves similarly to free Mu. Mu precession has been observed in quartz, ice and solid CO_2.

Mu-like states have also been observed in semi-conductors such as Ge and Si. The observed precession frequency is approximately half that of free Mu (Brewer, 1975). It is believed that Mu exists in the interstitial sites and is highly perturbed. The reduced precession frequency indicates that the binding energy is reduced by several electron volts.

In insulators and semi-conductors both free muon and Mu states exist simultaneously. This suggests one of two things (Brewer,1975).

1 Thermal formation of Mu does not occur.

2 A fraction of the Mu reacts epithermally and

exists in a diamagnetic environment producing what appears to be free muon precession.

The absence of thermal Mu formation is difficult to understand in the case of insulators where the binding energy of the Mu atom is 13.6 eV. It is difficult to comprehend how the $|Mu\ (n-1)e^-\rangle$ state could have an energy greater than that of the $|\mu^+\ ne^-\rangle$ state. However, a $|\mu^+\ ne^-\rangle$ state may be meta-stable to a transition into a lower energy state, $|Mu\ (n-1)e^-\rangle$, if the thermal muon is trapped in a diamagnetic state.

CHAPTER IV MEASUREMENTS OF FREE o-Ps PRODUCTION EFFICIENCIES IN OXIDE POWDERS AND AN ACCURATE DETERMINATION OF THE O_2 QUENCHING RATE COEFFICIENT FOR o-Ps

Sect IV.1 Introduction

The purpose of this experiment was:

1. To determine the fraction of injected positrons forming o-Ps and reaching the intergranular regions for various oxide powders.

2. To test the feasability of using fine oxide powders as high yield sources of free o-Ps to study the interactions of o-Ps with gas molecules.

The presence of free o-Ps in a sample is relatively easy to establish because of its characteristic 140 nsec lifetime and continuous 3 γ annihilation energy spectrum. However, measuring the fraction of positrons in a free o-Ps state is more difficult. The 140 nsec component in the lifetime spectrum is difficult to normalize to the prompt components because they result from 2 γ decays which yield monoenergetic gamma rays. Similarly, normalizing 3γ coincidence rates to 2γ coincidence rates is difficult because it involves knowing the detector efficiency as a

function of energy and the effective solid angle subtended by the detectors. This technique also suffers from low counting rates (typically 3 or 4 counts/1000 sec.), even with a 200 μCi source (Celitans, 1964).

More subtle techniques for measuring the o-Ps fraction involve quenching the o-Ps by a known amount using magnetic or chemical means. The application of a large (20 KG) magnetic field mixes the o-Ps (m=0) substate with p-Ps and causes 1/3 of the o-Ps to decay into 2γ s. Chemical quenching is the introduction of some o-Ps reactant which either induces an o-Ps→p-Ps conversion through a spin flip mechanism or results in an o-PsX compound which is followed by pickoff annihilation within a few nanoseconds.

In this experiment samples of SiO_2 (35 Å radius), SiO_2 (70 Å radius), Al_2O_3 (150 Å radius), ZnO (560 Å radius) and MgO (fine) (see Appendix IV) were investigated. Using the technique described in Sect IV.2 the o-Ps fractions were determined for each powder. The largest producer was found to be the 35Å radius SiO_2 powder where approximately 25% of the injected positrons emerged from the powder grains as o-Ps. This powder was then used to measure the mean decay rate of o-Ps as a function of O_2 pressure. The relationship was found to be linear, giving a quenching rate coefficient of 35.5±1.0 μsec^{-1}/atmos. The reaction mechanism was determined to be spin changing in nature by using a high resolution GeLi detector to monitor the pair momentum distribution.

Sect. IV.2 Technique For Measuring Free o-Ps Fraction

The production efficiency of o-Ps in the intergranular region of a powder sample can be determined by measuring the 2 γ counting rate and the o-Ps mean decay rate(=1/lifetime) in the powder under vacuum and again with a gas quencher in the intergranular region. In the special case where the gas quencher eliminates all 3 γ decays and the powder surfaces produce no quenching affect, the free o-Ps fraction may be written

$$f_{o\text{-}Ps} = \frac{\frac{dN}{dt}_Q - \frac{dN}{dt}_v}{\frac{dN}{dt}_Q} = \{1 + \frac{\frac{dN}{dt}_v}{\frac{dN}{dt}_Q - \frac{dN}{dt}_v}\}^{-1}$$

where dN/dt_v and dN/dt_Q are the 2 γ counting rates in the evacuated powder sample and in the powder sample plus gas quencher respectively.

In a more realistic situation where the powder surfaces have a quenching effect on the o-Ps and the gas quencher does not completely quench the o-Ps , $f_{o\text{-}Ps}$ may be written (see Appendix VI)

$$f_{o\text{-}Ps} = \{1 - \frac{\lambda_v - \lambda_o}{\lambda_v} + \frac{\frac{dN}{dt}_v}{\frac{dN}{dt}_Q - \frac{dN}{dt}_v}\left[\frac{\lambda_Q - \lambda_o}{\lambda_Q} - \frac{\lambda_v - \lambda_o}{\lambda_v}\right]\}^{-1}$$

eqn IV.1

where λ_v , λ_o and λ_Q are the mean decay rates in the evacuated powder sample,in true vacuum and in the presence of the gas quencher respectively.

Eqn IV.2 is based on the assumption that the gas quencher serves only to quench the o-Ps in the intergranular region and does not alter the fraction of o-Ps in the intergranular region. In this experiment O_2 at 1 atmosphere was used because of its effectiveness as a quencher (80%) and its non toxic nature. However, O_2 may indeed alter the fraction of o-Ps reaching the intergranular region in two possible ways.

1. The powder surfaces are known to adsorb gases (Steldt and Varlashkin, 1972). A layer of O_2 on the powder surfaces might alter the transmission properties of o-Ps through the surfaces.

2. Small concentrations of O_2 are known to increase Ps formation in gases. It is conceivable that this could also happen for very fine powders

However, if the quenching is nearly complete as is the case with O_2 at 1 atm then the result from eqn IV.1 is insensitive to the fraction of o-Ps in the intergranular region in the presence of the quencher.

In order to estimate the error due to this effect, one quenching run in the 35 $\mathring{A}$ radius SiO_2 powder was repeated using 750 torr of Cl_2 for which $\lambda_Q-\lambda_o/\lambda_Q \sim 1.00$. The

results were as follows:

$$f_{o\text{-}Ps} = 26.4 \pm .8 \text{ \% using 750 torr of } O_2$$

$$f_{o\text{-}Ps} = 24.8 \pm .3 \text{ \% using 750 torr of } Cl_2$$

This difference was taken into account in the final error estimate on the o-Ps fractions.

Sect. IV.3 Experimental Details

i Target Assemblies

Two 15 μCi Na^{22} sources were prepared in the following manner. Several drops of NaCl solution were deposited on 1.9 μm nickel foil and allowed to dry. A very thin coat of lacquer was applied to hold the NaCl in place

There were basically two types of target assemblies. For the low density SiO_2 powders the source was suspended in the centre of a 17 cm diameter flask filled with SiO_2. It was calculated that 7 cm of SiO_2 (ρ=.035 g/cm^3) was sufficient to stop even the most energetic (544 KeV) positrons from Na^{22} decays. For the high density powders (ρ>.13 g/cm^3) a second Na^{22} source was suspended 2 cm from the bottom of a large 4 cm diameter test tube filled with powder to a height of 5 cm. It is estimated that >95% of the positrons were stopped in the powder for both types of target.

All runs in vacuum were performed after outgassing at less than 10^{-3} torr for a period of six hours. A Wallace and Tiernan precision vacuum guage, accurate to ±2 torr, was used to monitor the O_2 pressure when required.

ii Detectors

Lifetime measurements were made using two 8.9 cm dia x 8.9 cm long NaI crystals mounted on RCA XP1140 photomultiplier tubes. They were arranged at 70° to one another approximately 15 cm from the source (see fig IV.1).

Measurements of the Doppler broadening of the 511 KeV annihilation line and the 2 γ counting rate were made using an lithium drifted germanium (GeLi) detector with an active volume of 104 cc measuring 5.2cm diax5.6cm long and possessing a resolution of 1.32 KeV at 567 KeV. The detector was placed 25 cm from the source.

iii Electronics for Lifetime Measurements

Fig IV.1 contains a schematic diagram of the electronics used in the lifetime measurements. The electronics were set up to measure the decay rate of o-Ps as a function of time after a positron stop. A Na^{22} source was chosen because the emission of a positron is followed in 10^{-11}sec by the emission of a nuclear gamma at 1.28 MeV (see fig II.3). The method of constant fraction discrimination was used to time the fast anode pulses from detectors 1 & 2. The spectrum of time delays was accumulated by using a time to amplitude converter and a pulse height analyzer. Pileup gates on each discriminator were used to reject events that came within 4 μsec of one another.

Single channel pulse height analysis was performed on the slow dynode pulses from detectors 1 & 2 to select decays of o-Ps. Fig IV.2 shows the Na^{22} energy spectrum from one of the NaI detectors showing the single channel analyzer windows for the start and stop. The important feature in fig IV.2 is that the stops required a gamma ray just below 511 KeV. This maximized the ratio

$$\frac{\text{stops from } 3\gamma \text{ annihilation}}{\text{stops from } 2\gamma \text{ annihilation}} = \frac{\text{long lifetime component}}{\text{prompt lifetime component}}$$

This ratio was unity for the 35 $\mathring{A}$ radius SiO_2 in vacuum which implies that half the events in the lifetime spectrum were from o-Ps decays.

The timing resolution was measured to be 4 nsec using a

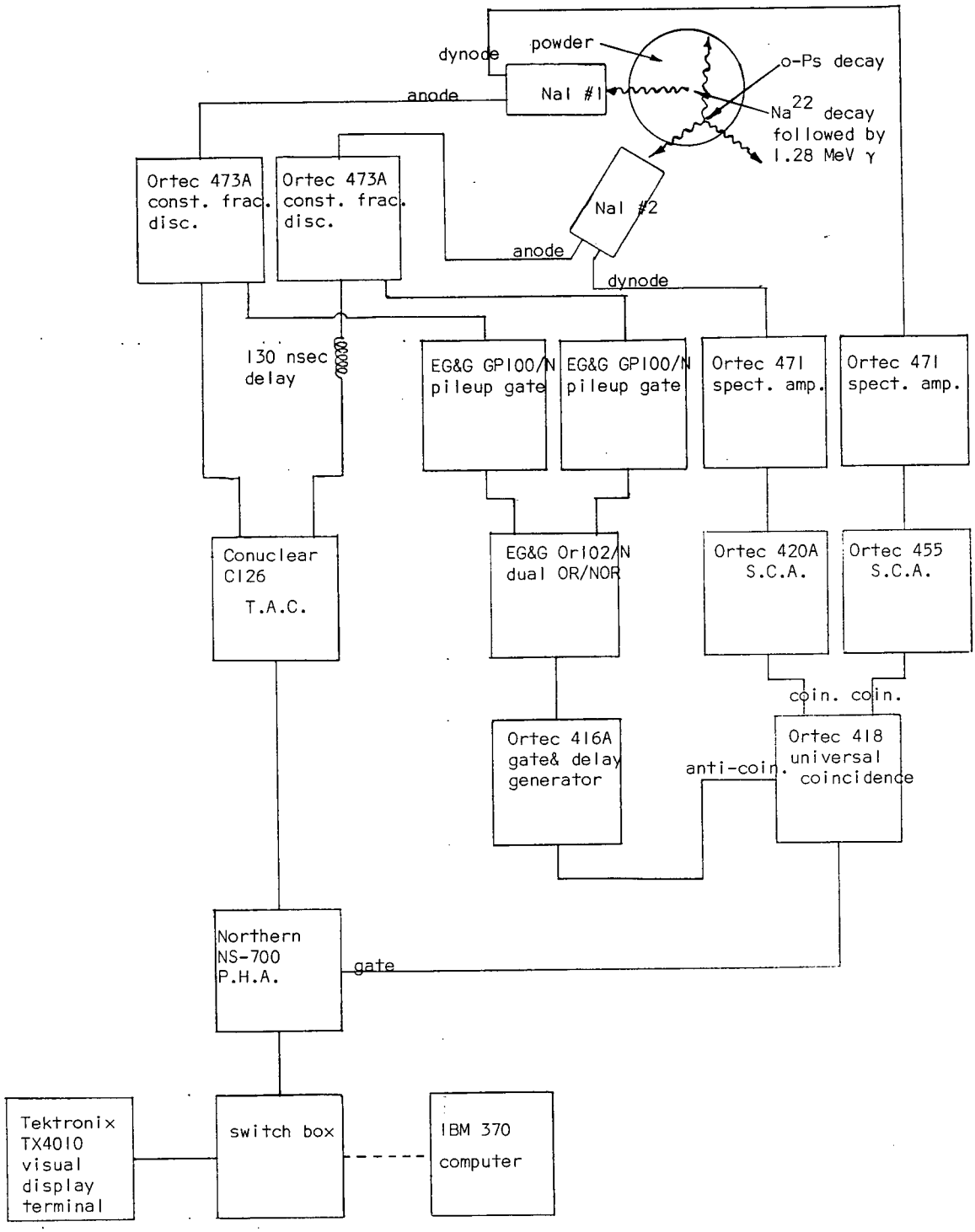

Fig IV.1 . Electronics used to measure o-Ps lifetime in powders.

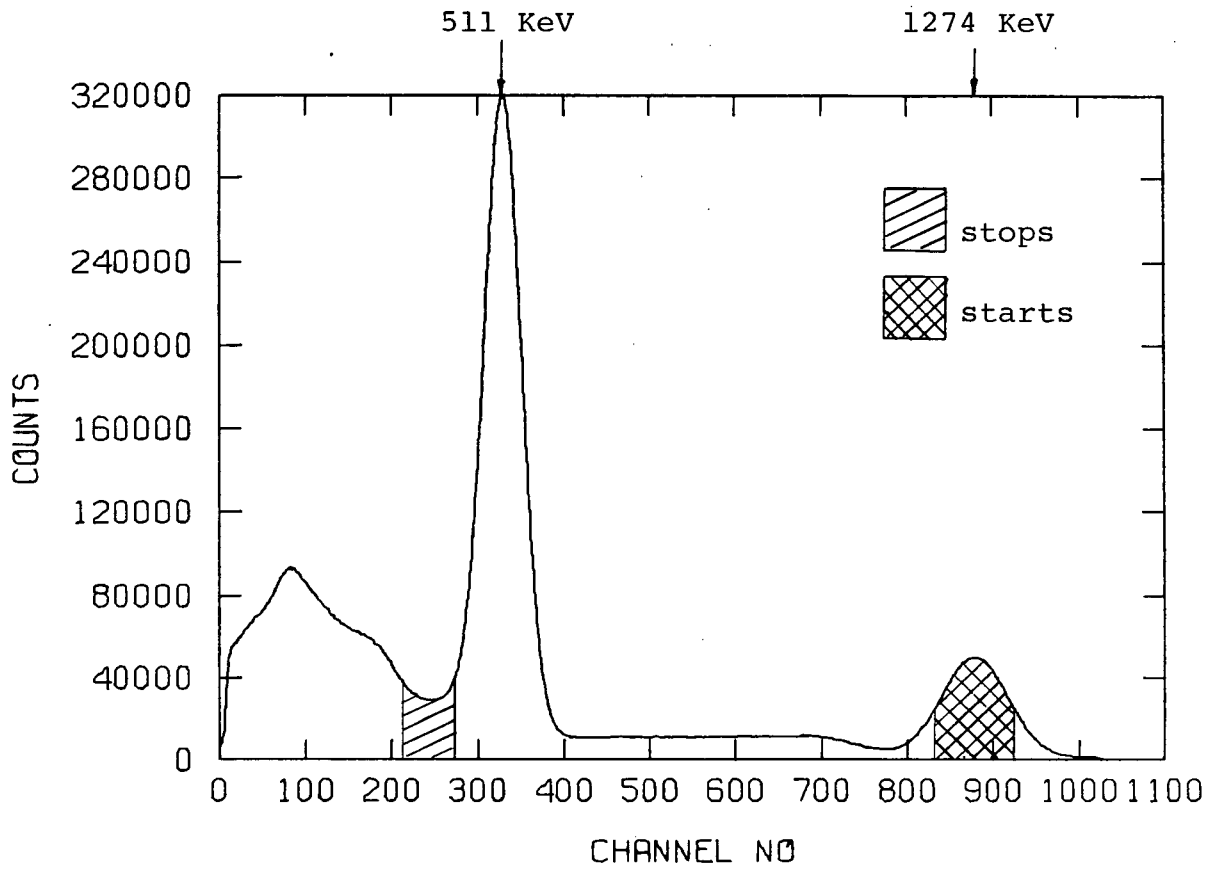

Fig IV.2. Na^{22} spectrum from one of the NaI detectors, showing the single channel analyzer window settings for the starts and stops in the lifetime determinations. 1 channel= 1.46 KeV

Co^{60} source which emits two, virtually simultaneous, gamma rays.

An ORTEC time calibrator was used to calibrate the TAC output and to check the differential linearity of the system. No non-linearity was observed using 20 nsec intervals over a range of 600 nsec. The average time per channel was .942 nsec.

The pulse height analyzer was operated in the 1024 channel mode. The stop was delayed so that time zero occurred in channel 130. This was done so that negative time could be used to evaluate the random coincidence rate (see Sect IV.3.x).

iv Electronics For Measuring The 2 γ Annihilation Rate and The Doppler Broadening of the 511 KeV Line

Fig IV.3 shows the electronics for the energy spectrum analysis used in the determination of the 2 γ counting rate. The time constant on the amplifier was set at 3 μsec. The pulse height analyzer was operated in the 1024 channel mode. The energy per channel was 580 eV.

The electronics for the Doppler broadening measurements were virtually the same as that for the 2 γ counting rate measurements. A biased amplifier was inserted as indicated in fig IV.3. Additional gain, heavy biasing and 2048 channels on the PHA were used to lower the energy per channel to 73.3 eV. This was necessary for an accurate determination of Doppler broadening of the annihilation line at 511 KeV.

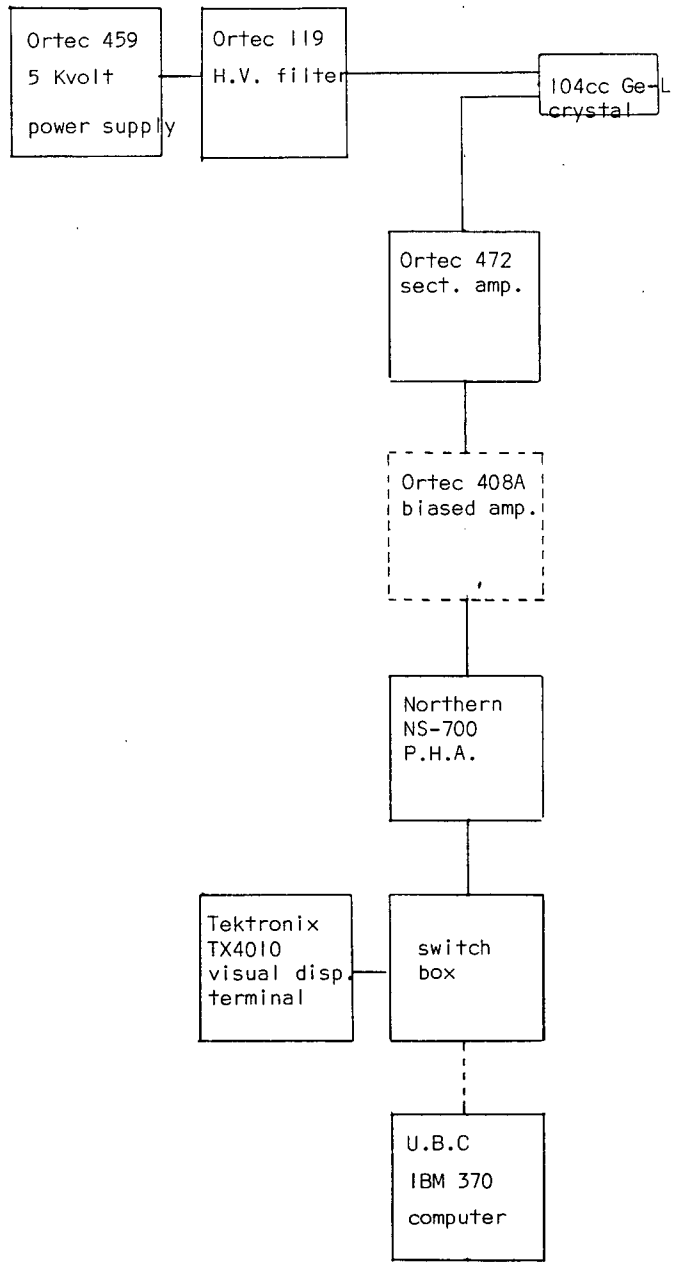

Fig IV.3 .Electronics used to measure total 2γ annihilation rates and Doppler broadening of the 511 KeV line. The biased amplifier was only used in the Doppler broadening measurements.

v Computer Link

A novel technique (Clarke, 1978) was used to transfer the data from the pulse height analyzer directly into the IBM 370 computer where the data analysis and plotting were performed. A switch box (see figs IV.1 and IV.3) between the computer terminal and the pulse height analyzer made such a transfer possible. A slight modification to the PHA was necessary to synchronise the transfer of data to the computer.

vi Procedure for o-Ps Production Measurements

Each sample was evacuated to a pressure of 10^{-3} torr for a period of three hours prior to running. Four runs were required to evaluate the o-Ps production efficiency in the intergranular regions as described in Sect IV.2. First a lifetime spectrum was accumulated for approximately 2×10^4 sec (333 min.) collecting 5×10^5 events. The count rates in the NaI counters were typically 2×10^4/sec. Then an energy spectrum using the GeLi detector was accumulated for 5×10^3 sec. 750 torr of O_2 (see Appendix V) was bled into the target chamber. Then another lifetime spectrum and energy spectrum were accumulated in the manner described above. Care was taken not to disturb the position of the GeLi detector in relation to source because the nuclear gamma ray from Na^{22} was used to normalize the energy spectrum in vacuum to that in 750 torr of O_2 (see Sect. IV.3.ix).

In the case of SiO_2 (35 Å) two additional spectra were taken using Cl_2 as a quencher.

vii Procedure for the O_2 Quenching Rate Coefficient Determination

35 Å radius SiO_2 moderator was used to determine the the dependence of the o-Ps mean decay rate on O_2 pressure. The system was pumped down to 10^{-3} torr, after which 750 torr of O_2 was bled in. Lifetime runs of duration 2 x 10^4 sec, collecting $5x10^6$ events, were taken at oxygen pressures of 750, 600, 450, 300, 200, 100, 50 and 10^{-3} torr.

viii Procedure for Doppler Broadening Measurements

Doppler broadening measurements were performed on the 35 Å SiO_2 powder sample at 10^{-3} torr, at 750 torr of O_2, and at 750 torr of Cl_2. These runs were 5×10^3 sec in duration collecting roughly 5×10^6 events in the annihilation photopeak. A Bi^{207} source with a nuclear gamma ray at 567 KeV was placed nearby in order to monitor the system resolution.

ix Analysis of the Annihilation Spectra

The purpose of this part of the analysis was to evaluate the 2γ counting rate in vacuum and in 750 torr of O_2 to within a constant of proportionality. This constant of proportionality cancels out in calulating $f_{o\text{-}Ps}$ which contains only the ratio of counting rates (see eqn IV.1).

This task was acccmplished for each annihilation spectrum by evaluating the total number of counts in the 511 KeV photopeak (see fig IV.4) and dividing by the number of Compton events from the 1.274 MeV nuclear gamma ray in the flat region above 511 KeV. This choice of energy range (see fig IV.5) desensitises the normalization to small changes in gain (Sen and Patro, 1972).

The 2γ counting rates can then be written

$$\frac{dN}{dt} = \frac{k(P-B1-B2)}{N}$$

where $k=N/t$ and t is the counting time.

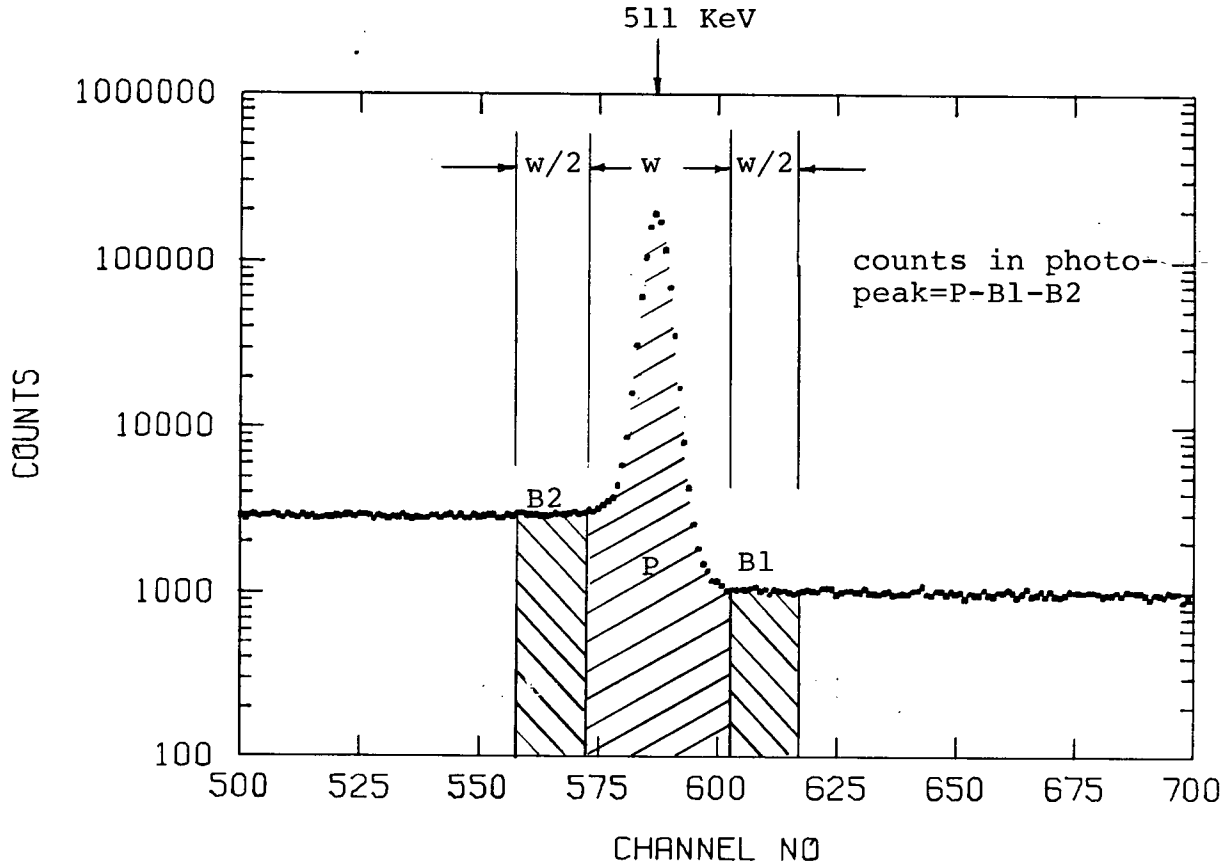

Fig IV.4. Annihilation spectrum from the Ge-Li detector, expanded about 511 KeV. 1 channel = 580 eV

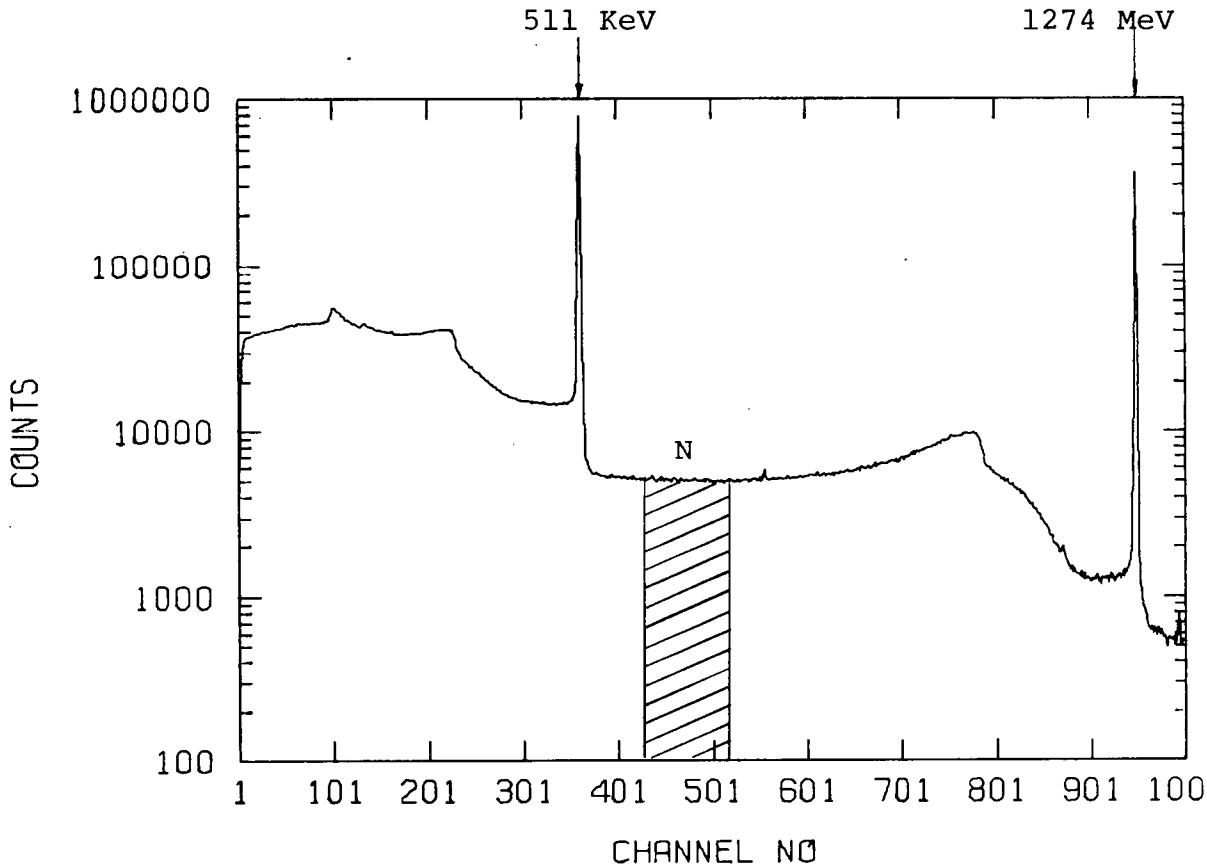

Fig IV.5. The Na^{22} spectrum in SiO_2(35 Å) at 10^{-3} torr. The annihilation spectra in vacuum and O_2 were normalized over the range indicated. The gain has been lowered to show the nuclear γ at 1274 KeV, which was off scale for the actual runs.

x Analysis of the Lifetime Spectra

The lifetime spectra were fitted to the function

$$\frac{dN}{dt} = \begin{cases} N e^{-\lambda t} + B & t>0 \\ B & t<0 \end{cases}$$

over the two regions indicated in fig IV.6. The starting time for region 2 was always 48 nsec. The finishing time was extended to where the count rate was twice the background or to 95 nsec whichever was largest. A maximum likelihood program (Albrecht, 1978) assuming Poisson statistics was used to determine the best fit. The χ^2 was calculated by binning the data appropriately so that Gaussian statistics could be applied. Although reasonable χ^2 s were obtained in all cases, the decay rates did show some dependence on the fitting region. For the long lifetimes this dependence was less than 1% whereas decay rates in the highly quenched runs varied as much as 5% after shifting region 2 inwards by 15 nsec. This deviation from a single exponential behaviour is not well understood. A systematic error of 5% was attached to all decay rates obtained from these highly quenched runs.

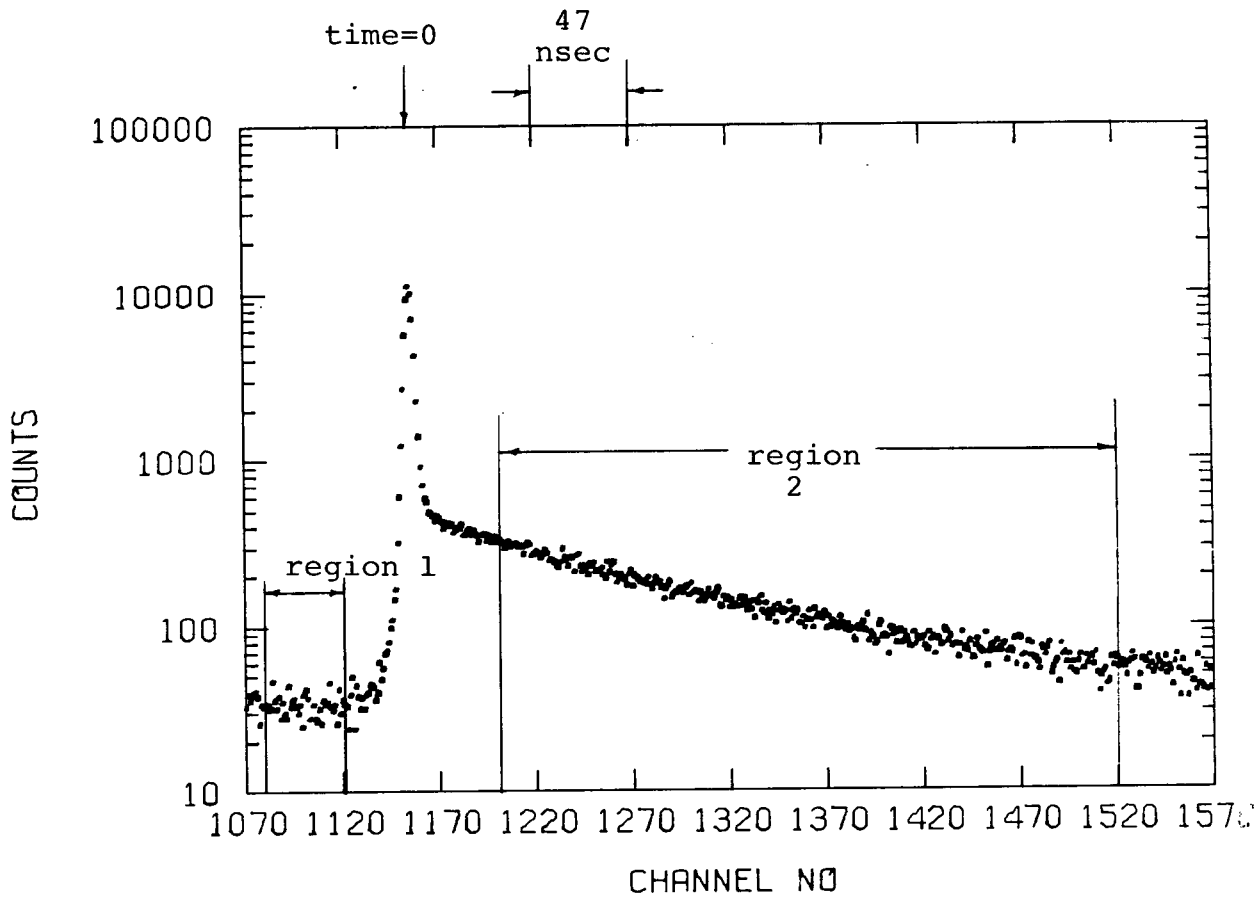

Fig IV.6. Decay rate versus time after the positron emission, in Al_2O_3 (150Å), showing the fitting regions. 1 channel = .942 nsec.

Sect. IV.4 Results and Discussion

i o-Ps Production Measurements

Columns 2, 3 & 4 of table I give some physical properties of the powders listed in column 1. Columns 5 & 6 give the mean decay rates in vacuum and at 750 torr of O_2, respectively. The errors quoted for the O_2 mean decay rates originate primarily from the estimated 5% systematic error associated with the dependence of the answer on the fitting region (see Sect IV.3.x). Column 7 contains the fraction of positrons reaching the intergranular regions in the form o-Ps as calculated from equation IV.1. Column 8 contains calculations of the ratio $\bar{\sigma}_{qp}/\pi R^2$ where $\bar{\sigma}_{qp}$ is the mean quenching cross section at room temperature of the powder grains (see Appendix III(a)) and πR^2 is the physical cross section of the grains. These quenching cross sections are consistent with calculations assuming that the o-Ps is moving freely between the grains but decays at a pickoff annihilation rate while it is within a few $\mathring{A}$ of a powder grain.

It is clear from column 8 that the quenching probability during a collision is of order 10^{-5} - 10^{-6}. It is interesting to compare this with the corresponding probability in gases. In Cl_2, I_2, Br_2 and NO_2 gases, the quenching cross sections are of the order 10^{-16} - 10^{-15} cm^2 and are due to chemical reactions (Tao, 1974). For these gases the quenching probability in a collision is of the

TABLE II. Results of the Positronium Experiment

Sample	Intrinsic Powder Density ρ^I g/cm^3	Bulk Density ρ^B g/cm^3	Mean Radius R 10^{-8}cm	Mean Decay Rate in Vac. λ_v μsec^{-1}	Mean Decay Rate in O_2 λ_q μsec^{-1}	Intergranular o-Ps Fraction $f_{o\text{-}Ps}$ %	Quench Cross Section(powd.) / Physical Cross Section $\bar{\sigma}_{qp}/\pi R^2$
SiO_2	.035	2.2	35	7.22±.08	40.1±2.0	26.4±2.6	.8 ±.3x10^{-6}
SiO_2	.035	2.2	70	7.23±.12	40.0±2.0	21.5±2.0	1.6±.8x10^{-6}
Al_2O_3	.56	3.7	150	8.39±.14	37.5±1.9	24.6±2.4	2.9±.4x10^{-6}
ZnO	.65	5.6	560	7.30±.09	44.5±2.1	19.2±1.9	2.6±1.x10^{-6}
MgO	.13	3.6		7.43±.09	39.0±2.0	14.3±1.4	

order unity since the physical cross sections are typically 7×10^{-16} cm^2. Where spin exchange is the dominant process, such as in O_2 or NO, this quenching probability decreases to 10^{-2} or 10^{-3} (Tao, 1972). For argon and the other inert gases the probability for quenching drops to 10^{-4} or 10^{-5} (Celitans, 1964b). It appears there is no large surface interaction for any of the powders. The noticeably larger decay rate for Al_2O_3 is primarily a density and particle size effect.

ii Quenching Rate Coefficient for O_2

Fig IV.7 shows explicitly the quenching effect of O_2 at 1 atmosphere on o-Ps using the 35 Å SiO_2 powder as a moderator. Fig IV.8 shows graphically the dependence of the o-Ps decay rate on O_2 pressure . A reasonable fit was obtained by assuming a linear relationship. The best fit gives a quenching rate coefficient of 35.6±.8 $\mu sec^{-1} atm^{-1}$, which at 22°C corresponds to $\sigma_q v = 1.43 \pm .03 \times 10^{-12}$ cm^3 sec^{-1} where σ_q is the quenching cross section and v is the o-Ps velocity. Using an argon moderator with O_2 partial pressures greater than 1 atmos Tao (1964) measured the oxygen quenching rate coefficient, $\sigma_q v$, to be $.94 \pm .12 \times 10^{-12}$ cm^3 sec^{-1}. More recently the quenching rate coefficient was measured using porous silica gel with a large surface area (800 m^2/g) as a moderator (Chuang and Tao, 1974b). They reported a long lived component in the lifetime spectrum ,attributed to o-Ps within the pores, possessing a mean decay rate of 31.3 μsec^{-1}. By adsorbing different amounts of O_2 onto the gel they calculated a quenching rate coefficient $\sigma_q v = 1.75 \times 10^{-12}$ $cm^3 sec^{-1}$.[1] The O_2 adsorbed samples showed an increased low momentum component in the angular correlation data which establishes that the quenching process is spin flip in nature.

---

[1] no error given

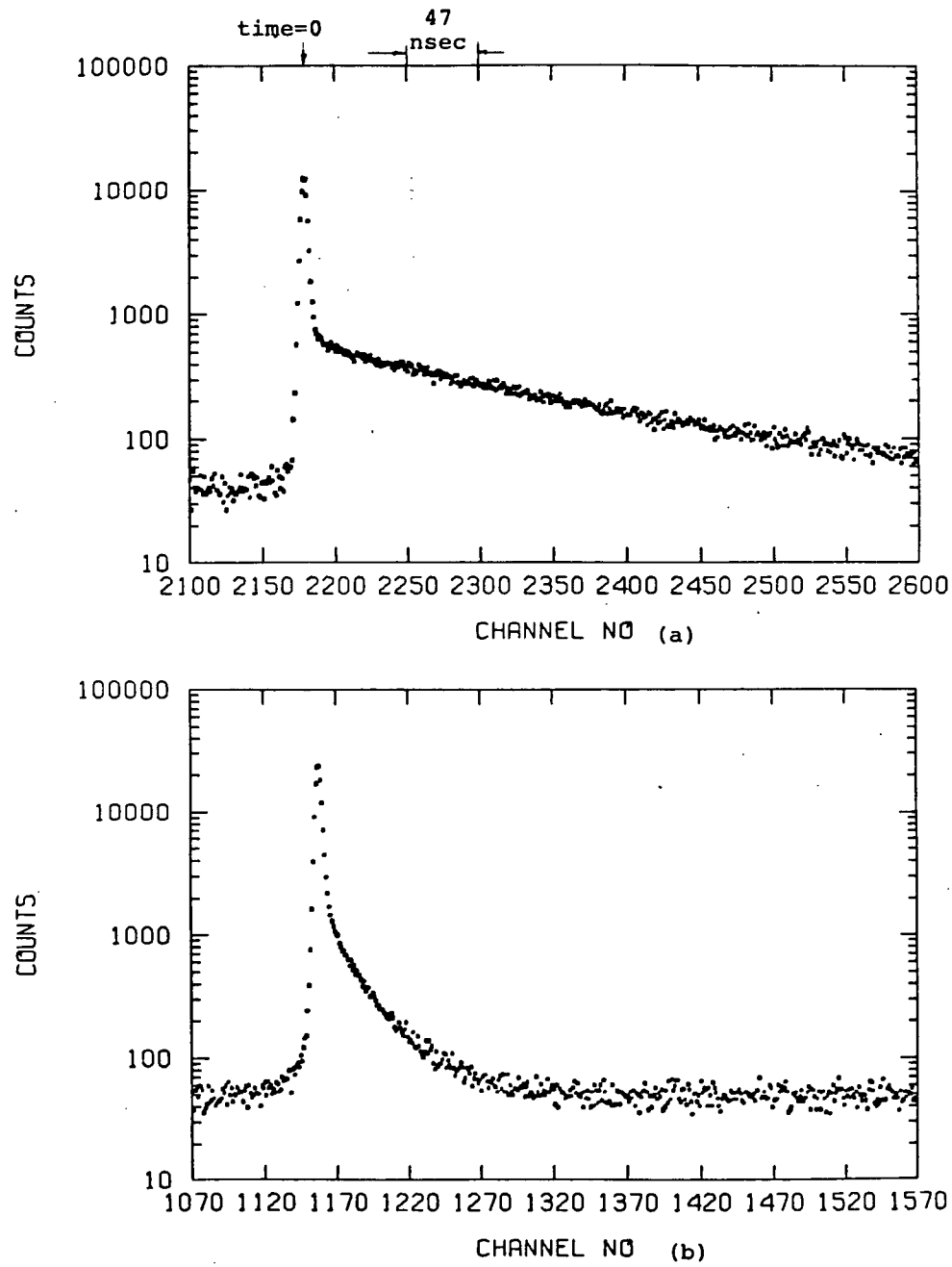

Fig IV.7(a) .Lifetime spectrum in 35Å radius SiO_2 powder at 10^{-3} torr. (b) Same at 750 torr O_2 . 1 channel=.942 nsec.

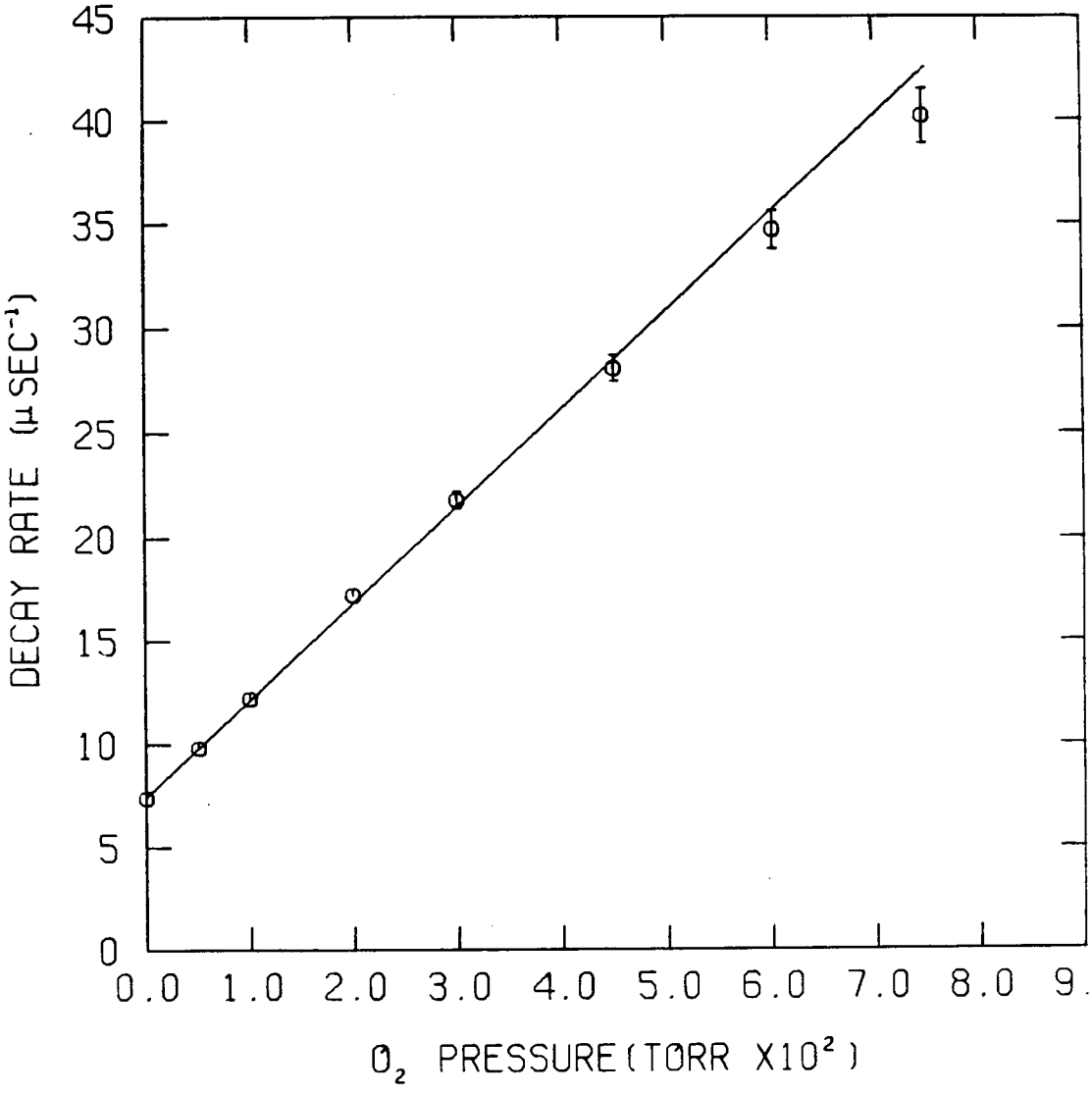

Fig lV.8. The o-Ps mean decay rate versus the O_2 pressure. The best fit gives a reaction rate coefficient of $\sigma_q \bar{v} = 1.43 \pm .04 \times 10^{-12}$ cm^3 sec^{-1}.

The fact that all three moderators give approximately the same answer indicates that no large systematic errors are introduced by the moderators.

iii Doppler Broadening Measurements in SiO_2 (35 Å) in Vacuum, O_2 and Cl_2

In this part of the experiment a GeLi detector with a resolution of 1.32 KeV at 567 KeV (see fig IV.9) was used to determine the o-Ps quenching mechanism in O_2 and Cl_2.

Fig IV.10 shows the line shape in 35 Å SiO_2 with and without O_2 present. The counting time was adjusted so that the peak heights were the same. The line shape corresponds to the distribution of the parallel component of the pair momentum (see Sect II.3.iv). The enhancement of a narrow component which is characteristic of thermalized p-Ps is clearly visible when O_2 is added. This indicates that the quenching process is spin exchange in nature.

The lifetime spectrum in SiO_2 (35 Å) with 750 torr of Cl_2 (see fig IV.11) shows no long component, indicating that the quenching is complete. In contrast to O_2, the line width with Cl_2 shows a slight broadening (see fig IV.12). The absence of a narrow component rules out a spin flip quenching process. The slight broadening can be understood if it is assumed there is a certain fraction of the positrons which form p-Ps directly and produce a small narrow component. The narrow component fraction of the 511 KeV line will then decrease as pickoff quenching of o-Ps is increased.

The broad line width in Cl_2 is not surprising since Cl_2 has no unpaired electrons. This result is in agreement with angular correlation studies on the PsCl system (Tao, 1974).

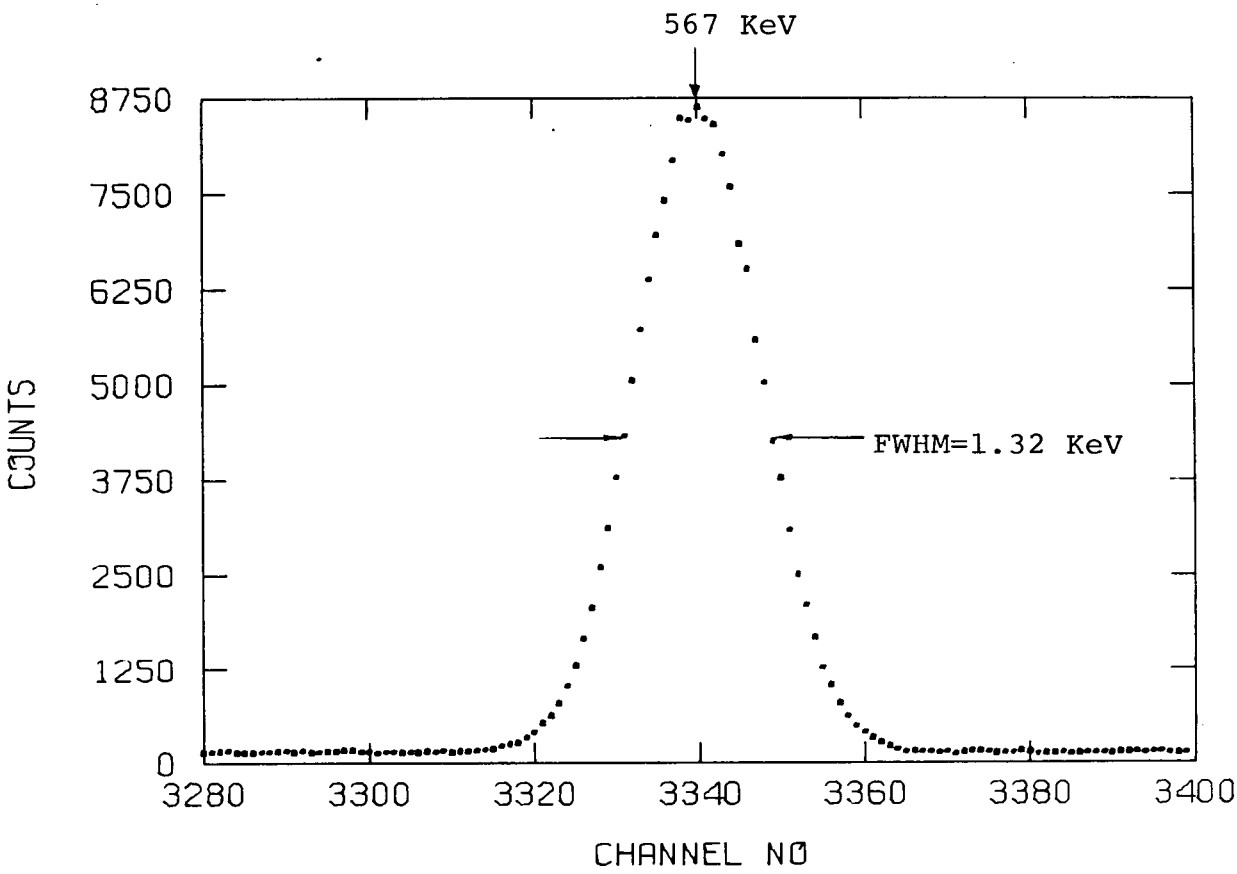

Fig 1V.9. The detector resolution curve at 567 KeV, measured with a Bi^{207} source.

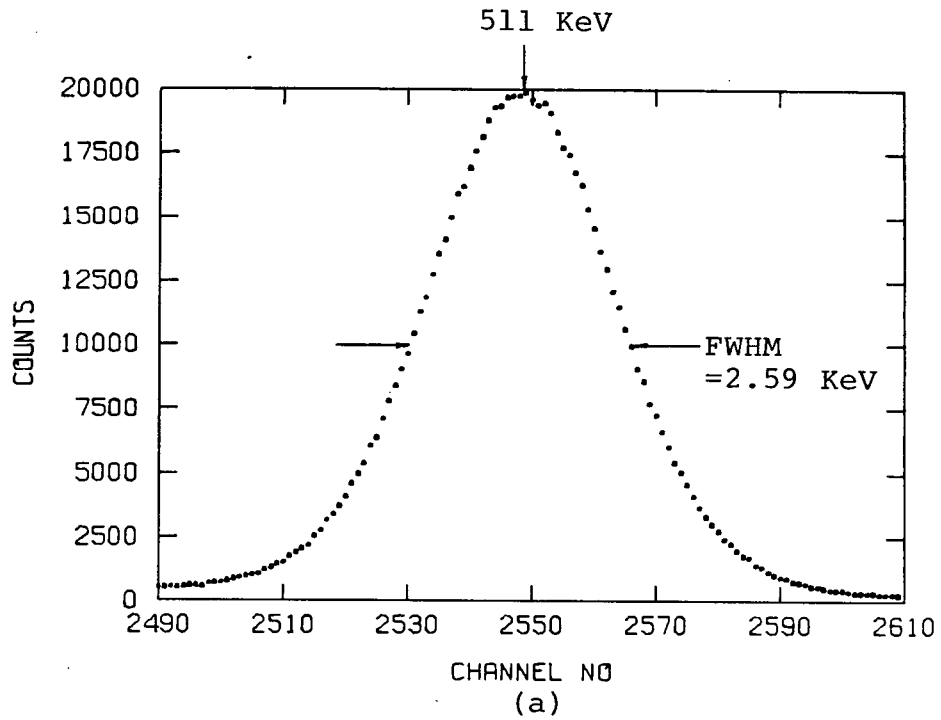

(a)

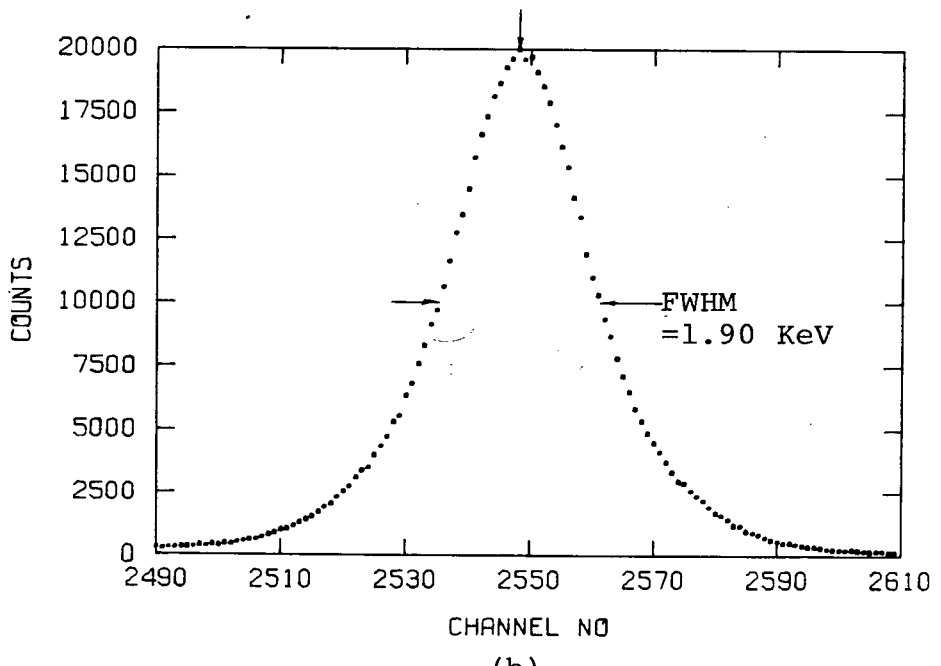

(b)

Fig IV.10(a) . Annihilation radiation in 35Å radius SiO_2 powder at 10^{-3} torr. (b). Same at 750 torr of O_2.1channel = 73 eV.

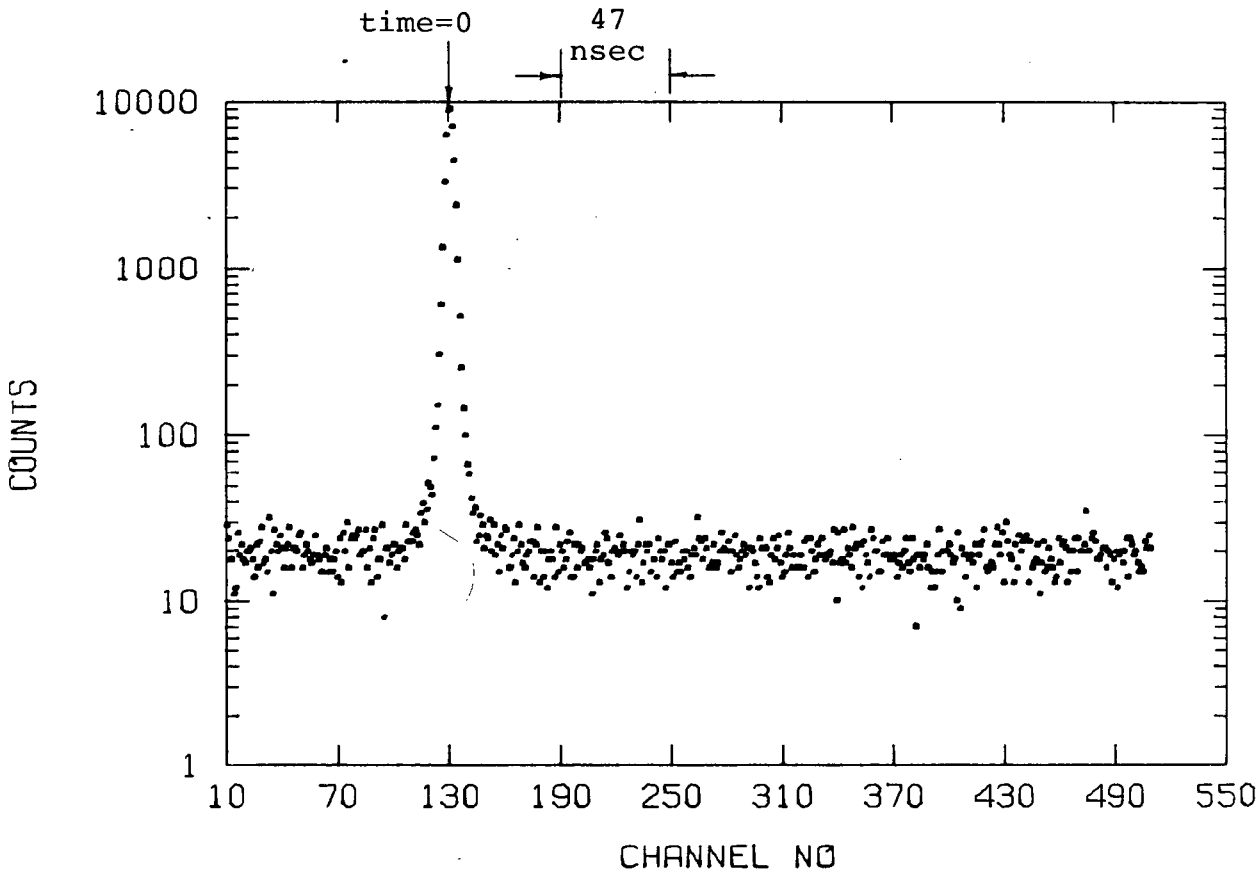

Fig lV.11. Lifetime spectrum in 35Å SiO_2 at 750 torr Cl_2. 1 channel = .942 nsec.

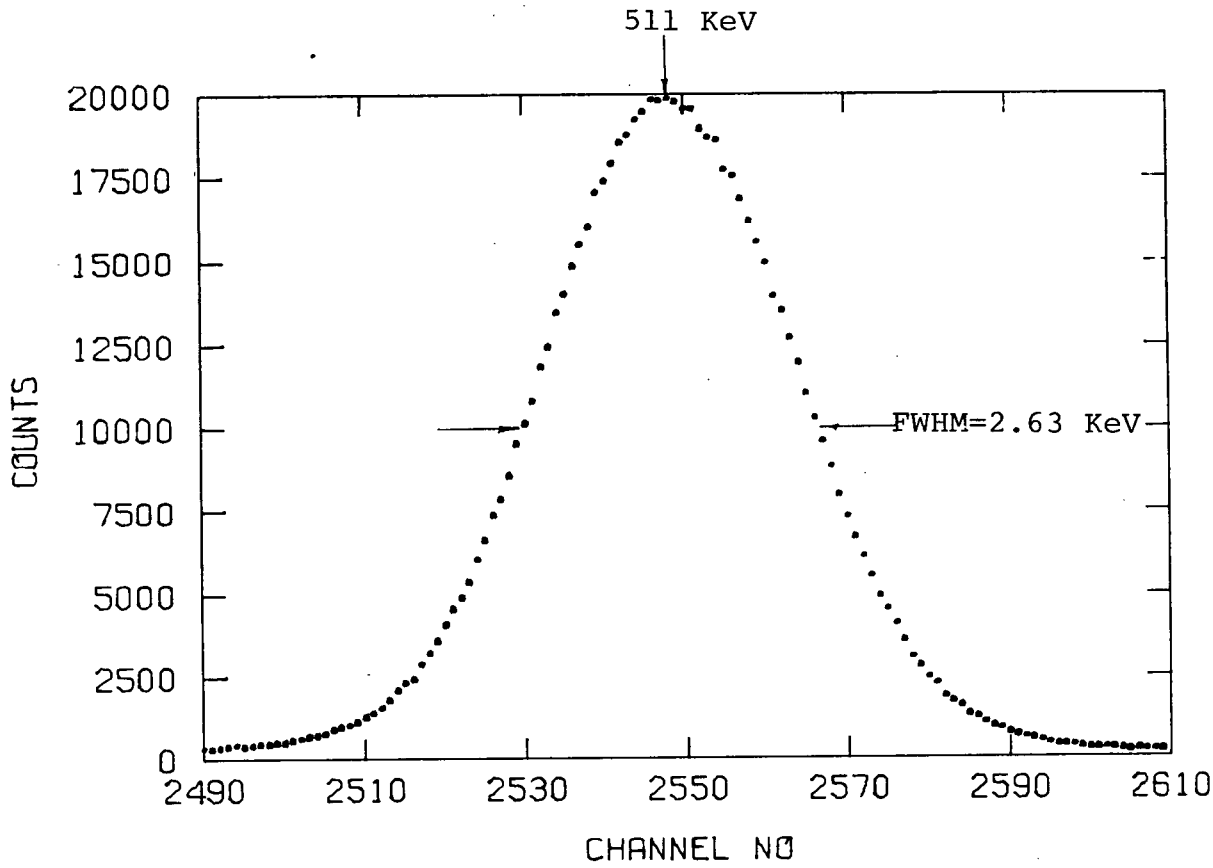

Fig lV.12. Annihilation radiation in 35Å SiO_2 at 750 torr Cl_2. 1 channel = 73 eV.

The chemical reaction

$$o\text{-}Ps + Cl_2 \rightarrow o\text{-}PsCl + Cl$$

is believed to be responsible for the large quenching cross section. The o-PsCl compound is very short lived because the positron picks off a valence electron from the Cl atom.

Sect IV.5 Conclusions

In conclusion of this chapter we state

1. Fine grain oxide powders are high yield sources of thermalized, virtually free, o-Ps, ideal for studying o-Ps interactions with gases.

2. The present state of GeLi detectors is such that they are able to distinguish quenching due to bond formation from quenching due to a spin exchange process, by the technique of Doppler broadening. Considering the simplicity ,speed and feasability for all density targets of such a technique, compared with the technique of angular correlation, GeLi detectors could prove to be very useful tools in physical gas chemistry.

CHAPTER V MEASUREMENTS OF μ^+ AND Mu FRACTIONS IN OXIDE POWDERS

Sect V.1 Introduction

The purpose of this experiment was

1. To search for Mu in powdered insulators using a transverse field MSR apparatus.

2. To measure both the free muon and Mu initial asymmetries and thus determine upper and lower limits on the Mu fraction in these powders.

3. To look for evidence that the Mu is diffusing out of the powder grains and into vacuum.

Powdered samples of SiO_2 (35 Å), GeO_2 (coarse), SnO_2 (coarse), CaO (coarse), MgO (fine), SiO (coarse) and Al_2O_3 (150 Å) were investigated. The ZnO (560Å) that was examined in the positronium experiment (Chapter IV) was investigated in a previous Mu experiment (Spires, 1977). The result was negative on the basis of a large muon asymmetry and the lack of Mu precession. That experiment also looked at Al_2O_3 (150 Å) which showed what appeared to be a large

Mu asymmetry relaxing very fast. It was felt that further evidence was required in order to make a positive identification.

Sect V.2 Technique

A standard two telescope MSR apparatus for transverse fields (see Sect III.3) was used to measure the time evolution of the muon polarization. In low fields (B<10G) there are two resolvable precession frequencies, one due to free muons in a $|\alpha\rangle$ spin state at 13.6 KHz/G and the other due to Mu in a $|\alpha\ \alpha\rangle_{Mu}$ [1] spin state at 1.4 MHz/G (see Sect III.3.iii). Each precession frequency is characterized by an amplitude or asymmetry which relaxes with time. The asymmetries at time=0 are in direct proportion to the fraction of the muon ensemble initially in a $|\alpha\rangle$ state and $|\alpha\ \alpha\rangle_{Mu}$ state respectively. The proportionality constant was determined experimentally by measuring the initial free muon asymmetry in Al for which it is assumed that all muons are initially in a free muon state.

$$f = k\ Asy(t=0) \quad \text{where} \quad k=[Asy_{\mu+}(t=0)]^{-1}$$
$$\text{for Al}$$

If all the muons stop in the powder then the free muon fraction and the Mu fraction in the powders are

$$f_{\mu+} = Asy_{\mu+}(powder)/Asy_{\mu+}(Al) \quad \text{eqn V.1(a)}$$

$$f_{Mu} = 2Asy_{Mu}(powder)/Asy_{\mu+}(Al) \quad \text{eqn V.1(b)}$$

where Asy(powd) is the measured initial Mu asymmetry for the powder, and

---

[1] Notation : $\alpha \rightarrow \frac{\sigma}{2} = \frac{1}{2} \quad \beta \rightarrow \frac{\sigma}{2} = -\frac{1}{2}$

where $Asy_{\mu+}$(powder), and $Asy_{\mu+}$(Al) are the measured initial free muon asymmetries for the powder and aluminum, respectively. The factor of 2 in the expression for f_{Mu} arises because half of the Mu ensemble is in a $|\alpha\ \beta>$ spin state which is not observable.

In a real situation the muons do not all stop in the powder, as intended, so that the effect of muons stopping elsewhere must be subtracted. The contribution to $Asy_{\mu+}$(powder) and $Asy_{\mu+}$(Al) due to muons stopping in the vacuum vessel,target holder,etc. was determined by measuring the free muon asymmetry for Fe_2O_3 in which there is no coherent free muon precession at 13.6 KHz/G. Sutracting this asymmetry from the free muon asymmetries in eqn V.1 yields

$$f_{\mu+} = \frac{Asy_{\mu+}(\text{powder}) - Asy_{\mu+}(Fe_2O_3)}{Asy_{\mu+}(\text{Al}) - Asy_{\mu+}(Fe_2O_3)} \qquad \text{eqn V.2}$$

$$f_{Mu} = \frac{2\ Asy_{Mu}(\text{powder})}{Asy_{\mu+}(\text{Al}) - Asy_{\mu+}(Fe_2O_3)} \qquad \text{eqn V.3}$$

Sect V.3 Experimental Details

i The Polarized Beam

The experiment was performed on M20, a stopping muon channel at TRIUMF. The channel was tuned to accept muons of momentum 29 Mev/c resulting from the decay of pions which had stopped on the surface of a Be production target. The polarization of such muons is close to 100% (see Sect III.3.v). Their range in carbon is 140 mg/cm^2 so that it was possible to stop all the muons in the target.

ii The Experimental Setup

Fig V.1 shows the counter arrangement used for the experiment. A thin (40 mg/cm^2) beam defining counter functioned as a 95% efficient muon counter, able to discriminate cleanly against positrons of 29 MeV/c because the dE/dX for muons is much greater than that for positrons at 29 MeV/c. The 5 cm of carbon degrader between R1 and R2 and between L1 and L2 discriminated against low energy positrons and thus served to increase the maximum experimental asymmetry (see Sect III.2.i). Using an aluminum target this maximum experimental asymmetry was measured to be .347±.004 and .336±.003 for the left and right telescopes respectively. The muon stop rates were typically 40 K/sec with 15 μA of primary proton beam incident on a 10 cm Be production target.

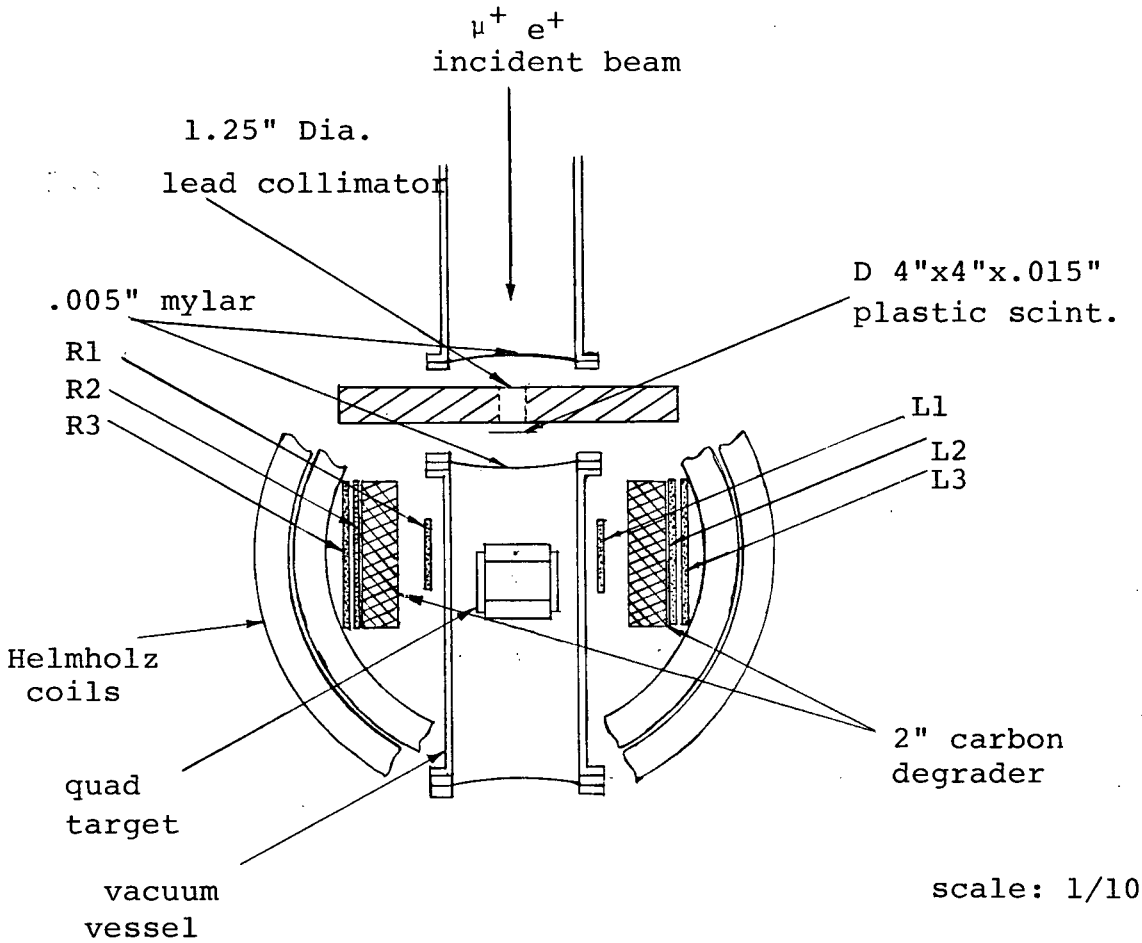

Fig V.1 Experimental setup for observing free muon and Mu precession in powders.

iii Electronics

The logic was designed to measure the time delay between the muon stop and a high energy positron passing through one of the telescopes (see fig V.2) . The details of the electronics are written up elsewhere (Garner, 1978) but the main features are:

1 Timing resolution = 5 nsec

2 Time/channel = 2 nsec

3 Total range = 4 μsec

4 Second muon rejector : If a second muon entered the target within 4 μsec of the first muon, the event was rejected.

5 Second electron rejector: If a second electron was observed in either the left or right telescope within 4 μsec after the muon stop, the event was rejected.

The time delay between the μ^+ stop and the e^+ event was digitized with an EG&G TDC100 clock connected to a CAMAC interface. A microprogrammable branch driver (MBD) was used to transfer data from CAMAC to a PDP-11/40 computer. Events where the second μ^+ or e^+ arrived within 4 μsec of the first μ^+ stop, but after the first e^+ were rejected by the MBD. The MBD also routed the event to the appropriate left or right spectrum.

90°/270° or "Arizona" data acquisition mode logic diagram

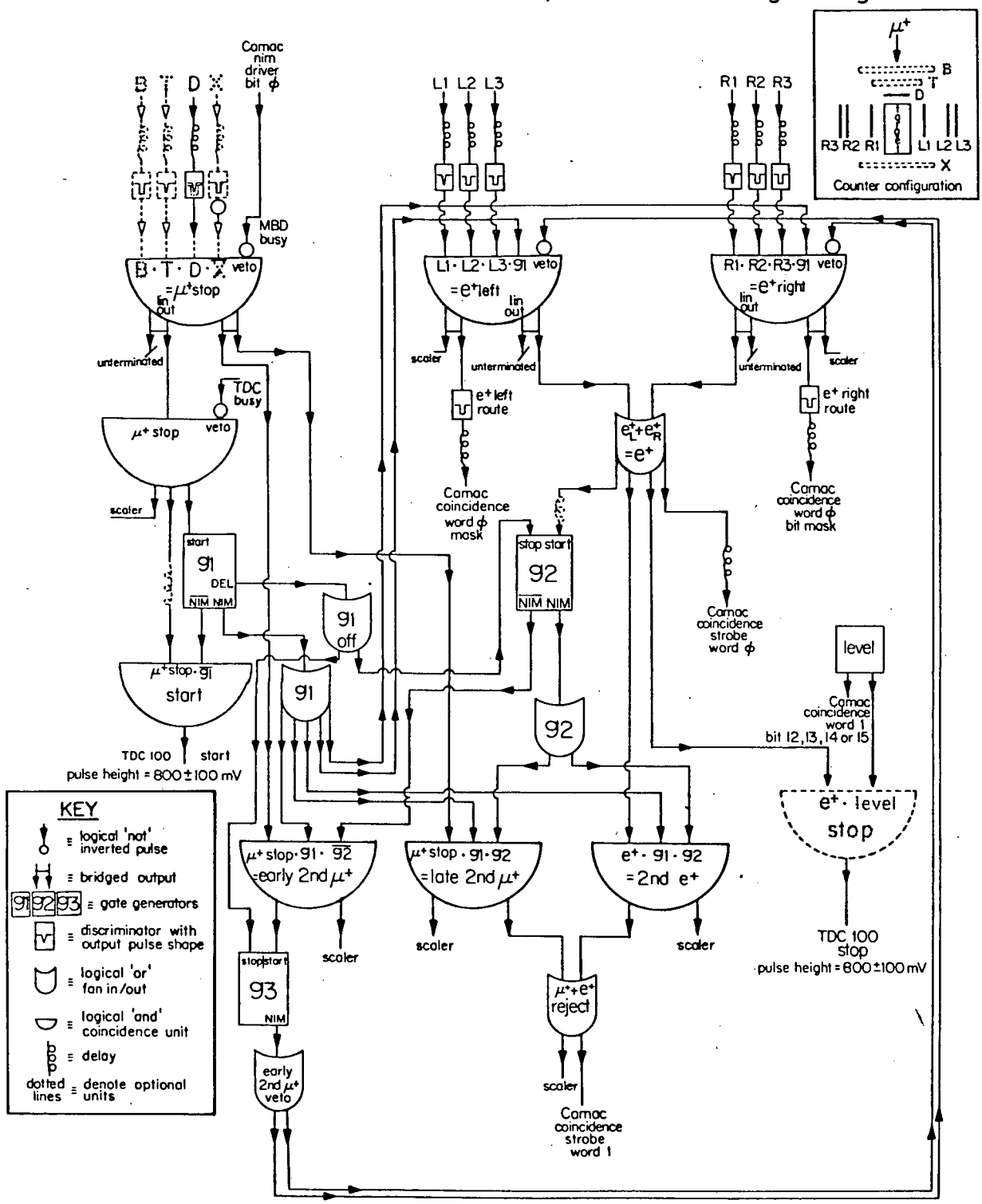

Fig V.2 . The logic used to collect the left and right spectra of time delays between a μ^+ stop (signaled by D) and a fast positron event (signaled by L1.L2.L3 or R1.R2.R3). The optional units denoted by the dotted lines were not used.

iv Procedure

A four sided multiple target attached to a mechanical feedthrough allowed four targets to be run in succession without disturbing the vacuum vessel. Another dual target consisting of aluminum (for normalization) on one side and a powder target on the other was used alternately with the quad target. Powder samples were contained by using .0013 cm aluminized mylar windows. The target areas were all 50 cm^2 in area whereas the collimated beam was 8 cm^2 upon entering the vacuum vessel.

During the runs the vacuum vessel was maintained at 10^{-5} torr. At least two runs were made for each powder, one at 69G and one at 7.8G . If the higher frequency muonium precession was visible at 7.8G, the run was repeated later on after bleeding in $\sim$ 5 torr of O_2. This was the case for Al_2O_3, MgO and CaO. The exception to this was for SiO_2 where the behaviour of Mu in powder + O_2 had already been investigated (Marshall, 1978).

v Target Preparation

The first four powders, SiO_2, GeO_2, SnO_2, and Al_2O_3, were pumped down to 10^{-5} torr for a period of 24 hours in advance of the run. They were installed within the MSR apparatus without disturbing the vacuum. The fifth and sixth samples to be run, Al and SiO (coarse) were not pumped in advance since surface effects were not expected to be important. The next three targets, Fe_2O_3, MgO, and CaO were pumped down to 10^{-1} torr for a period of 3 hours in advance of their running. In addition, the CaO, which is commonly found as $CaCO_3$, was baked for 24 hours at 600 C° to ensure the reaction

$$CaCO_3 \rightarrow CaO + CO_2$$

had taken place.

vi Analysis

a) High Field Runs

Since the positron telescopes, initial muon polarization (the beam direction), and magnetic field of 69G were all at 90^{o} to one another the positron counts versus time after the μ^{+} stop were fitted to the following 6 parameter function.

$$S^{high}(t) = N[1 + A(0)e^{-\lambda_R t}\cos(\omega t+\phi)]e^{-t/\tau_\mu} + B \qquad \text{eqn V.4}$$

where N = the normalization

A(0) = initial asymmetry

λ_R = relaxation rate for the asymmetry

ω = angular velocity of the free muon polarization vector

ϕ = phase of this precession

B = flat background term

τ_μ = 2199.4 nsec (the μ^{+} lifetime)

The spectra were fitted over a 3.6 μ sec range using 20 nsec bins starting at approximately 20 nsec. The function

$$\chi^2 = \sum_n [\, S^{high}(n) - S(n)\,]^2/S^{high}(n) \qquad \text{eqn V.5}$$

was minimized using the computer program MINUIT where S(n) is the number of events in bin n and $S^{high}(n)$ is the number of events in the time interval corresponding to bin n as calculated from eqn V.4.

Fig V.3(a) shows the raw time spectra for aluminum at 69 G along with the best fit. Fig V.3(b) shows the data after subtracting the flat background term and folding out the exponential. More explicitly it is a plot of

$$C^{high}(t) = \frac{S(n) - (E(n)+B(n))}{E(n)} \qquad \text{eqn V.6}$$

where E(n) and B(n) are the number of events in the time interval corresponding to bin n as calculated from

$$E(t) = Ne^{-t/\tau_\mu}$$
$$B(t) = B \qquad \text{eqn V.7}$$

The amplitude of the oscillating function, $C^{high}(t)$, is defined as the experimental asymmetry $Asy_{\mu+}(t)$. The solid line in fig V.3(b) represents the best fit to $C^{high}(t)$ defined as

$$C^{high}_{fit}(t) = A(0)\ e^{-\lambda_R t}\ \cos(\omega t+\phi)$$

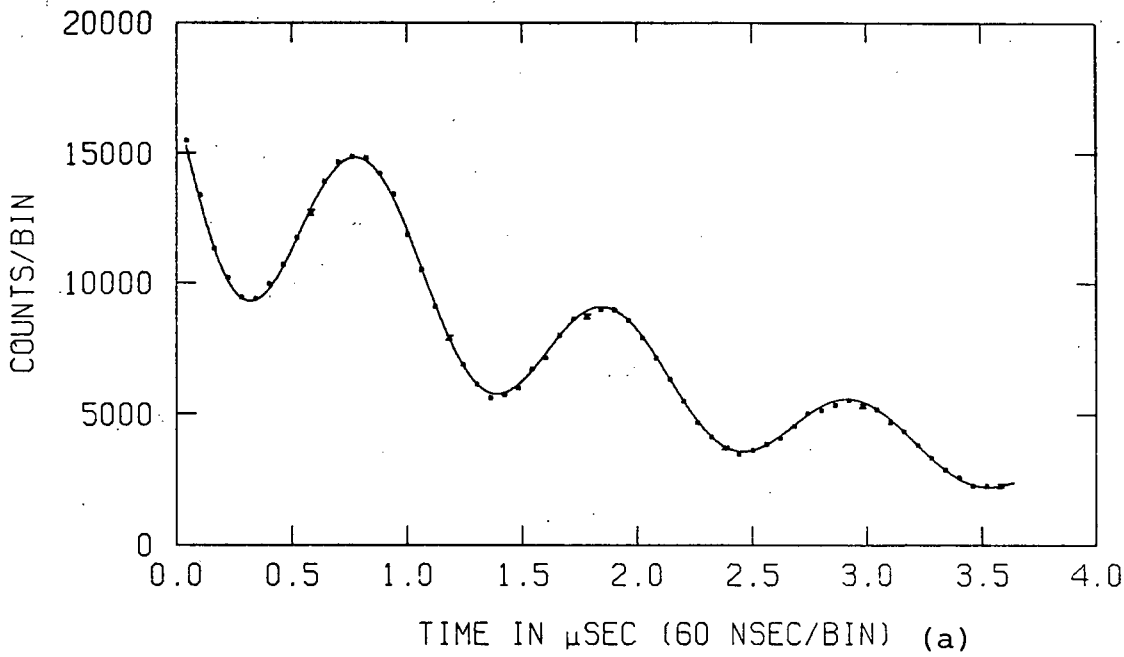

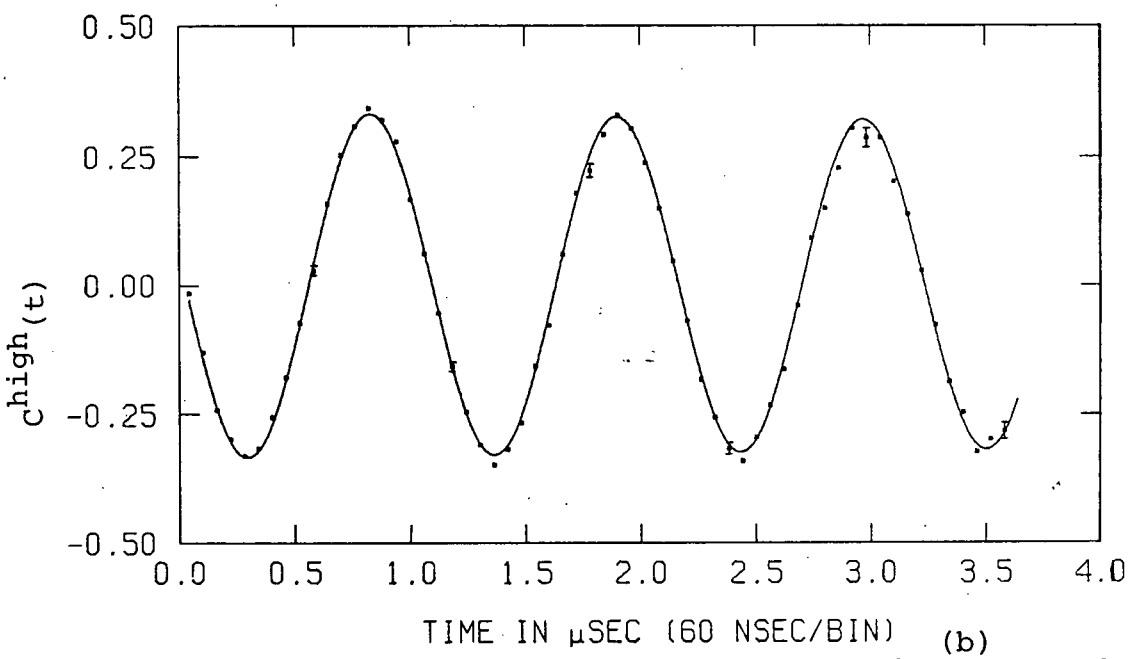

Fig V.3(a) . Number of positron events versus time after the muon stop in aluminum. The transverse field was 69 G .The solid line represents the best fit. (b) Same as (a) except the exponential has been folded out.The amplitude of the oscillation is the asymmetry due to free muon precession.

b Low Field Runs

For the runs at 7.8G the number of positron events versus time after the μ^+ stop was fitted to the following 8 parameter function using 8 nsec bins

$$S^{low}(t) = N[1+A_{Mu}(0)e^{-\lambda_{Mu}t}\cos(103\omega_{\mu+}t-\phi_{Mu}) + A_{\mu+}(0)\cos(\omega_{\mu+}t+\phi_{\mu+})]e^{-t/\tau_\mu} + B$$

where N = the normalization

$A_{Mu}(0)$ = the initial Mu asymmetry

λ_{Mu} = relaxation rate of the Mu asymmetry

$103\omega_{\mu+}$ = angular velocity of the muon polarization in mucnium

ϕ_{Mu} = the corresponding phase

$A_{\mu+}(0)$ = the initial free muon asymmetry

$\omega_{\mu+}$ = angular velocity of the muon polarization for free muons

$\phi_{\mu+}$ = corresponding phase

B = flat background term

Again this done by using the computer program MINUIT to minimize the χ^2 according to eqn V.5 . Fig V.4(a) is the raw time spectrum for SiO_2 (35Å) at 7.8G at 10^{-5} torr. Fig V.4(b) is a plot of

$$C^{low}(n) = \frac{S(n) - [E(n)-B(n)]}{E(n)}$$

where E(n) and B(n) are defined as in eqn V.6 . The solid

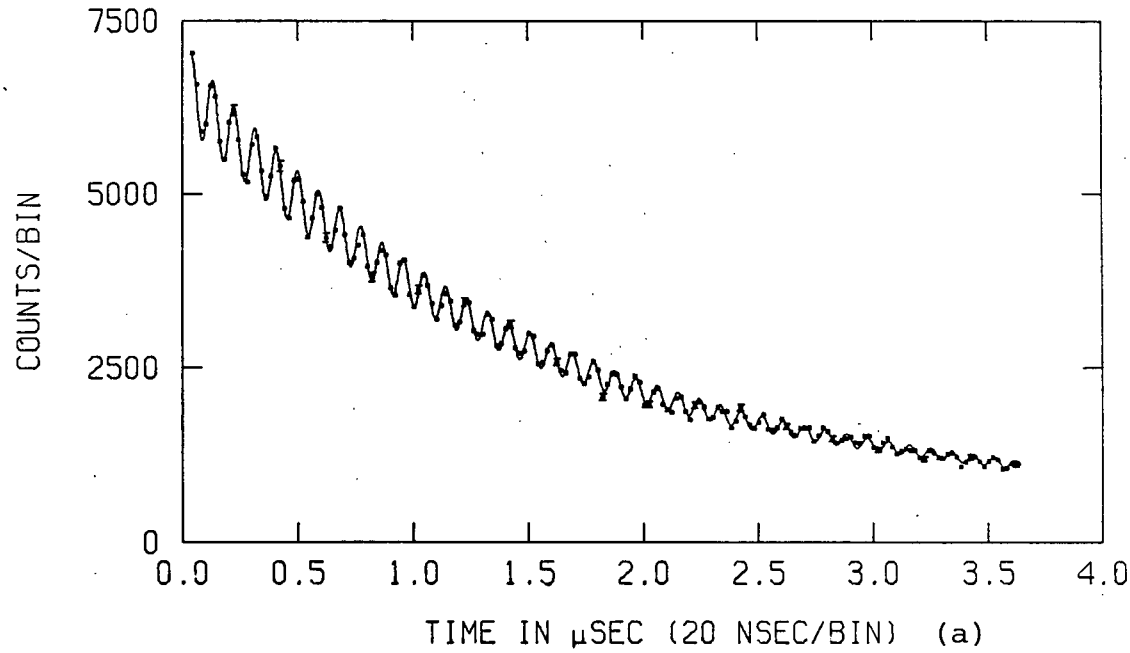

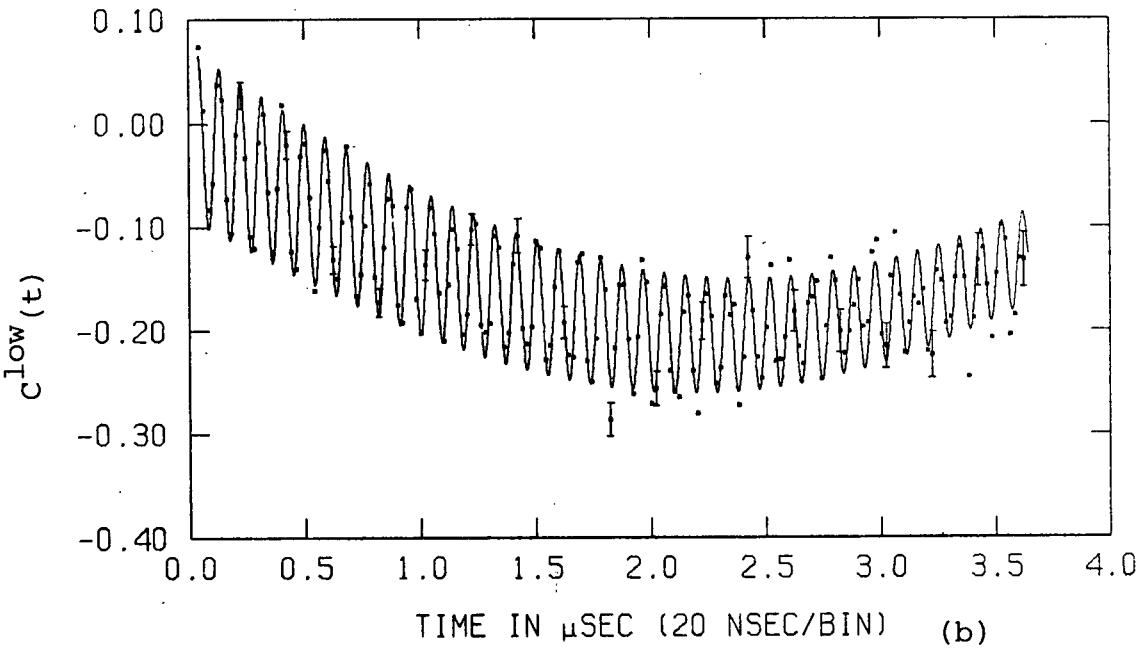

Fig V.4(a).Number of positron events versus time after the muon stop in SiO_2(35Å).The transverse magnetic field was 7.8 G.The pressure inside the vacuum vessel was 10^{-5} torr.The solid line is the best fit. (b) The same as (a) except the exponential has been folded out.The fast oscillation is due to muonium precession whereas the slow one is due to free muon precession.

line in fig V.4(b) is the function

$$C^{low}_{fit}(t) = A(0)e^{-\lambda_{Mu}t}\,[\,\cos(103\omega_{\mu^+}t - \phi_{Mu})] + A_{\mu^+}(0)\cos(\omega_{\mu^+}t + \phi_{\mu^+})$$

properly normalized to 20 nsec bins. The amplitude of the fast oscillation in fig V.4(b) is defined as the muonium asymmetry , $Asy_{Mu}(t)$. The base line for the Mu asymmetry oscillates in time at a frequency reduced by a factor 103 (see Sect III.3). The amplitude of this precession is defined as the free muon asymmetry , $Asy_{\mu^+}(t)$.

Sect V.4 Results and Discussion

Table III summarizes the results of all runs in vacuum. The free muon and Mu fractions were calculated according to eqns V.2 and V.3 respectively. The left and right telescopes were analyzed seperately. In some cases the values calculated for the left and right hand sides differed by several standard deviations. The errors listed in Table III are either the MINUIT errors or half the difference between the left and right hand telescopes, whichever was largest.

The Mu asymmetry in Al_2O_3 relaxes very rapidly and is only marginally indentifiable (see fig V.5). There are three factors which strongly support the claim the observed oscillation is actually Mu precession

1. The frequency corresponds to Mu to within a relatively large fitting error.
2. The precession signal for the left side is 180° out of phase in relation to the right side (see fig V.5)
3. The addition of 5 torr or O_2 destroys the signal (see fig V.6).

The cause of this fast depolarization is not clear. If the precession signal is due to muonium within the grains then the random local magnetic field (RLMF) of Al_2O_3 is responsible. The RLMF due to the nuclear magnetic moment of the Al^{27} nucleus definitely contributes to the

TABLE III. Results of the Muonium Experiment

Sample	μ^+ Asymmetry at Time=0	μ^+ Relaxation Rate μsec^{-1}	Mu Asymmetry at Time=0	Mu Relaxation Rate μsec^{-1}	Polarized μ^+ Fraction %	Polarized Mu Fraction %	Missing Fraction %
Aluminum	.342±.006	.031±.009			100 by assumption		
Fe_2O_3	.070±.006	.009±.009					
SiO_2	.17 ±.02	.03 ±.02	.083±.004	.18±.04	35±5	61±3	4±6
CaO	.185±.010	.07±.02	.047±.005	2.5±.6	43±3	35±4	22±5
MgO	.262±.016	.05±.04	.020±.004	1.9±.5	71±6	15±3	14±7
Al_2O_3	.267±.013	.08±.02	.047±.018	11.3±4.4	72±4	35±14	-7±15
GeO_2	.18 ±.03	.044±.016	no signal		40±7	0	60±7
SnO_2	.336±.019	.056±.025	no signal		98±5	0	2±5
SiO	.24 ±.01	.049±.009	no signal		63.5±1	0	36±1

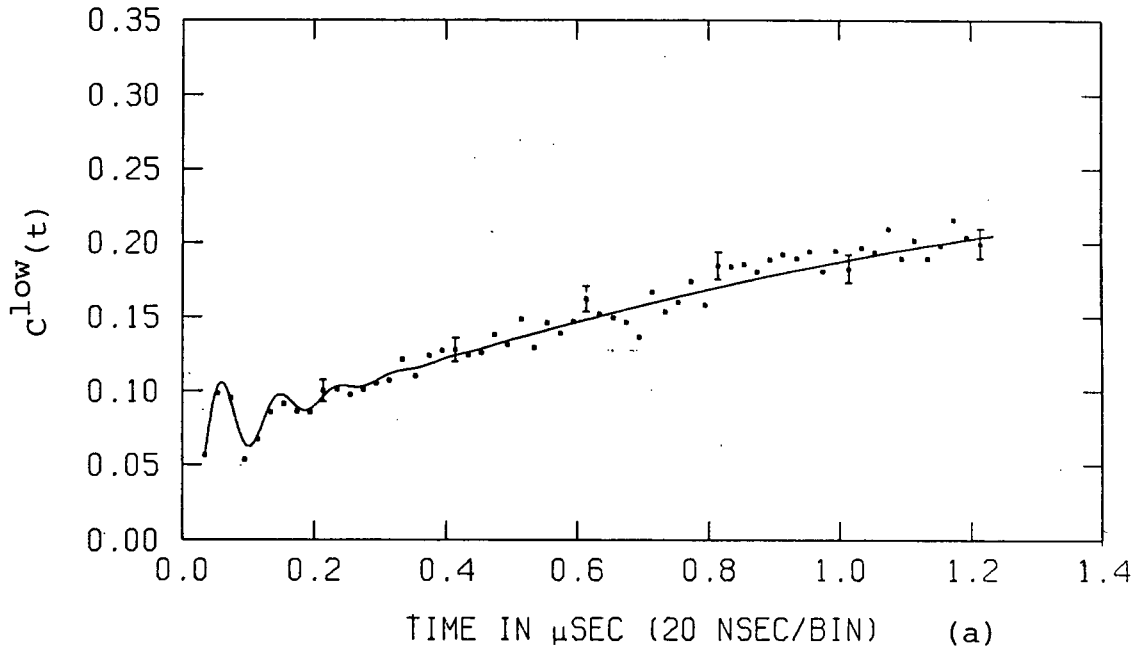

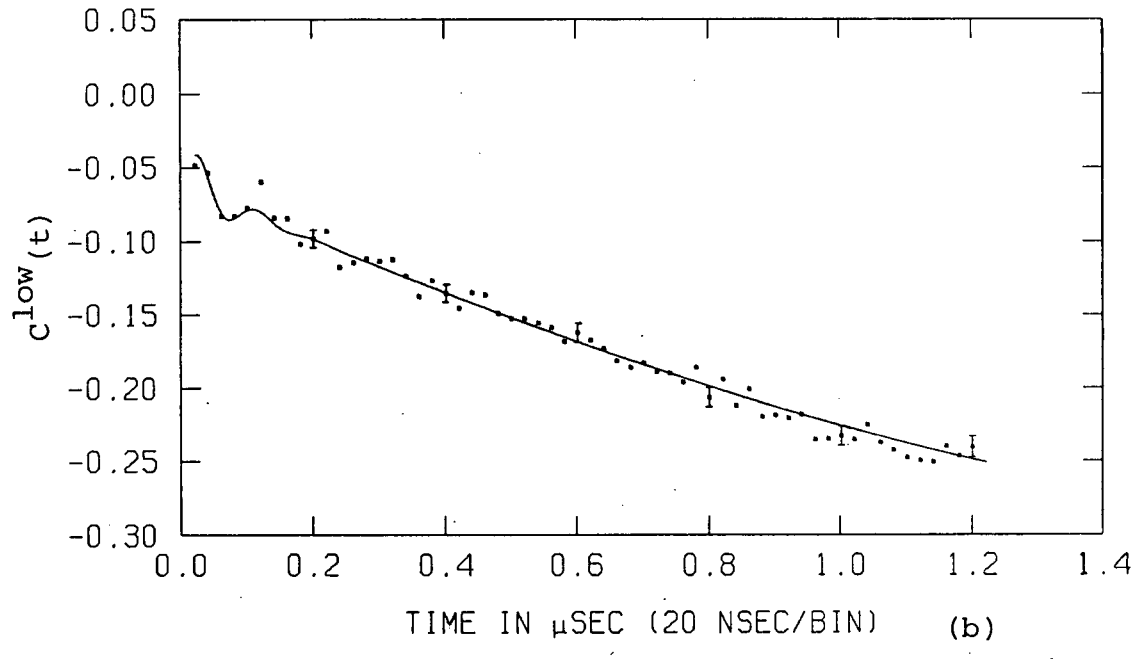

Fig V.5(a). Number of positron events versus time after the muon stop, with the exponential folded out, in Al_2O_3 (150Å) for the left telescope. The transverse field was 7.8 Gauss. The pressure in the vacuum vessel was 10^{-5} torr.. (b). Same as (a) except for the right telescope.

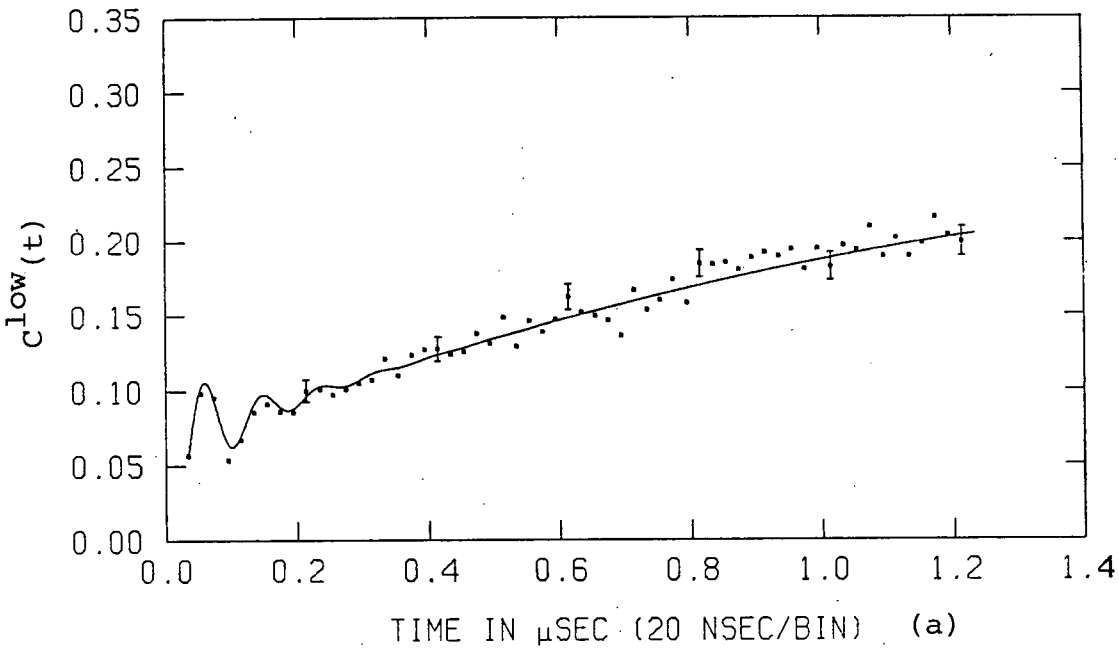

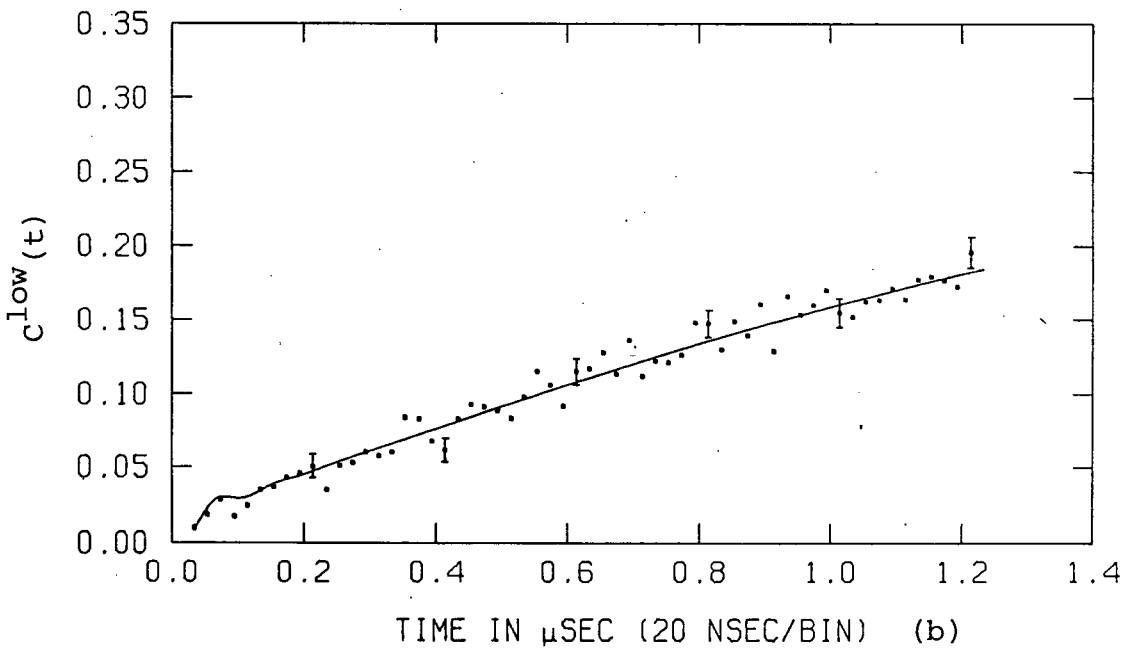

Fig V.6 (a). Number of positron events versus time after the muon stop, with the exponential folded out, in Al_2O_3 (150Å). The pressure in the vacuum vessel was 10^{-5} torr. The transverse field was 7.8 Gauss.

(b). Same as (a) except with 5 torr of O_2 in the vacuum vessel.

depolarization but it is probably not the only cause since this fast depolarization is not present in ice where the proton nuclear magnetic moment is present. Physical inpurities may also contribute to this RLMF. If the mucnium is in the intergranular regions then the affect of adsorbed gases on the surface must also be considered.

Figs V.7(a) and V.7(b) show the effect of 5 torr of O_2 on the Mu precession signal in MgO. Again the precession signal is destroyed. Such is not the case for coarse CaO (see figs V.8(a) & V.8(b)), which is clearly a particle size effect. The SiO_2 (35Å) in an O_2 environment has been investigated by Marshall (1977). The quenching rate coefficient was measured and found to be consistent with measurements using an argon moderator (Garner, 1978). This is strong evidence that the Mu was in the intergranular regions.

GeO_2 showed the largest missing fraction. There was no mucnium precession observed despite the fact that the free muon precession accounted for only 40±7 % of the muons (see figs V.9(a) and V.9(b)). It is very probable that the missing fraction is due to fast depolarization of Mu since

1. GeO_2 and SiO_2 are chemically very similar sc one would expect that Mu formation in SiO_2 would imply Mu formation in GeO_2.
2. Mu precession is 100 times more sensitive to RLMF than μ^+ precession. The fact that a long

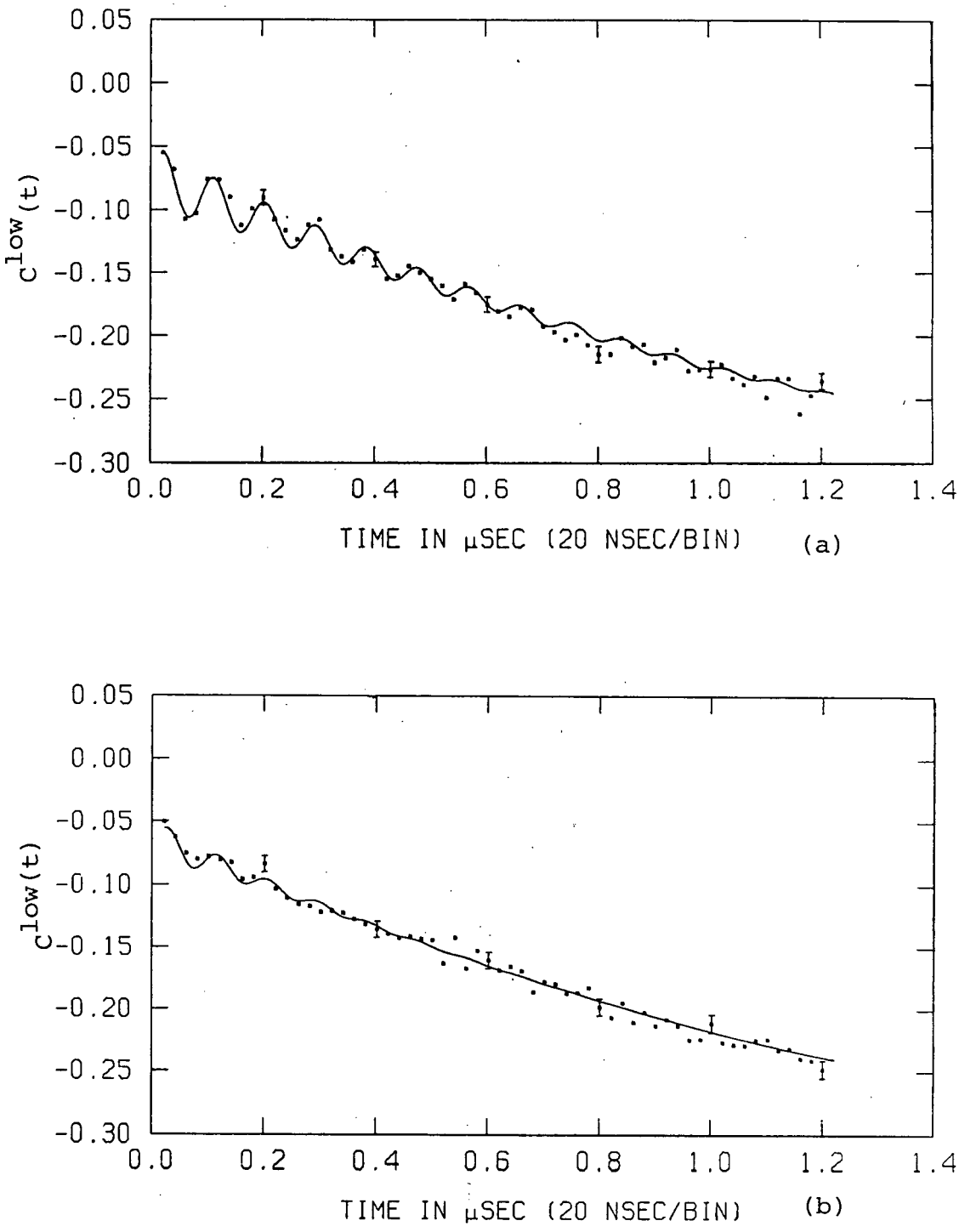

Fig V.7 (a). Number of positron events versus time after the muon stop, with the exponential folded out, in fine MgO. The pressure in the vacuum vessel was 10^{-5} torr. The transverse field was 7.8 Gauss.

(b) Same as (a) except with 5 torr of O_2 in the vacuum vessel.

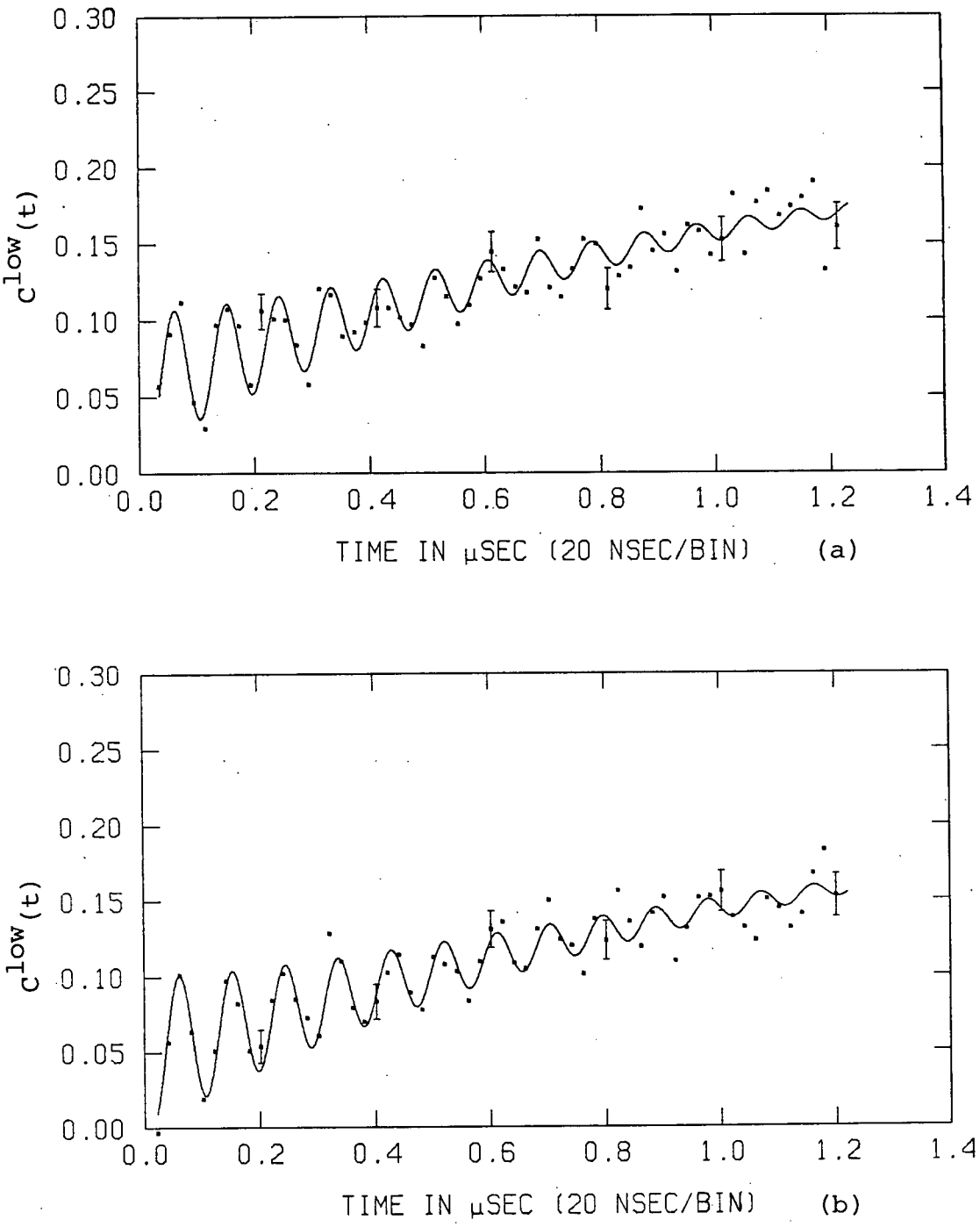

Fig V.8 (a). Number of positron events versus time after the muon stop, with the exponential folded out, in coarse CaO. The pressure in the vacuum vessel was 10^{-5} torr. The transverse field was 7.8 Gauss.

(b) Same as (a) except with 5 torr of O_2 in the vacuum vessel.

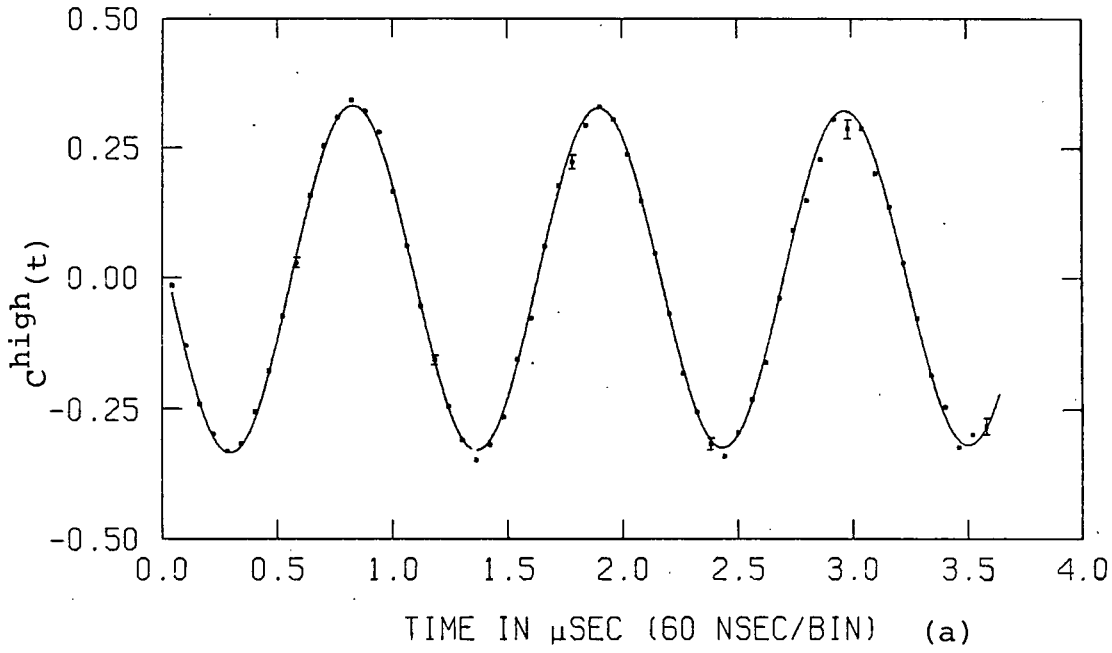

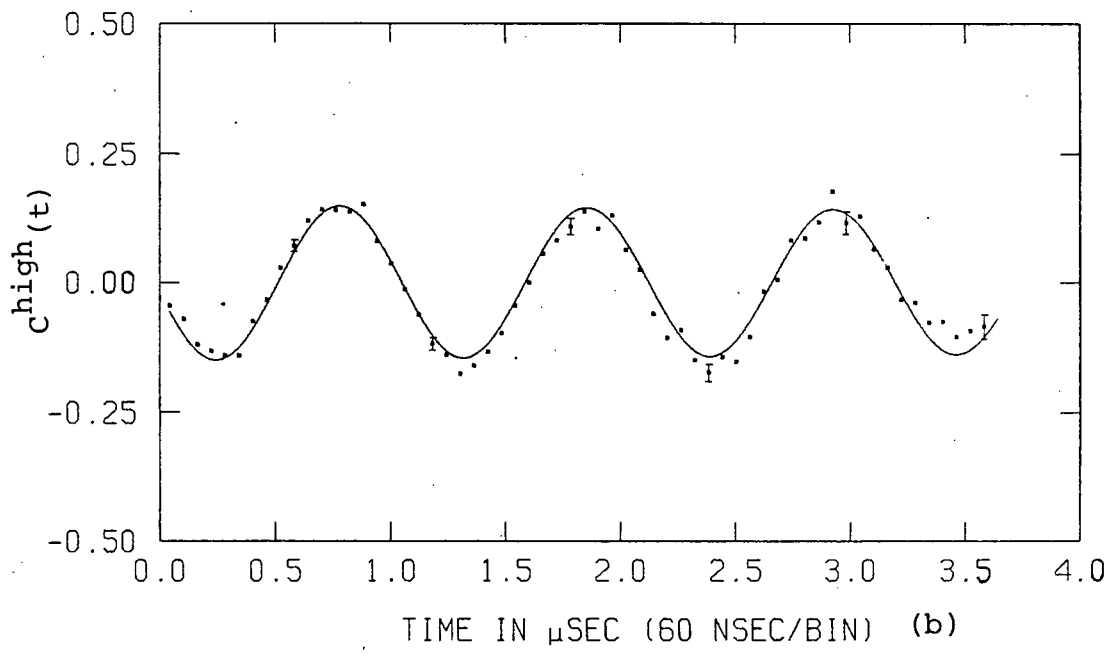

Fig V.9 (a). Number of positron events versus time after the muon stop, with the exponential folded out, in aluminum. The pressure in the vacuum vessel was 10^{-5} torr. The transverse field was 69 Gauss.

(b) Same as (a) except in GeO_2.

lived μ^+ precession was observed in GeO_2 suggests that the missing component is Mu.

The missing fraction in MgO (14±7%) could be due to Mu within the grains and the observed fraction due to Mu in the intergranular region. This would be possible if the variance on the particle size is large as expected. On this assumption the observed Mu relaxation rate is a result of surface depolarization.

The missing fraction in CaO (22±7%) cannot be explained this way because the addition of O_2 had no affect on the Mu precession. This implies the particle size is much larger than the mean diffusion length before decay. However it is possible that the observed precession signal is due to Mu trapped in pores within the grains. The missing fraction would then correspond to Mu depolarizing fast within the solid CaO regions.

Sect V.6 Future Muonium Experiments

The results of this experiment leave many questions unanswered which should be re-examined in the future.

The origin of the missing fraction, especially in GeO_2, should be investigated. Isotopically pure samples of GeO_2 are now available. If the nuclear magnetic moment of Ge^{73}, which composes 7.76% of the natural Ge , is responsible for the fast depolarization of Mu then an isotopically pure GeO_2 sample will show Mu precession. Fine GeO_2 powder should also be examined since it is expected that muonium will diffuse into the intergranular regions before it has a chance to depolarize.

A single run with oxygen is not the best technique in order to determine whether Mu has reached the intergranular regions because the oxygen will also depolarize Mu which is on the surface. It is then neccessary to examine the relaxation rate as a function of O_2 pressure in order to establish that the Mu is in the intergranular regions (Marshall, 1978). One fairly simple way to establish that the Mu is in between the grains is to show a linear dependence between powder density and relaxation rate. Such a dependence is only possible if the Mu is moving freely between grains.

The diffusion model should be tested thoroughly by doing studies of the vacuum fraction of Mu versus temperature and particle size for all powders which form Mu. In this regard it would be very interesting to compare the

diffusion constants for muonium and positronium in the various oxides .

Finally , the possibility of depositing chemicals on the surface of these powders clearly suggests a series of experiments in surface chemistry.

CHAPTER VI CONCLUDING REMARKS

It has been shown that fine powdered oxides can be used to efficiently produce muonium and positronium. Furthermore, the results indicate that if these oxides are in a fine powdered form Mu like Ps reaches the intergranular regions. The applications in gas chemistry, surface chemistry, diffusion studies and the study of fundamental properties of Mu and Ps are numerous.

Careful measurements have revealed Mu precession in CaO, MgO, and Al_2O_3 where they had not been seen before. These results indicate that the formation processes for Mu and Ps are closely linked at least in a qualitative sense despite the large mass difference.

Clearly future investigations in this area should be very rewarding in many branches of physics and physical chemistry and will help clarify our understanding of one of the most fundamental of physical systems the hydrogen atom.

BIBLIOGRAPHY

Albrecht,R. (1978). Ph.D Thesis, University of British Columbia, Physics Department.

Anderson,C.D. (1933). Phys.Rev. 43 ,491.

Anderson,C.D and Neddermeyer,S.H. (1937). Phys. Rev. 51 , 884.

Bailey,J. et al. (1977). Phys. Lett. 67B,225.

Bird,H.M. And Jones,G. (1973). Can. J. Phys. 51 ,537.

Blackett,P.M. And Occhianlini,G.P. (1933). Proc. Roy. Soc. (London) A139 ,699.

Brandt,W. and Paulin,R. (1968). Phys. Rev. 21 ,193.

Brewer,J.H., Crowe,K.M., Gygax,F.N., and Shenck,A. (1975) Muon Physics Vol. II, edited by Hughes,V.W., and Wu,C.S. ,Academic Press,New York,p. 3-39.

Calmet,J. et al. (1977). Rev. Mod. Phys. 49,21.

Canter,K.F.,Coleman,P.G.,Griffith,T.C. and Heyland,G.R. (1972). J. Phys. , B5,L167.

Canter,K.F.,Coleman,P.G.,Griffith,T,C and Heyland,G.R. (1974). Appl. Phys. 4 ,89.

Canter,K.F., Mills,A.P. and Berko,S. (1975). Phys. Rev., Lett. 34 ,177.

Caswell,W.E., (1977). Phys. Rev. Lett. 38 ,488.

Celitans,G.J., Tao,S.J. and Green,J.H. (1964a). Proc., Phys., Soc., 83 ,833.

Celitans,G.J. and Green,J.H. (1964b). Proc. Phys. Soc. 83 ,823.

Charlambois,S., Chardalas,M. and Dedoussis,S. (1976). Phys. Lett. 59A 235.

Chuang,S.Y. and Tao,S.J. (1974a). Phys. Rev. A9 ,989.

Chuang,S.Y. and Tao,S.J. (1974b). Appl. Phys. 3 ,199.

Clarke,G. (1978). Honours Thesis,University of British

Columbia, Engineering Department.

Conversi,M., Pancini,E., and Piccioni,O. (1947). Phys. Rev. 71 ,209.

Cronin,J.W.(1968). Proc.Conf. High Energy Physics,14th,p289.

Deutch,M. (1951). Phys. Rev. 83 ,866; 82 ,455.

Dirac,P.A.M. (1930). Proc. Roy. Soc. A126 ,360.

Feinberg,G. and Weinberg,S. (1961). Phys. Rev. 123 ,1439.

Garner,D. (1978). Ph.D. Thesis, University of British Columbia, Chemistry Department.

Gidley,D.W. et al (1978). Phys. Rev. Lett. 40,737.

Gidley,D.W., Marko,K.A. and Rich,A. (1976). Phys. Rev. Lett. 36,395.

Gittleman,B. and Deutch,M. (1958). Ann. Progr. Report ,Lab. Nucl. Sci. Massachusetts Institute of Technology.

Harris,F.M. (1976). Comments Atom. Mol. Phys. ,6,49.

Hotz,H.P., Mathiesen,J.M., and Hurley,J.P. (1968). Phy. Rev. 170,351.

Kolbig,K,S., Mignaco,J.A. and Remiddi,E. (1970). BIT 10 ,38.

Lattes,C.J. et al. (1947). Nature (London) 160,453.

Lee,J., Tao,S.J. and Celitans,G.J. (1967). Positron Annihilation ,edited by Stewart,A.T. and Rolling,L.O., Academic Press,371.

Marshall,G.M., Warren,J.B., Garner,D.M., Clark,G.S., Brewer,J.H. and Fleming,D.G. (1978). Phys. Lett. 65A,351.

Mogensen,O. et al. (1971). Phys. Rev. B4,71.

Mohorovicii,S. (1934). Astron. Nachr. , 94

Ore,A. and Powell,J.L. (1949). Phys Rev. 75, 1696.

Pifer,A.E.,Bowen,T.,and Kendall,K.R.(1976) Nucl. Inst. And Meth. 135,39.

Pirenne,J. (1946). Arch. Sci. Phys. et Nat. 28,273; (1947) 29,121,207.

Paulin,R. and Ambrosino,G. (1968). J. Phys. 29,263.

Pond,T.A. (1952). Phys. Rev. 94,489.

Segre,E. (1964a,b). Nuclei And Particles, W.A. Benjamin Inc.,New York,38,57.

Reddy ,K.R. and Carrigan,R.A. (1970). Nuovo Cimento LXVIB,105.

Sen,P. and Patro,A.P. (1969). Nuovo Cimento LXIVB,324.

Shimizu,S. Et al.(1968). Phys. Rev. 173, 405.

Sodickson,L. et al.(1961). Phys. Rev. 124, 1851.

Spires,L.D., Judd,D.J., Brewer,J.H. and Kiefl,R.F., unpublished work performed at TRIUMF in 1978.

Stambaugh,R.D. et al. (1974). Phys. Rev. Lett. 33,568.

Stedlt,F.R. and Varlashkin,P.G. (1972). Phys. Rev. B5,4265.

Street,C. and Stevenson.E. (1937). Phys. Rev. 51,1005.

Tawara,H. and Russek,A. (1973). Rev. Mod. Phys. 45,178.

Theriot,E.D.Jr., Beers,R.H. and Hughes,V.W. (1967). Physics Reports 5,215.

West,R.N. (1973). Advances in Physics 22,263.

Wheeler,J.A. (1946). Ann. N.Y. Acad. Sci. 46,221.

Williams,W.S.C. (1971). An Introduction To Elementary Particles, 2nd edition, Academic Press, New York ,303.

Wu,C.S. et al. (1957). Phys. Rev. 105,1413.

APPENDIX 1(A) CHARGE CONJUGATION PARITY FOR AN $e^+ e^-$ STATE

The charge conjugation operator acts on a state vector by reversing the sign on all the internal quantum numbers of the paricles involved such as the charge, strangeness, baryon number, lepton number, etc.

Consider a spin 1/2 fermion - antifermion state vector

$$| F \bar{F} > = | \overset{1}{a}, \overset{2}{-a}, \overset{3}{L(L+1)}, \overset{4}{L_Z}, \overset{5}{S(S+1)}, \overset{6}{S_Z} >$$

where quantum number

1 = internal quantum numbers of fermion # 1

2 = internal quantum numbers of fermion # 2

3 = (orbital angular momentum)^2

4 = z component of orbital angular momentum

5 = (total spin)^2

6 = z component of spin

Now expanding $| F \bar{F} >$ in terms of the kets

$$| \overset{1}{a}, \overset{2}{-a}, \overset{3}{\theta}, \overset{4}{\phi}, \overset{5}{S1_Z}, \overset{6}{S2_Z} >$$

where quantum number

1 & 2 = as defined before

3 & 4 = spherical angles between fermion 1 & 2

5 = third component of spin for fermion 1

6 = third component of spin for fermion 2

Gives

$$|F\ \bar{F}> = \sum_{S1_z}\sum_{S2_z} \int d\Omega Y_{LM}(\theta,\phi)\chi_S(S1_z,S2_z)\,|a,-a,\theta,\phi,S1_z,S2_z>$$

Applying the operators which exchange space variables (E_{space}), spin variables (E_{spin}), and internal quantum numbers (C) gives

$$E_{space}E_{spin}\ C|F\ \bar{F}>$$

$$= \sum_{S1_z}\sum_{S2_z} \int d\Omega Y_{LM}(\theta,\phi)\chi_S(S1_z,S2_z)\,|-a,a,-\theta,-\phi,S2_z,S1_z>$$

$$= \sum_{S1_z}\sum_{S2_z} \int d\Omega Y_{LM}(-\theta,-\phi)\chi_S(S2_z,S1_z)\,|-a,a,\theta,\phi,S1_z,S2_z>$$

$$= (-1)^L(-1)^{S+1}(-1)^{\eta}|F\bar{F}>$$

where $C|F\ \bar{F}> = (-1)^{\eta}|F\ \bar{F}>$

Since the state vector for two identical fermions must be antisymmetric under such an exchange

$$(-1)^{L+S} = (-1)^{\eta}$$

Thus the C parity $(-1)^{\eta}$ for positronium obeys this rule.

APPENDIX 1 (B) CHARGE CONJUGATION PARITY FOR AN n PHOTON STATE

Classically, the vector potential for the electromagnetic fields must change sign when all charges are reversed in sign since the fields

$$\bar{B} = \text{Curl } \bar{A}$$

$$\bar{E} = -\frac{\partial \bar{A}}{\partial t} - \text{Grad}\phi$$

are observed to reverse their signs.

The photon field operator in Fock space is defined as

$$A(x) = \frac{1}{(2\pi)^{3/2}} \int \frac{d\bar{k}}{(2k_o)^{1/2}} \sum_{j=1}^{2} \{ A_{kj} \hat{e}_j e^{-ik.x} + A_{kj}^{\dagger} \hat{e}_j e^{ik.x} \}$$

where $A_{kj}^{\dagger}$ creates a photon of momentum $\bar{k}$ and polarization j and A_{kj} annihilates one of the same.

Since the field theoretic vector potential must have the same symmetry as the classical vector potential, this implies

$$C \; A_{kj}^{\dagger} C^{\dagger} = -A_{kj}^{\dagger}$$

Thus an n photon state has C parity $(-1)^n$ since

$$C \, A_{k_1 j_1}^{\dagger} A_{k_2 j_2}^{\dagger} \cdots A_{k_n j_n}^{\dagger} |0\rangle$$

$$= CA_{k_1 j_1}^{\dagger} C^{\dagger} CA_{k_2 j_2}^{\dagger} C^{\dagger} \cdots CA_{k_n j_n}^{\dagger} C^{\dagger} C |0\rangle$$

$$= (-1)^n A_{k_1 j_1}^{\dagger} A_{k_2 j_2}^{\dagger} \cdots A_{k_n j_n}^{\dagger} |0\rangle$$

APPENDIX II (A) MEAN QUENCHING CROSS SECTION OF A POWDER FOR o-Ps

Let n be the number density for a powder with intrinsic density ρ^I, bulk density ρ^B, and mean radius R

$$\frac{1}{n} = \frac{4}{3}\pi R^3 \rho^B/\rho^I \qquad \text{eqn AII.1}$$

Assume there exists a o-Ps atom at time=0. Let P(t) be the probability that it still exists at time t. Define σ_{qp} as

$$\frac{dP}{dt} = -[\sigma_{qp} nv + \lambda_o] \qquad \text{eqn AII.2}$$

where v is its velocity and λ_o is the mean decay rate of free o-Ps.

From eqn AII.2 it follows:

$$P(t) = \exp[-(\sigma_{qp} nv + \lambda_o)t] \qquad \text{eqn AII.3}$$

From eqn AII.3 the observable mean decay rate in an evacuated powder is

$$\lambda_v = \sigma_{qp} vn + \lambda_o$$

Using eqn AII.1 it follows

$$\sigma_{qp} = \frac{4}{3} \frac{\lambda_v - \lambda_o}{v} \pi R^3 \rho^B/\rho^I$$

If it is assumed that the σ_{qp} varies as 1/v so that the λ_v is independent of v then the mean cross section

$$\overline{\sigma_{qp}(v)} = \frac{(\lambda_v - \lambda_o)}{n} \left(\overline{\frac{1}{v}}\right)$$

For a Maxwellian speed distribution

$$\frac{\bar{l}}{v} = \left(\frac{2m}{\pi k\theta}\right)^{-\frac{1}{2}} = [5.92 \times 10^{6} \text{cm/sec}]^{-1}$$

where

$m = 1.02$ MeV

$k = 1.38 \times 10^{-16}$ erg/deg

$\theta = 295^{\circ}$ K

APPENDIX II (B) QUENCHING RATE COEFFICIENT OF A GAS FOR O-PS

Equation AII.3 can be rewritten for a gas

$$P(t) = \exp[-(\sigma_q vn + \lambda_o)t] \qquad \text{AII.4}$$

where σ_q is the cross section at velocity v, n is the number density for the quenching gas and λ_o is the mean decay rate in the absence of the quenching gas. It follows from eqn AII.4 that

$$\lambda_q = \lambda_o + \sigma_q vn$$

where λ_q is the observed decay rate in the presence of the quencher. The quenching rate coefficient for the gas is defined as $\sigma_q v$ and is independent of v provided σ_q goes as 1/v.

APPENDIX III THE MUON POLARIZATION VECTOR FOR A FREE MUON IN A STATIC MAGNETIC FIELD

The task is to evaluate

$$\bar{P}(t) = \langle\psi(0)| e^{\frac{iH^{\mu}t}{\hbar}} \bar{\sigma}^{\mu} e^{\frac{-iH^{\mu}t}{\hbar}} |\psi(0)\rangle$$

$$|\psi(t)\rangle = e^{-ia\sigma_z}|\psi(0)\rangle = e^{-ia\sigma_z}\frac{1}{\sqrt{2}}\{|S_z=\tfrac{1}{2}\rangle + |S_z=-\tfrac{1}{2}\rangle\}$$

where $a = \dfrac{g_{\mu}e|\bar{B}|}{4cm_{\mu}}$

$$= \frac{1}{\sqrt{2}}\{e^{-ia}|S_z=\tfrac{1}{2}\rangle + e^{ia}|S_z=-\tfrac{1}{2}\rangle\}$$

therefore $P_z(t) = \langle\psi(t)|\sigma_z|\psi(t)\rangle = \frac{1}{2}\{e^{-ia}e^{ia} - e^{-ia}e^{ia}\} = 0$

In order to evaluate $P_x(t)$ and $P_y(t)$ it is advantageous to define a complex polarization

$$P^c(t) = P_x(t) + iP_y(t)$$

$$= \frac{1}{2}[e^{ia}\langle S_z=\tfrac{1}{2}| + e^{-ia}\langle S_z=-\tfrac{1}{2}|\,]\,2S^{+}\,[e^{-ia}|S_z=\tfrac{1}{2}\rangle + e^{ia}|S_z=-\tfrac{1}{2}\rangle]$$

where $S^{+}=S_x+iS_y$ is the S_z raising operator

therefore $P^c(t) = [e^{ia}\langle S_z=\tfrac{1}{2}| + e^{-ia}\langle S_z=-\tfrac{1}{2}|\,]e^{ia}|S_z=\tfrac{1}{2}\rangle$

$$= e^{2ia}$$

$$= \cos(2at) + i\sin(2at)$$

therefore $\bar{P}(t) = \cos\dfrac{g_{\mu}e|\bar{B}|t}{2m_{\mu}c}\,\hat{x} + \sin\dfrac{g_{\mu}e|\bar{B}|t}{2m_{\mu}c}\,\hat{y}$

APPENDIX IV LIST OF THE FINE POWDERS

SAMPLE	MANUFACTURERS LISTED MEAN RADIUS (Å)	MANUFACTURER
SiO_2	35	Cabot Corp.[1]
SiO_2	70	Cabot Corp.
Al_2O_3	150	Davidson Chemical Division
		W. R. Grace & Co.
ZnO	560	New Jersey Zinc
MgO	light powder (radius not available)	Matheson Coleman & Bell

[1] Cabot Corp
Cabot-Sil Division
125 High Street
Boston Mass. 02110
U.S.A.

APPENDIX V THE o-Ps FRACTION IN VACUUM

Consider a large number of o-Ps atoms , N(0), at time=0. Let N(t) be the number of atoms after time t. Then

$$dN(t) = -\lambda_o N(t)dt \qquad \text{eqn AV.1}$$

where λ_o is the free o-Ps decay rate. If a quenching agent is present then eqn AV.1 must be rewritten

$$dN(t) = -\lambda_Q N(t)dt \quad \lambda_Q=\lambda_o+\lambda_q \qquad \text{eqn AV.2}$$

$$N(t) = N(0)\exp[-\lambda_Q t]$$

where λ_q is the mean quenching rate. The total number of 2γ decays resulting from the quenching process is

$$\int_o^\infty \lambda_q N(t)dt = \int_o^\infty (\lambda_Q-\lambda_o)N(0)\exp(-\lambda_Q t)\,dt$$

$$= (\lambda_Q-\lambda_o)/\lambda_Q N(0)\,[\exp(-\lambda_Q t)]_\infty^o$$

$$= (\lambda_Q-\lambda_o)/\lambda_Q N(0)$$

It follows that if the o-Ps is being produced at a constant rate , dX/dt , then the 2γ decays will occur a rate

$$\frac{dX^{2\gamma}}{dt} = (\lambda_Q-\lambda_o)/\lambda_Q \frac{dX}{dt} \qquad \text{eqn AV.3}$$

Define

$(dN/dt)_v$ = 2γ counting rate in the evacuated powder

$(dN/dt)_Q$ = 2γ counting rate in the powder+quencher

$(dN/dt)_o$ = 2γ counting rate due e+ s that do not reach the intergranular regions as o-Ps

$(dN/dt)_{CQ}$ = the 2γ counting rate if the quenching were complete and there were no 3γ decays

λ_o = the true vacuum mean decay rate of o-Ps

λ_Q = the mean decay rate in the powder sample + quencher

λ_V = the mean decay rate in the evacuated powder

Then it follows that o-Ps fraction in vacuum is

$$f_{o\text{-}Ps} = [(dN/dt)_{CQ} - (dN/dt)_o]/(dN/dt)_{CQ}$$

$$= \{ 1 + (dN/dt)_o/[(dN/dt)_{CQ} - (dN/dt)_o] \}^{-1} \qquad \text{eqn AV.4}$$

Since $(dN/dt)_{CQ}$ and $(dN/dt)_o$ are not observable the problem is to express $f_{o\text{-}Ps}$ in terms of the observables λ_Q, λ_V, $(dN/dt)_V$, $(dN/dt)_Q$ and the known $\lambda_o = 7.05$ μsec^{-1}. By definition of $(dN/dt)_{CQ}$ and $(dN/dt)_o$ the rate of o-Ps production is

$$dX/dt = \frac{1}{k}[(dN/dt)_{CQ} - (dN/dt)_o] \qquad \text{eqn AV.5}$$

where k is the efficiency for detection. In the powder+quencher the rate of 2γ decays resulting from the quenching of o-Ps is

$$(dX/dt)_Q^{2\gamma} = \frac{1}{k}[(dN/dt)_Q - (dN/dt)_o] \qquad \text{eqn AV.6}$$

Substituting eqns AV.5 and AV.6 into eqn AV.3 yields

$$(dN/dt)_Q - (dN/dt)_o = \frac{(\lambda_Q - \lambda_o)}{\lambda_Q}[(dN/dt)_{CQ} - (dN/dt)_o] \qquad \text{eqn AV.7}$$

Similarly

$$(dN/dt)_V - (dN/dt)_o = \frac{(\lambda_V - \lambda_o)}{\lambda_V}[(dN/dt)_{CQ} - (dN/dt)_o] \qquad \text{eqn AV.8}$$

Subtracting eqn AV.7 from eqn AV.8 yields

$$(dN/dt)_Q-(dN/dt)_v = [(dN/dt)_{CQ}-(dN/dt)_o]\left[\frac{\lambda_Q-\lambda_o}{\lambda_Q} - \frac{\lambda_v-\lambda_o}{\lambda_v}\right]$$

Rewritng this gives

$$(dN/dt)_{CQ}-(dN/dt)_o = [(dN/dt)_Q-(dN/dt)_v]\left[\frac{\lambda_Q-\lambda_o}{\lambda_Q}-\frac{\lambda_v-\lambda_o}{\lambda_v}\right]^{-1}$$

eqn AV.9

Rewriting eqn AV.8

$$\frac{(dN/dt)_o}{(dN/dt)_{CQ}-(dN/dt)_o} = -\frac{\lambda_v-\lambda_o}{\lambda_v} + \frac{(dN/dt)_v}{(dN/dt)_{CQ}-(dN/dt)_o}$$

eqn AV.10

Using eqn AV.9

$$\text{L.H.S.} = -\frac{\lambda_v-\lambda_o}{\lambda_v} + \frac{(dN/dt)_v}{(dN/dt)_Q-(dN/dt)_v}\left[\frac{\lambda_Q-\lambda_v}{\lambda_Q} - \frac{\lambda_v-\lambda_o}{\lambda_v}\right]$$

eqn AV.11

Substituting eqn AV.11 into eqn AV.4

$$f_{o-Ps} = \left\{1 - \frac{\lambda_v-\lambda_o}{\lambda_v} + \frac{(dN/dt)_v}{(dN/dt)_Q-(dN/dt)_v}\left[\frac{\lambda_Q-\lambda_o}{\lambda_Q} - \frac{\lambda_v-\lambda_o}{\lambda_v}\right]^{-1}\right\}$$

eqn AV.12

qed

APPENDIX VI OXYGEN IMPURITIES

The following is the manufactures list of impurities for the 99.65% oxygen used in this experiment.

.3% argon

.05% nitrogen

2ppm carbon dioxide

20ppm hydrocarbons)